UNIVERSITY OF CALIFORNIA
SANTA CRUZ

GEOMORPHOLOGICAL ANALYSIS OF BOULDERS AND POLYGONS ON MARTIAN PERIGLACIAL PATTERNED GROUND TERRAINS

A dissertation submitted in partial satisfaction
of the requirements for the degree of

DOCTOR OF PHILOSOPHY

in

EARTH AND PLANETARY SCIENCE

by

Travis C. Orloff

December 2012

The Dissertation of Travis C. Orloff is approved:

Professor Erik Asphaug, chair

Professor Noah Finnegan

Mikhail Kreslavsky, Ph.D.

Tyrus Miller
Vice Provost and Dean of Graduate Studies

TABLE OF CONTENTS

LIST OF FIGURES

Chapter 1

Chapter 2

Chapter 3

ABSTRACT

GEOMORPHOLOGICAL ANALYSIS OF BOULDERS AND POLYGONS ON MARTIAN PERIGLACIAL PATTERNED GROUND TERRAINS

Travis Orloff

Images from the High Resolution Imaging Science Experiment Camera onboard the Mars Reconnaisance Orbiter show the surface in higher detail than previously capable. I look at a landscape on Mars called permafrost patterned ground which covers ~10 million square kilometers of the surface at high latitudes (>50°). Using the new high resolution images available we objectively characterize permafrost patterned ground terrains as an alternative to observational surveys which while detailed suffer from subjective bias. I take two dimensional Fourier transforms of individual images of Martian permafrost patterned ground to find the scale most representative of the terrain. This scale acts as a proxy for the size of the polygons themselves. Then I look at the distribution of spectral scales in the northern hemisphere between 50-70° and find correlations to previous studies and with the extent of ground ice in the surface. The high resolution images also show boulders clustering with respect to the underlying pattern. I make the first detailed observations of these clustered boulders and use crater counting to place constraints on the time it takes for boulders to cluster. Finally, I present a potential mechanism for the process that clusters the boulders that takes the specifics of the Martian environment to account. Boulders lying on the surface get trapped in seasonal CO_2 frost while ice in the near surface contracts in the winter. The CO_2 frost sublimates in spring/summer allowing the boulders to move when the near surface ice expands in summer.

Repeated iterations lead to boulders that cluster in the polygon edges. Using a thermal model of the subsurface with Mars conditions and an elastic model of a polygon I show boulders could move as much as ~0.1mm per year in the present day.

ACKNOWLEDGEMENTS

The text of this dissertation includes reprints of the following previously published material: Orloff, T., M. Kreslavsky, E. Asphaug, and J. Korteniemi 2011. Boulder movement at high northern latitudes of Mars. *J. Geophys. Res.*, 116, E11006 and Orloff, T., M. Kreslavsky, and E. Asphaug in press, A Possible Mechanism for Boulder Clustering on Mars. *Icarus*. The co-author Prof. Erik Asphaug listed in this publication supervised the research which forms the basis for the dissertation. I'd also like to thank my other coauthors Dr. Mikhail Kreslavsky and Dr. Jarmo Korteniemi. Dr. Kreslavsky provided immense efforts in the publication of these papers including research direction, crater statistics analysis (in Orloff et al., 2011), image capture automation, writing, editing, and countless fruitful discussions. Dr. Korteniemi provided a spectacular crater database on which to perform cratering statistics, participated in editing, and also took part in many research discussions. Prof. Quentin Williams, Prof. Noah Finnegan, Dr. Aaron Zent and Jonathon Perkins provided fruitful discussions that further advanced this research. This research would not be possible without funding from the University of California Santa Cruz Earth and Planetary Sciences Department and the NASA Mars Fundamental Research Program. This work is dedicated to the memory of my grandparents Joe and Ruetta Orloff and James and Arlene Wicker who passed away.

CHAPTER ONE

Characterization of Martian Patterned Ground in the Northern Hemisphere Using the Fourier Transform

Abstract

Permafrost patterned ground forms on the surface of nearly all landscapes between 50-70°N on Mars. This landform appears in satellite imagery as an interconnected network of polygonal shapes. Previous studies used geomorphologic observations to characterize patterned ground terrains on Mars. These classification systems prove useful but suffer from somewhat subjective methods. We find objective analysis of the polygons comprising patterned ground terrains on the surface of Mars feasible using HiRISE imagery acquired from orbit. We perform a two-dimensional Fourier transform on 124 images of polygonal surfaces to characterize the spatial scale pertinent to scenes and analyze the distribution of these properties on the surface of Mars between 50-70°N. We find two distinct sets of polygons: large polygons which form below 60°N and small polygons primarily above 60°N with exception for sites within Acidalia Planitia. Our findings show similar trends to those found in previous studies but also fundamental differences in the populations of polygons above and below 60°N. The polygons within 60-70°N share roughly the same polygonal scale implying that seasonal temperature change is not the only factor forcing polygon development as previous models found. In some cases our methods show polygons of multiple scales make up a scene. While we cannot yet objectively quantify the larger scale we do identify where multiple scales exist. This method in conjunction with observational analysis improves our ability to characterize surfaces and should prove a useful tool in examining patterned ground terrains on Mars.

1. Introduction

The surface of Mars displays a wide variety of permafrost patterned ground across a wide range of latitudes covering 10's of millions of square kilometers of the surface [*Costard and Kargel*, 1995; *Mangold*, 2005; *Balme and Gallagher*, 2008; *Levy et al.*, 2009; *Orloff et al.*, 2011]. The morphologic variations suggests high latitude (>50°) permafrost patterned ground forms due to a variety of environmental drivers dependent on local climate and setting and also potentially different mechanisms including thermal contraction of ground ice, frost heave, or ground ice sublimation [*Mellon*, 1997; *Seibert and Kargel*, 2001; *Marchant and Head*, 2007; *Morgenstern et al.*, 2007; *Balme et al.*, 2008; *Mellon et al.*, 2008; *Lefort et al.*, 2009]. Individual polygons in the different patterned ground terrains have distinct visual appearances from satellite imagery. Two such examples are shown in Figure 1. Figure 1a shows classic high latitude (>65°N) small polygons and Figure 1b shows significantly larger polygons common at lower latitude (50-55°N). Also note the differences in the polygonal edges and spacing of these polygonal networks.

Patterned ground has been classified, described, and mapped using primarily subjective methods based on geomorphological observations (polygon diameter, shape, slopes, presence of boulders) in satellite imagery from the Mars Orbital Camera (MOC [*Malin and Edgett*, 2001]) [*Mangold*, 2005, *Kostama et al.*, 2006] and the High Resolution Imaging Science Experiment (HiRISE [*McEwen et al.*, 2007]) [*Levy et al.*, 2009; *Korteniemi and Kreslavsky*, 2012]. These methods are applied to describe the variety of patterned ground and the characteristics of the different types

Figure 1

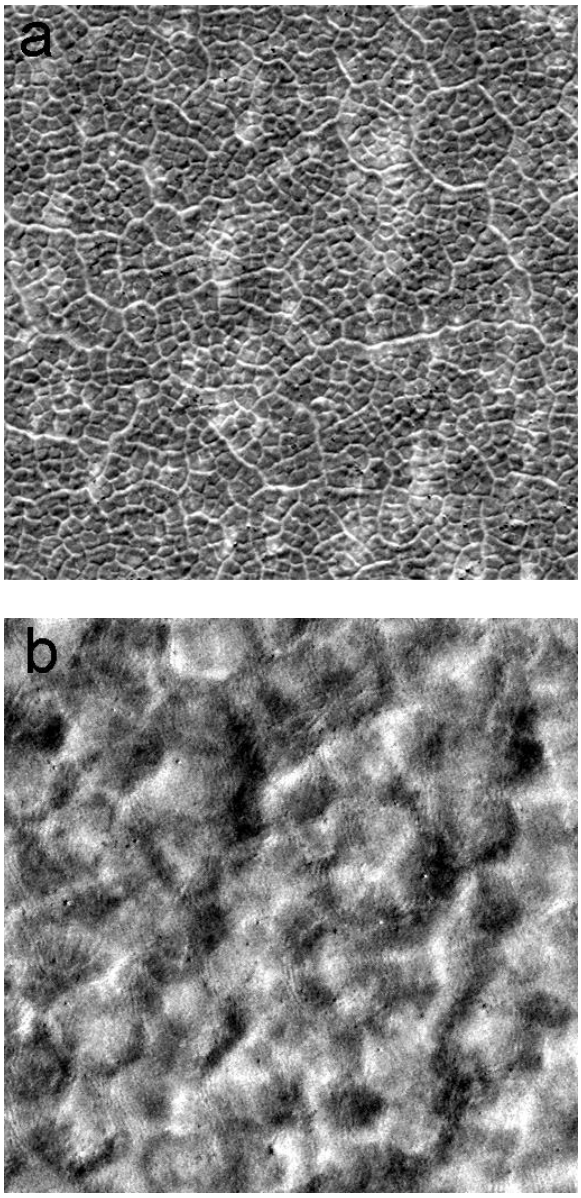

Figure 1: Images of two types of patterned ground. a) Picture of high latitude small polygons from PSP_001418_2495. b) Low latitude large polygons from ESP_018924_2365. Note the differences in the polygonal edges and spacing of these two types of polygons. Illumination of both images is from the right and images are ~125 meters across. Image: NASA/JPL/University of Arizona.

of patterned ground. These studies showed significant latitudinal trends in the types of patterned ground further supporting the idea that climate directly influences polygon formation.

While these studies provided useful observations, they did not provide an objective method to consistently analyze these terrains. *Pina et al.* [2006, 2008] developed a method using the dynamics of watershed contours [*Beucher and Meyer*, 1993; *Bleau and Leon*, 2000] to characterize polygonal networks and then measure average polygon size and count the number of polygonal neighbors for each polygon using both MOC and HiRISE images. They then use several statistical measures to characterize their network. Their findings do prove useful in characterizing polygonal networks but depend strongly on tuning filters for each individual image, which introduces a subjective element into processing. As of this writing they also have not applied their method systematically to a large number of sites.

Several studies have used the Fourier transform to analyze periodic structures in topographic and bathymetric data [*Rayner*, 1972; *Hanley*, 1977; *Stromberg and Farr*, 1986; *Ricard et al.*, 1987; *Mulla*, 1988; *Gallant*, 1997; *Perron et al.*, 2008] We use a two-dimensional Fourier Transform (2-D FT) to objectively analyze patterned ground terrains across Mars in northern high latitudes and determine a spatial characteristic which allow us to describe patterned ground. We intend to determine if this objective technique finds regional or latitudinal spacing variations similar to those found in previous geomorphological studies. Such variations would indicate regional and global scale differences in patterned ground formation.

2. Method

The goal of our study is to characterize permafrost patterned ground terrain using an objective measure and analyze the distribution of this objective measure on the surface of Mars between 50-70°. To do this we look at HiRISE images between 50-70°N on Mars and perform a Fourier transform on the images to determine the wavelength most representative of the terrain.

We start with a catalog of HiRISE images (Table 1) that we aim to analyze. We choose the same images as those used for a geomorphological study in *Korteniemi and Krelavsky* [2012]. The images chosen do not represent a random population, nor do they form a uniform distribution. Instead images were chosen such that no large craters or other large primary features would influence our results. Only full-resolution HiRISE images (map-projected with 25 cm sampling) were chosen. The distribution of images shows geographical biases, such as the fact that there are many more images acquired near the Phoenix landing site. Despite these biases, following *Korteniemi and Krelavsky* [2012] we believe that the chosen images are reasonably representative of all patterned ground terrains within 50-70°N.

We take each chosen HiRISE image and identify a sub-image with polygons representative of the entire image. We choose locations with as few boulders as possible to minimize their effects on further processing. We also tried to avoid obvious albedo variations. We pick a center point of a 1460 × 1460 pixel sub-image chosen via visual inspection of the image.

The illumination conditions (direction of the sun) directly influence the patterns of bright and dark within an image: surface facets tilted toward the sun are systematically brighter than those tilted in the opposite direction. Because of this, the 2-D power spectra resulted from the 2-D Fourier transform are not isotropic: illumination direction is seen as a peculiar direction in the spatial frequency domain. To analyze chosen sub-images consistently, we rotate them so that the sun direction is the same in all images (directly from the right), then cut out a 512 × 512 pixel region (128 m × 128 m) and a 1024 × 1024 pixel region (256m × 256m) from the center of the 1460 × 1460 sub-image. This gives us a set of images the proper size for an efficient 2-D Fourier transform and with uniform lighting conditions.

With our images now ready for analysis we run them through code presented by Taylor Perron from the 'New Tools in Process-Based Analysis of Lidar Topographic Data' 2010 workshop (available at www.opentopography.org/index.php/resources/short_courses/lidar2_2010/) which we modified to work on brightness values in grayscale images. In our case we look at patterns of brightness within an image rather than patterns of elevation in Lidar Topographic Data. Like *Perron et al.* (2009), we use a Hann window to remove edge effects; then we perform a 2-D Fourier transform on both the 512 × 512 pixel and 1024 × 1024 pixel sub-image providing us with a spatial power spectrum, which we then examine (an example of which is shown in Figure 2). In Figure 2 the color corresponds to the spectral power, $P(k_x, k_y)$ at a given vector of spatial frequency (wave number) with Cartesian components k_x, k_y. Due to symmetry in the spectra we

only look at the positive x-frequencies. Then we artificially set P to zero for the 3 pixels adjacent to the 0 frequency (one directly to the right, and the two above and below the pixel to the right) because of influence from the Hann window and large scale (~100 meter) albedo patterns. We also disregard frequencies with either an k_x or k_y component greater than 1 m^{-1}, because the wavelengths corresponding to these frequencies (<1 m) are at, close to, or below the resolution of the original images; in result, P at these frequencies is strongly affected by details of interpolation algorithms used in map-projecting HiRISE images and subsequent rotation and bear little information about the real surface.

We use reciprocal power-weighted-mean x-component of the spatial frequency as a measure of the spatial scale most representative of the image:

$$\lambda = \frac{\sum_{k_x}\sum_{k_y} P(k_x, k_y)}{\sum_{k_x} k_x \sum_{k_y} P(k_x, k_y)} \qquad (1)$$

We chose this measure after a series of trials. The use of x-component was dictated by the fact that in this direction the topography-controlled variations of brightness are greatest (x direction is the direction to the Sun), and our goal is topographic rather than albedo pattern. We assessed the choice of the characteristic spatial scale measure performing three tests. For the first test we magnify the image 2x and expect to double the original characteristic spatial scale. For the second test we compare the characteristic spatial scale of similar polygons at different locations

Figure 2

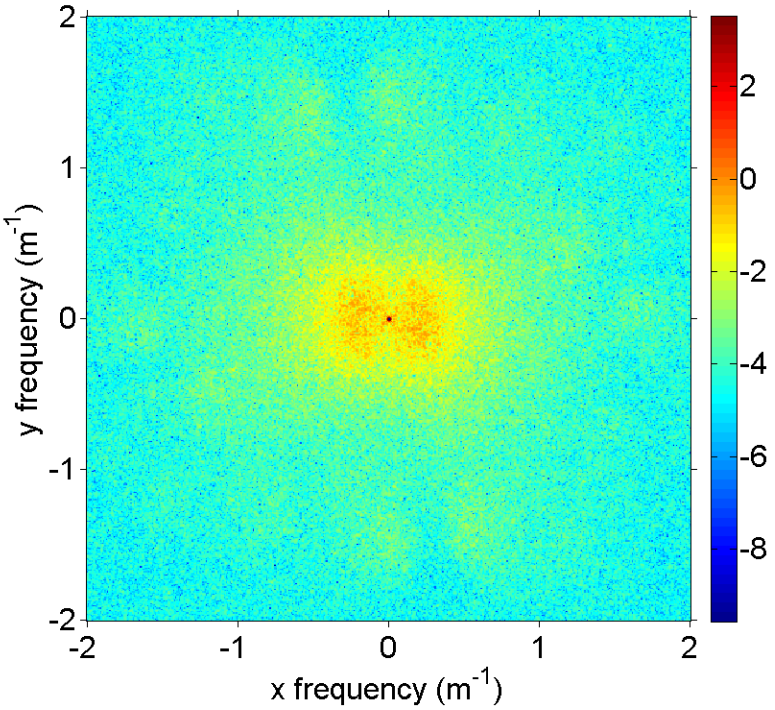

Figure 2: Example of our discrete Fourier transform spectra. Colors correspond to the power associated with a given orientation and radial frequency. In our analysis we fold the spectra in half due to symmetry and then we sum all the powers at each x-component frequency. In all cases the illumination of the image from which we take the Fourier transform is from the right.

within the same HiRISE image and expect roughly the same scale. In the third test we analyze the actual image itself to see if the inferred characteristic spatial scale indeed represents the characteristic size of the polygons. The measure λ defined in (1) was successful at these tests within less than 20% variation in all our test cases.

3. Results

The characteristic spatial scales λ we report do not directly correspond to polygon size or spacing but we interpret them as a proxy for these characteristics. Figures 3 and Figure 4 show the results of our analyses on 124 512 × 512 pixel images of patterned ground in the northern high latitudes of Mars.

First we look at how characteristic spatial scales varied across the surface of Mars. Figure 3 shows the distribution of images across Mars with colored dots representing each image location where the color of the dot corresponds to the characteristic scale we found for that image. Blue dots show the locations of short scales, red dots show the locations of long scales, and green or yellow dots show the locations of intermediate spatial scales. We find that all images northward of 60°N are at the lower range of our color scale indicating small polygons. Southward of 60°N we find large, small, and intermediate spatial scales indicating a greater diversity in polygon appearances.

Previous studies [*Mangold*, 2005; *Levy et al.*, 2009] noted variations of patterned ground type with latitude and so we looked if we could find similar trends in our results. Figure 4 shows the characteristic scale of each image as a function of latitude. Like Figure 3 we clearly see a different trend in characteristic spatial scale

Figure 3

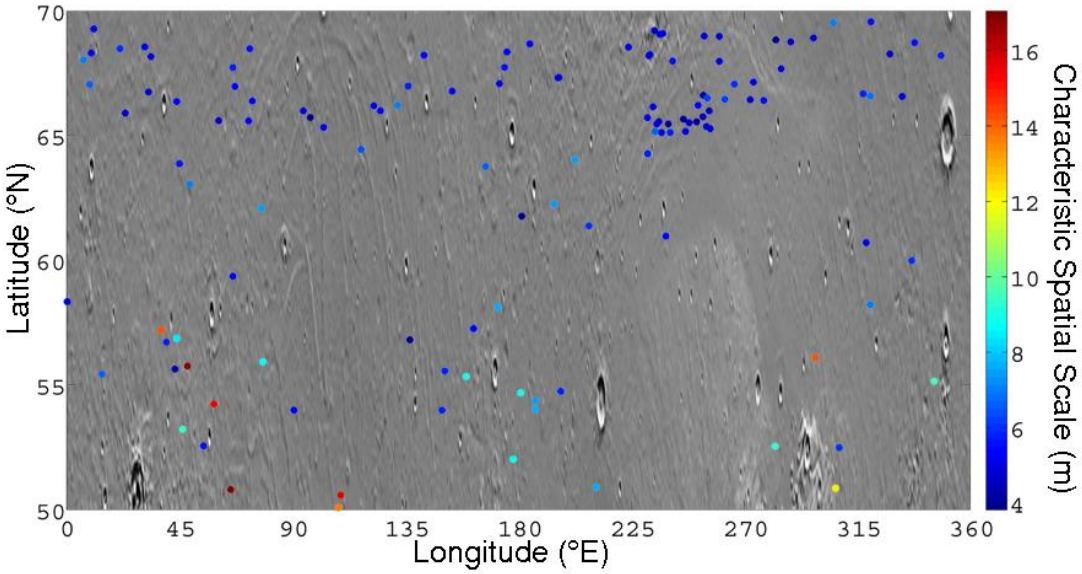

Figure 3: Map of Mars showing locations of images and characteristic spatial scale associated with each 512 × 512 pixel image. Colors correspond to characteristic spatial scale. Note primarily blue colors corresponding to low characteristic spatial scales above 60°N and a variety of colors below. Background shows a shaded relief map of the region derived from Mars Orbiter Laser Altimeter data.

between 50-60°N and between 60-70°N. The polygons at lower latitudes display a greater range in polygon sizes while those at higher latitudes cluster between ~4-8 meters.

To see if our results are robust we compared 512 × 512 pixel images to the results for 1024 × 1024 pixel images of the same location. If we missed certain portions of the spatial power spectrum by using the 512 × 512 pixel image we should find additional power at longer wavelengths in the larger image. Figure 5 shows that for most images both sets of images provide nearly the same results. However, we find 11 images (denoted with triangles and grouped together with a box) in Figure 5 with significantly larger characteristic spatial scales in the 1024 × 1024 images. Upon inspection of the images (an example is shown in Figure 6) we see that the polygons present have multiple dominant scales: a small scale around 3-5 meters and a larger scale comprising groups of these polygons. While we can identify that these polygons show multiple scales, with the technique we use, we cannot reliably and objectively measure the larger scale.

Many boulders lie on top of polygons in the images in our survey but we chose portions of the HiRISE image with as few boulders as possible to perform our analysis. Still, boulders appear in many of the images we study. To determine how boulders influence characteristic spatial scale we choose three additional subimages from four HiRISE images in our survey and analyze them in the same fashion noted in Section 2. We specifically choose HiRISE images to look at the presence of boulders on small polygons, boulders on large polygons, rubble piles on small

Figure 4

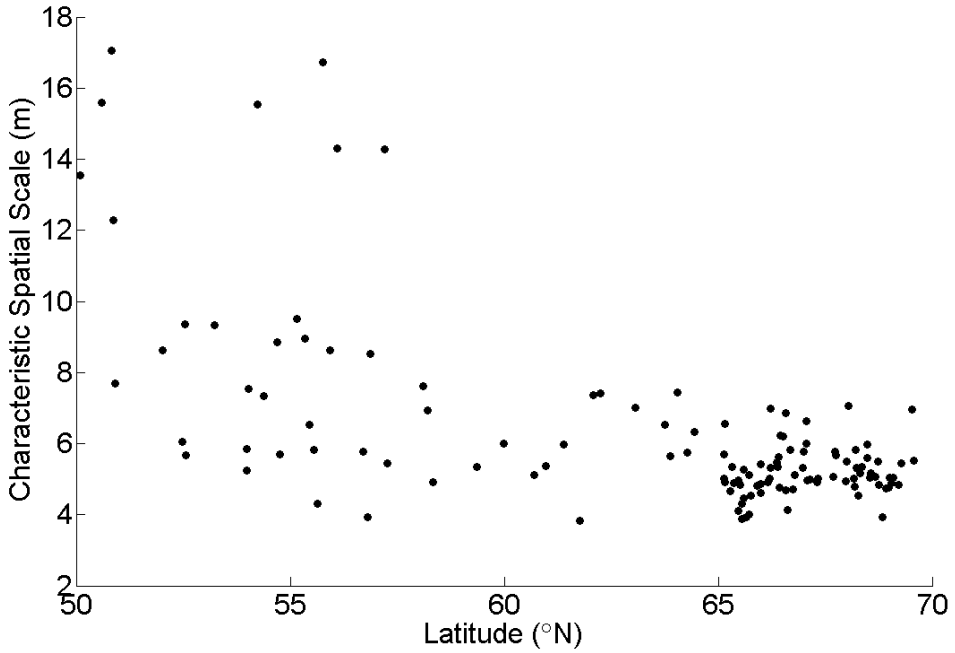

Figure 4: Characteristic spatial scale as a function of latitude for 512 × 512 pixel images. Each point corresponds to an image from our study. Note that no large scale polygons are present above 60°N.

polygons, and additional boulder free areas on small polygons. For small polygons the presence or lack of boulders does not significantly alter the characteristic spatial scale of the terrain. However for larger scale polygons the presence of boulders greatly reduces the characteristic spatial scale we find for boulder free regions. This means that more care is necessary for picking images displaying the larger scale polygons to be sure boulders do not significantly influence the analysis.

4. Discussion

Our results show significant differences between patterned ground terrains pole-ward of 60°N and patterned ground terrains equator-ward. Specifically, we find regions with large characteristic spatial scales in low latitudes and much shorter characteristic spatial scales in higher latitudes as shown in Figures 3 and 4. This same trend has previously been found in observational geomorphological surveys [*Mangold*, 2005; *Levy et al.*, 2009; *Korteniemi and Kreslavsky*, 2012]. Additionally, *Levy et al.* [2009] and *Korteniemi and Kreslavsky* [2012] found small scale polygon morphologies extending across the entire range of latitudes we study. We too find short characteristic spatial scales across nearly all latitudes with our more objective method. This suggests to us that our method performs similarly to observational surveys.

Unlike *Mangold* [2005] and *Levy et al.* [2009], however, we do not find trends within 60-70°N, nor do we find trends within 50-60°N. This is not unexpected, though, because polygons of the same scale would give similar λ despite different

Figure 5

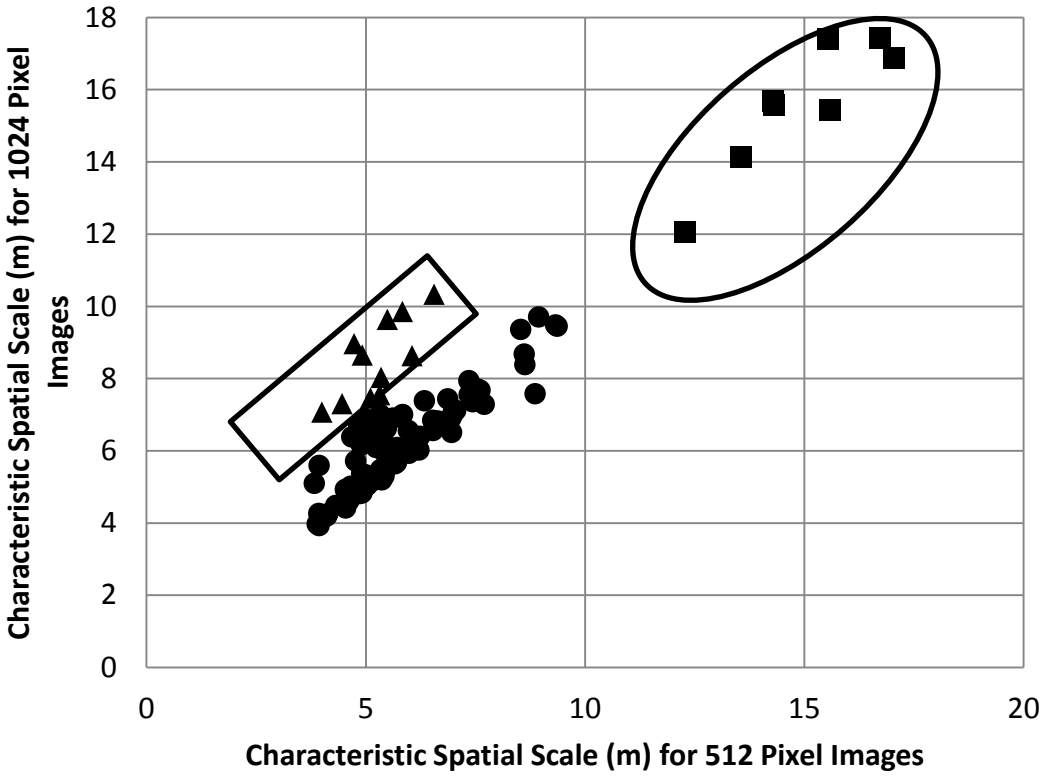

Figure 5: Characteristic spatial scale of 512 × 512 pixel images vs characteristic spatial scale of 1024 × 1024 pixel images. Those values far from 1:1 show regions where multiple scales influence polygons. Squares represent large polygonal surfaces, diamonds represent small scale polygonal surfaces and triangles represent multi-scale polygonal surfaces. Large polygonal surfaces are grouped within an ellipse and the multi-scale polygonal surfaces are grouped within a rectangle.

morphological appearances, given that several of *Levy et al.*'s [2009] polygon classes have nearly the same diameter.

Our inability to distinguish polygon morphology of similar scales may prove this method's greatest weakness because this means that visual inspection of polygonal surfaces is still necessary in mapping and characterizing the variety of patterned ground terrains. However, *Korteniemi and Kreslavsky* [2012] agree that the morphological variations of similar scale polygons do not indicate fundamentally different polygon types. *Korteniemi and Kreslavsky* [2012] find two primary types of polygons they call Type 1 (a larger (10-20 m diameter) smoothly undulating or hummocky ground pattern) and Type 2 (clear, angularly connected sharp polygons) instead of the 5 or more classes of polygons in *Levy et al.* [2009] and *Mangold* [2005]. Our findings support this type of classification scheme and we find a similar distribution of polygons amongst our survey. Our method adds a more objective and quantitative approach, and when combined with observations can prove more predictive.

Models [*Mellon*, 1997; *Mellon et al.*, 2008] predict that the size of the polygons depend on the amplitude of seasonal temperature change which depends in large part on climatic conditions. Larger temperature changes lead to greater thermal stresses which should generate smaller polygons because peak stresses form in the center of polygons. *Mellon* [1997] estimated the tensile strength of ice-cemented Martian soil to be between 2 and 3 MPa at Martian temperatures and for length scales comparable to permafrost polygons. More recently *Mellon et al.* [2008] predicts 3.5

Figure 6

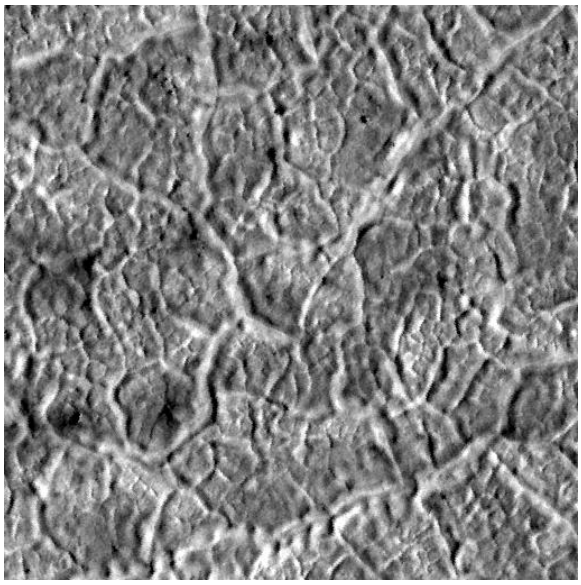

Figure 6: Example of an image with multiple polygonal scales. In this image from PSP_001559_2485 there are at least two primary polygon sizes. The smallest diameter polygons have diameters of approximately 3-4 meters and sets of these polygons make larger polygons with diameters > 10 meters. Illumination of image is from the right and image is ~125 meters across. Image: NASA/JPL/University of Arizona.

MPa stresses in the center of a polygon with cracks 10 meters apart for a seasonal temperature change less than 50° K. Under these conditions *Mellon et al.* [2008] predicts subdivision of such a polygon, so that polygon size decreases with the increase of the seasonal temperature amplitude, all other parameters being the same.

Since at the high latitudes the summer day-average temperature increases equatorward, while the winter day-average temperatures are fixed at the CO_2 frost point, the seasonal temperature amplitude increases from higher to lower latitudes. Thus, smaller characteristic polygon sizes are predicted at lower latitudes based on simple thermal contraction considerations. This is in contrast with our findings, that show small polygons (< 6m characteristic spatial scale) across almost the entire range of latitudes (~55-70°N) in the survey and large polygons only at low latitudes (< 60°N). A purely temperature driven mechanism would predict a gradient of sizes. This suggests that other factors must play a role in polygon development.

We suspect the extent of shallow ground ice down to ~60°N deduced from the Gamma Ray Spectrometer onboard Mars ODYSSEY [*Boynton et al.*, 2002; *Feldman et al.*, 2002; *Mitrofanov et al.*, 2002] may cause polygons below this latitude to appear different than those above. Namely, larger polygons form where ice is not present, or is deeper than Mars ODYSSEY can detect. At the same time, however, polygons close to 60°N have less ice present than those at 70°N but the same characteristic spatial scales. These findings suggest to us that the presence of high volumes of near surface ice, in addition to climatic seasonal temperature shifts, is an important factor in the development of polygons.

Figure 7

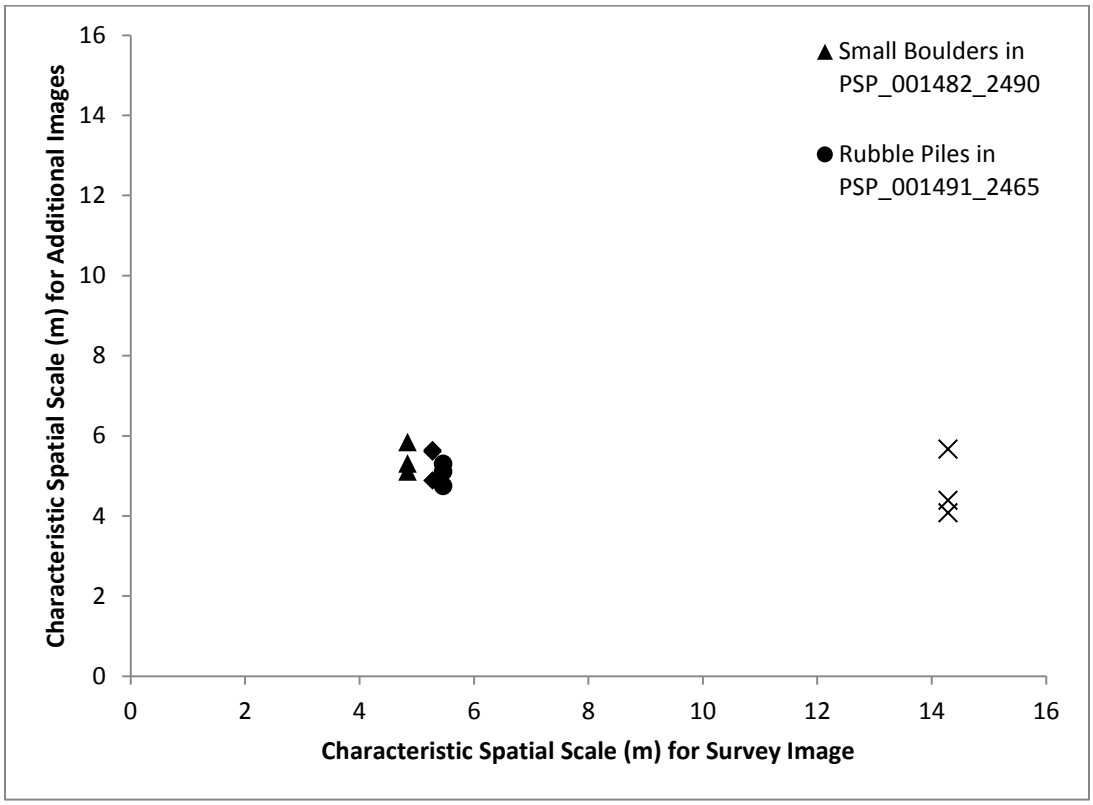

Figure 7: Multiple locations within a single image. We look at the cases where boulders appear on small polygons (triangles), rubble piles form on small polygons (circles), additional cases of no boulders (diamonds), and boulders appear on large polygons (x symbols). For the small polygons the additional images show good agreement with the survey image and the boulders do not seem to affect the characteristic spatial scale. For large polygons though the presence of boulders significantly lowers the characteristic spatial scale compared to a relatively boulder free terrain.

5. Conclusions

We show that our analysis of the spatial power spectrum produced from the 2-D FT is indeed capable of providing characteristic spatial scales comparable to the actual diameter of individual polygons in an image and multi-polygon features. Applying this technique to HiRISE images of patterned ground gives an objective way to characterize patterned ground terrains. Our results mostly agree with those of *Mangold* [2005] and *Levy et al.* [2009].

Like *Korteniemi and Kreslvasky* [2012] we find two primary types of polygons. We only find large scale polygons at lower latitudes and small scale polygons at higher latitudes (with some also at lower latitudes in Acidalia Planitia). We do not discern differences in polygon morphology of the same scale but we do find multi-scale polygons in certain regions although we cannot yet objectively discern the larger scale. Our results suggest that the presence of ground ice and seasonal temperature changes both influence polygon morphology. We conclude that spatial spectral characteristics can objectively determine features of landscapes in HiRISE images and will be a powerful tool of Mars patterned ground research and geomorphology.

Acknowledgements

Research by T.O., M.K. and E.A. was supported by NASA Mars Fundamental Research Program award NNX08AT13G. M.K. was also supported by NASA Mars Data Analysis award NNX08AL07G. We appreciate fruitful discussions regarding the use of Fourier transforms on terrain with Noah Finnegan and Jon Perkins. We also

would like to acknowledge the HiRISE team for the spectacular images of the surface of Mars which allowed us to perform this study.

References

Balme, M. R. and C. Gallagher (2008), An equatorial periglacial landscape on Mars, *Earth and Planet. Sci. Lett.*, *285*(1-2), 1-15, doi:10.1016/j.epsl.2009.05.031.

Balme, M. R., C. J. Gallagher, D. P. Page, J. B. Murray, and J. -P. Muller (2008), Sorted stone circles in Elysium Planitia, Mars: Implications for recent martian climate, *Icarus*, *200*(1), 30-38, doi:10.1016/j.icarus.2008.11.010.

Beucher, S., and F. Meyer (1993), The morphological approach to segmentation: The watershed transformation. In *Mathematical Morphology in Image Processing*. (E.R. Dougherty, Ed.) 433-482, Marcel Dekker, New York.

Bleau, A., and L.J. Leon (2000), Watershed-based segmentation and region merging. *Computer Vision and Image Understanding*, 77, 317-370.

Boynton, W.V., W. C. Feldman, S. W. Squyres, T. H. Prettyman, J. Brückner, L. G. Evans, R. C. Reedy, R. Starr, J. R. Arnold, D. M. Drake, P. A. J. Englert, A. E. Metzger, I. Mitrofanov, J. I. Trombka, C. d'Uston, H. Wänke, O. Gasnault, D. K. Hamara, D. M. Janes, R. L. Marcialis, S. Maurice, I. Mikheeva, G. J. Taylor, R. Tokar, and C. Shinohara (2002), Distribution of hydrogen in the near surface of Mars: Evidence for subsurface ice deposits, *Science*, *297*, 81–85, doi:10.1126/science.1073722.

Costard, F. M., and J. S. Kargel (1995), Outwash Plains and Thermokarst on Mars, *Icarus*, *114*(1), 93- 112.

Feldman, W. C., W. V. Boynton, R. L. Tokar, T. H. Prettyman, O. Gasnault, S. W. Squyres, R. C. Elphic, D. J. Lawrence, S. L. Lawson, S. Maurice, G. W. McKinney, K. R. Moore and R. C. Reedy (2002), Global distribution of neutrons from Mars: Results from Mars Odyssey, *Science*, *297*(5578), 75-78, DOI:10.1126/science.1073541.

Gallant, J. C. (1997), Scale and structure in landscapes, PhD thesis, Australian National University.

Hanley, J.T. (1977), Fourier analysis of the Catawba Mountain knolls, Roanoke county, Virginia, *Mathematical Geology*, *9*(2), 159-163.

Korteniemi, J., and M. A. Kreslavsky (2012). Patterned ground in Martian high northern latitudes: Morphology and age constraints. *Icarus*, in press.

Kostama, V.-P., M. A. Kreslavsky, and J.W. Head (2006), Recent high latitude icy mantle in the northern plains of Mars: Characteristics and ages of emplacements, *Geophys. Res. Lett.*, 33, L11201, doi:10.1029/2006GL025946.

Lefort, A., P. S. Russell, N. Thomas, A. S. McEwen, C. M. Dundas, and R. L. Kirk (2009), Observations of periglacial landforms in Utopia Planitia with the High Resolution Imaging Science Experiment (HiRISE), *J. Geophys. Res.*, *114*(E4), E04005, doi:10.1029/2008JE003264.

Levy, J. S., J. W. Head, and D. R. Marchant (2009), Thermal contraction crack polygons on Mars: Classification, distribution, and climate implications from HiRISE observations, *J. Geophys. Res.*, *114*(E1), E01007, doi:10.1029/2008JE003273.

Malin, D.R. and K.S. Edgett (2001), Mars Global Surveyor Mars Observer Camera: Interplanetary cruise through primary mission, *J. Geophys. Res.*, *106*(E10), 23429-23570, doi:10.1029/2000JE001455.

Mangold, N. (2005), High latitude patterned ground on Mars: Classification, distribution and climate control, *Icarus*, *174*, 336– 359, doi:10.1016/j.icarus.2004.07.030.

Marchant, D. R., and J. W. Head (2007), Antarctic dry valleys: Microclimate zonation, variable geomorphic processes, and implications for assessing climate change on Mars, *Icarus*, *192*(1), 187-222, doi:10.1016/j.icarus.2007.06.018.

McEwen, A.S., E. M. Eliason, J.W. Bergstrom, N.T. Bridges, C.J. Hansen, W.A. Delamere, J.A. Grant, V.C. Gulick, K.E. Herkenhoff, L. Keszthelyi, R.L. Kirk, M.T. Mellon, S.W. Squyres, N. Thomas, and C.M. Weitz (2007), Mars Reconnaissance Orbiter's High Resolution Imaging Science Experiment (HiRISE), *J. Geophys. Res.*, *112*, E05S02, doi:10.1029/2005JE002605.

Mellon, M. T. (1997), Small-scale polygonal features on Mars: Seasonal thermal contraction cracks in permafrost, *J. Geophys. Res.*, *102*(E11), 25617–25628, doi:10.1029/97JE02582.

Mellon, M. T., R. E. Arvidson, J. Marlow, R. Phillips, and E. Asphaug (2008), Periglacial landforms at the Phoenix landing site and the northern plains of Mars, *J. Geophys. Res.*, *113*, E00A23, doi:10.1029/2007JE003039.

Mitrofanov, I., D. Anfimov, A. Kozyrev, M. Litvak, A. Sanin, V. Tret'yakov, A. Krylov, V. Shvetsov, W. Boynton, C. Shinohara, D. Hamara, and R. Saunders (2002), Maps of Subsurface Hydrogen from the High Energy Neutron Detector, Mars Odyssey, *Science*, *297*(5578), 78-81, doi:10.1126/science.1073616.

Morgenstern, A., E. Hauber, D. Reiss, S. van Gasselt, G. Grosse, and L. Schirmeister (2007), Deposition and degradation of a volatile-rich layer in Utopia Planitia and implication for climate history on Mars, *J. Geophys. Res.*, *112*(E6), E06010, doi:10.1029/2006JE002869.

Mulla, D. J. (1988), Using geostatistics and spectral analysis to study spatial patterns in the topography of southeastern Washington state, *USA Earth Surface Processes and Landforms*, *13*, 389-405.

Orloff, T., M. Kreslavksy, E. Asphaug, and J. Korteniemi (2011), Boulder movement at high northern latitudes of Mars, *J. Geophys. Res.*, *116*, E11006, doi:10.1029/2011JE003811.

Perron, J.T., J.W. Kirchner and W.E. Dietrich (2008), Spectral signatures of characteristic spatial scales and nonfractal structure in landscapes, *J. Geophys. Res.*, *113*, F04003, doi:10.1029/2007JF000866.

Pina, P., J. Saraiva, L. Bandeira, and T. Barata (2006), Identification of Martian polygonal patterns using the dynamics of watershed contours, *Lect. Notes Comput. Sci*,. 4142, 691–699.

Pina, P., J. Saraiva, L. Bandeira, and J. Antunes (2008), Polygonal terrains on Mars: A contribution to their geometric and topological characterization, *Planet. And Space Sci., 56*, 1919-1924.

Rayner, J. N. (1972) The application of harmonic and spectral analysis to the study of terrain, in *Spatial Analysis in Geomorphology*, edited by R. J. Chorley, pp. 283-302, Methuen.

Ricard, Y., C. Froidevaux, and R. Simpson (1987), Spectral analysis of topography and gravity in the Basin and Range Province, *Tectonophysics*, *133*, 175-187.

Seibert, N. M., and J. S. Kargel (2001), Small-scale Martian polygonal terrain: Implications for liquid surface water, *Geophys. Res. Lett.*, *28*(5), 899-902.

Stromberg, W. D., and T. G. Farr (1986), A Fourier-based textural feature extraction procedure, *IEEE Transactions on Geoscience and Remote Sensing*, *24*, 722-731.

Table 1: HiRISE Image Information

Image Name	Subsolar Azimuth (°)	Subimage X-Pixel Coordinate	Subimage Y-Pixel Coordinate	Characteristic Scale λ (m)
PSP_001333_2485	110.6	6114	9745	5.0234
PSP_001337_2480	219.9	8546	6597	5.0546
PSP_001338_2480	247.2	10729	13907	4.9465
PSP_001341_2485	328.7	2702	3042	5.3438
PSP_001344_2465	51.7	5145	7029	4.8591
PSP_001345_2480	78.14	14150	12749	5.7829
PSP_001351_2490	241.1	11477	4586	4.7617
PSP_001358_2485	72.5	12455	25384	5.5904
PSP_001373_2460	122.7	6523	4235	4.8172
PSP_001375_2485	176.2	4333	3495	4.5305
PSP_001377_2475	231.3	3314	6143	4.9796
PSP_001389_2500	197.6	11306	6570	6.9587
PSP_001391_2465	253.9	8820	17483	4.615
PSP_001392_2490	279.8	6425	7376	5.0472
PSP_001395_2485	1.85	7144	2078	5.3295
PSP_001404_2490	246.8	13350	1681	5.0379
PSP_001413_2495	132.3	5113	3572	5.4329
PSP_001415_2470	188	2893	9810	5.8287
PSP_001418_2495	268.7	6073	9597	4.8336
PSP_001421_2470	351.7	1424	8667	5.1204
PSP_001422_2465	19.25	14400	12664	5.4138
PSP_001430_2470	236.9	16460	22307	6.0071
PSP_001448_2470	8.064	7963	15588	5.7853
PSP_001464_2460	85.13	9825	5124	4.4587
PSP_001467_2490	165.6	2586	6287	5.4908
PSP_001473_2480	329.6	8517	12543	5.6775
PSP_001475_2465	25.01	5402	13756	5.0116
PSP_001477_2470	79.19	8637	21624	5.3304
PSP_001481_2410	150.3	18410	20249	5.1059
PSP_001482_2490	214.7	3998	4849	4.8406
PSP_001483_2465	243	5610	14449	6.2369
PSP_001484_2455	270.7	12158	3832	4.9778
PSP_001491_2465	101.2	16033	9658	5.4646

PSP_001497_2480	264.3	7904	21592	5.5067
PSP_001505_2485	122.2	6730	9407	5.9707
PSP_001520_2470	172.2	12985	4761	4.6783
PSP_001523_2465	254.2	19175	11300	5.3165
PSP_001525_2475	308.2	8846	15851	5.023
PSP_001531_2470	112.1	5942	7464	4.7229
PSP_001535_2490	220.4	8441	8330	3.9378
PSP_001556_2460	74.63	5060	23848	5.2765
PSP_001559_2485	155.3	11296	2423	5.8337
PSP_001565_2490	318.7	9258	11585	5.0676
PSP_001575_2465	232.4	11795	4768	4.7644
PSP_001576_2460	260	9941	3885	3.9242
PSP_001588_2465	227	5571	3255	5.6217
PSP_001591_2475	308.5	9044	7041	4.9176
PSP_001611_2485	133.6	7288	11200	5.1732
PSP_001614_2490	215.2	7261	2633	4.733
PSP_001615_2470	243.1	7670	26108	6.2093
PSP_001629_2455	265.7	5604	12605	4.1117
PSP_001635_2465	68.99	11520	23547	5.3538
PSP_001655_2460	254.9	18666	27264	3.8911
PSP_001663_2490	111.9	18185	12986	5.1644
PSP_001668_2460	249.3	7071	23505	4.5413
PSP_001669_2460	276.8	30247	12096	5.1152
PSP_001681_2455	243.9	3077	29376	4.66
PSP_001682_2465	271.1	21081	15011	4.9087
PSP_001695_2455	266.1	10418	27592	5.7012
PSP_001708_2455	260.7	31132	19583	4.9132
PSP_001721_2460	255	15216	27289	4.8388
PSP_001734_2470	249.2	1917	24451	4.1341
PSP_001738_2345	155.4	7205	9385	5.8409
PSP_001741_2395	152.3	6443	8496	5.336
PSP_001742_2370	152.4	14391	12111	5.7803
PSP_001744_2355	152.7	20836	12227	9.511
PSP_001748_2460	271.6	10750	28870	4.3199
PSP_001753_2460	47.89	10402	7539	3.9978
PSP_001761_2495	264.9	11354	26774	5.0438
PSP_001785_2330	155.4	3933	12224	6.0548

PSP_001801_2455	277.7	24197	39107	6.5572
PSP_001803_2475	331.5	7906	4901	4.9737
PSP_001813_2455	244.9	20534	9823	4.895
PSP_001814_2455	272.6	11397	29393	5.0084
PSP_001880_2485	273.3	26210	16902	4.7816
PSP_001946_2485	275	31966	18719	5.2813
PSP_002183_2495	264.6	18081	12768	4.8841
PSP_002317_2420	146.7	13678	33905	3.8231
PSP_002396_2345	151.1	11745	21614	7.3491
PSP_002455_2360	146.4	3322	13034	6.5362
PSP_002620_2345	145.1	26531	10071	7.5438
PSP_007803_2375	147.3	12004	33120	5.4472
PSP_008123_2310	156.3	15172	75875	17.046
PSP_008219_2470	181.5	12607	72809	6.8705
PSP_008266_2445	147.8	18361	25994	6.3388
PSP_008370_2355	153.6	12430	77855	8.9415
PSP_008372_2455	41.63	18769	57448	5.3486
PSP_008778_2325	160.6	19385	42313	8.6278
PSP_009086_2360	158.4	16138	38596	16.728
PSP_009112_2345	161.4	23454	37361	15.53
PSP_009604_2310	162.7	23588	17122	12.289
PSP_009664_2305	162.9	13519	38446	13.556
PSP_009713_2415	152.9	21788	4277	5.9729
PSP_010141_2360	154.6	1039	2376	4.3139
PSP_010164_2370	156	1799	5182	3.9319
PSP_010394_2405	154.6	8363	7745	5.988
PSP_010434_2500	182.6	1738	6042	5.5083
PSP_010625_2360	153.5	16260	29270	5.8181
ESP_011512_2330	149.3	3981	20875	5.665
ESP_016956_2310	156.1	25114	16369	15.6
ESP_016957_2425	144.4	26914	23239	7.3591
ESP_017112_2440	147.5	25647	38206	6.5276
ESP_017131_2485	133.5	3567	11104	7.0495
ESP_017146_2385	152	16710	28688	6.9347
ESP_017166_2465	10.52	33556	26130	6.9735
ESP_017494_2350	159.4	13269	15559	8.8639
ESP_017543_2330	159.6	12322	48302	9.3621

ESP_017632_2475	135.4	18592	22552	6.6367
ESP_018117_2345	160	3435	15855	5.2307
ESP_018125_2445	153.2	7244	30415	5.7487
ESP_018126_2445	151.3	6888	14768	7.4391
ESP_018139_2315	162.2	9365	31150	7.7005
ESP_018157_2365	156.7	19948	28681	8.6122
ESP_018158_2435	151.4	17036	26842	7.0081
ESP_018173_2385	155.3	5691	13136	4.9121
ESP_018211_2370	156.4	14887	20838	8.5332
ESP_018245_2425	151.6	18060	10804	7.4245
ESP_018259_2385	154.7	17998	10449	7.6061
ESP_018264_2375	157.1	19505	14961	14.288
ESP_018294_2365	156.9	11852	20507	14.305
ESP_018573_2415	150.4	14918	8926	5.363
ESP_018646_2440	150	13806	22497	5.6538
ESP_018746_2350	157	6215	17620	5.7097
ESP_019068_2335	156.3	11600	24514	9.3302

CHAPTER TWO

Boulder movement at high northern latitudes of Mars

Published in Orloff, T., M. Kreslavksy, E. Asphaug, and J. Korteniemi (2011), Boulder movement at high northern latitudes of Mars, J. Geophys. Res., 116, E11006, doi:10.1029/2011JE003811. Used with permission.

1.1 Abstract

We examine a narrow latitudinal band (60°N–70°N) on Mars to place constraints on the seasonally averaged velocity Q of boulder movements over patterned ground. These latitudes comprise a region of the northern lowlands where patterned ground covers nearly every surface. Here boulders meters in diameter are consistently found to be concentrated at or near the cracks that define the polygonal networks, indicating a mobilization process. Because impact craters are the source for many boulders, we can use craters and their degradation to estimate the time scales for boulder movement. We study and catalog 1018 degraded impact craters (100 m < D < 1 km) in 55 High Resolution Imaging Science Experiment (HiRISE) images. We find that crater degradation occurs on a time scale <∼1 Ma, which is too recent for melting-related mechanisms in a past, warmer epoch. Clustering of boulders occurs at a time scale of a few Ma or shorter, which means that boulders on 5–20 m diameter polygons move at seasonal velocities Q ∼1–10 mm/yr or faster.

2.1 Introduction

Patterned ground covers tens of millions of square kilometers of Mars and is found across a wide range of latitudes [Costard and Kargel, 1995; Mangold, 2005; Balme and Gallagher, 2008; Levy et al., 2009a]. The morphology of Martian patterned ground varies widely, suggesting differences in origin [Mellon, 1997; Seibert and Kargel, 2001; Morgenstern et al., 2007], age [Balme et al., 2009; Soare et al., 2008; Soare and Osinski, 2009; Gallagher et al., 2011], and type [Marchant and Head, 2007; Balme et al., 2009; Mellon et al., 2008, Lefort et al., 2009]. Latitudinal trends in patterned ground morphology allude to climatic influences in the development of certain patterned ground [Mangold, 2005; Balme and Gallagher, 2008; Levy et al., 2009a]. In this paper we focus on the northern plains between 60°N and 70°N where nearly every surface is uniformly patterned, and we examine polygonal networks where boulders tend to concentrate at or near the cracks making up the patterned ground.

Permafrost processes generate multiple types of patterned ground in cold-climate environments on Earth [e.g., Washburn, 1973; French, 1976]. Previous research of Martian patterned ground also predict formations that are due to ground-ice-related processes [e.g., Mellon, 1997; Seibert and Kargel, 2001], especially in our focus area [Mangold, 2005; Levy et al., 2009a]. Ice is known to be present on the near surface of certain regions of Mars, including our area of interest, today. Measurements from the Gamma Ray Spectrometer instrument suite onboard the Mars Odyssey mission indicate high abundances of hydrogen in the uppermost meter of the

surface at latitudes above 60°, but much lower content at lower latitudes [Boynton et al., 2002; Feldman et al., 2002; Mitrofanov et al., 2002]. This high hydrogen abundance has been interpreted as high fractions of water ice. In 2008 the Phoenix spacecraft landed on patterned ground terrain [Smith et al., 2008] within the 60°N–70°N zone and confirmed the presence of nearly pure ice within centimeters of the surface [Mellon et al., 2009a]. Models show that this ground ice is stable in the shallow subsurface at these latitudes against diffusive vapor exchange with the atmosphere [e.g., Mellon and Jakosky, 1993; Schorghofer and Aharonson, 2005].

Meter-sized and larger boulders are abundant in our study zone, and they tend to cluster [Mellon et al., 2008; Levy et al., 2008]. We start with a brief summary of the patterned ground landscape observed in the 60°N–70°N zone (Section 3), then we describe our survey of degraded craters (Section 4) and derive formal age constraints based on our survey (Section 5). In Section 6 we present our observations of boulder clustering and show that clustering is related to polygonal patterns and involve horizontal movement. We derive constraints on the time scale. The accuracy and implications of the results are discussed in the last section.

3.1 Background

3.1.1 Patterned Ground at 60°N–70°N

Patterned ground in the 60°N–70°N zone is formed on geologically rather uniform terrain, mostly the interior member of the Vastitas Borealis Formation [e.g., Tanaka et al., 2005], and on a surface, which is moderately smooth at kilometer to subkilometer scales. The smallest scale pattern is formed by polygonal networks of

cracks with average polygon diameters of 5–20 m and 0.1–1 m relief [Levy et al., 2009a; Mellon et al., 2009b]. Large-scale (~100 m) polygonal networks have been observed on Mars since the Viking era [Lucchitta, 1981; Squyres and Carr, 1986]. Increased image resolution showed these polygons have smaller polygons superimposed on them at these latitudes [Mellon et al., 2008], perhaps indicative of processes happening on different fundamental time scales. (There are also even larger polygons on Mars, which probably are not related to permafrost processes [McGill and Hills, 1992].)

Historically, efforts to understand patterned ground began on Earth, where studies show that the seasonal freeze thaw cycle plays an integral role in polygon evolution [Washburn, 1973; French, 1976, 2003; Yershov, 1998; Bockheim et al., 2007]. Physical processes responsible for pattern formation in the terrestrial permafrost regions include thermal cracking, flow of meltwater and water-saturated sediments, expansion of water when freezing, and frost heave that is due to cryosuction drawing water to the freezing front [Rempel, 2007]. Combinations of these processes in different settings form a large variety of morphologies, including ice wedge polygons [Leffingwell, 1915; Lachenbruch, 1962; Péwé, 1963; Murton and Bateman, 2007] and sorted polygons [Hallet, 1990; Francou et al., 2001]. Sorting is especially interesting because it effectively clusters pebbles, cobbles, and small boulders. On Earth, patterned ground in the permafrost environments often forms in the presence of abundant liquid water during the warm season; in particular, frost heave and sorting need saturation of the soil with meltwater.

The present climate conditions on Mars are known well enough to be sure that the seasonal freeze-thaw cycle does not operate on Mars today. Although temperatures at the surface routinely exceed 273 K at low latitudes as well as at steep slopes at high latitudes, the day-average surface temperature (which matters for seasonal thaw) is well below 273 K everywhere throughout the whole year. The Mars Climate Database (available at http://www-mars.lmd.jussieu.fr/mars/mars.html [Forget et al., 1999; Lewis et al., 1999]) contains an accurate proxy for the temperature regime of horizontal surfaces on Mars. This data set has been validated against remote sensing observations and is consistent with Phoenix in situ temperature measurements [Zent et al., 2010]. According to the climate database, the year-maximum day average temperature in the 60°N–70°N zone ranges from 223 to 234 K, with this variation mainly a function of albedo. These temperatures are too low to for seasonal thaws. A dedicated search at the Phoenix landing site confirmed the absence of any aqueous liquid phase in the soil [Stoker et al., 2010; Zent et al., 2010].

Whether and when the freeze-thaw cycle has operated on Mars in the recent geological past are interesting and important questions. Martian climate is known to change because of changes of spin obliquity and orbital parameters (astronomical forcing). Global climate models predict that the year-maximum day-average surface temperatures can reach the water melting point only if spin axis obliquity exceeds ~35° [e.g., Costard et al., 2002], which occurred for the last time about 3.1 Ma ago according to calculations by Laskar et al. [2004]. This would imply that thawing of

near surface ice has not occurred since at least ~3 Ma ago. The same conclusion can be obtained without resorting to global climate models and their associated implicit assumptions. On Mars the surface temperature is primarily controlled by direct insolation, all other factors being minor (unlike on the Earth). Presently, the maximum daily insolation at 60°S–70°S is 42% higher than that at 60°N–70°N because the southern summer is close to the perihelion and the northern summer is close to the aphelion. The present peak day average temperature at 60°S–70°S ranges from 238 to 244 K: a 42% insolation increase causes roughly a 10–15 K temperature increase.

From the known evolution of spin and orbit parameters [Laskar et al., 2004] we calculated that for the last 3 Ma the highest daily insolation at 60°N–70° N was 27% higher than the present-day peak daily insolation at 60°S–70°S. That maximum is predicted to have occurred 0.63 Ma ago, when a combination of high eccentricity, high obliquity, and northern hemisphere summer in perihelion favored high maximal daily insolation. Calculations suggest that these additional 27% did not give more than an additional 10–15 K temperature increase compared to today, and the daily average temperature at that time remained below ~255 K, still well below 273 K, the melting point of ice. In summary, it is highly improbable that seasonal thawing and related permafrost processes (like frost heaves and sorting) have occurred at 60°N–70°N (or elsewhere on Mars for that matter) for the last 3 Ma.

Polygons are often formed in frozen ground on Earth even in the absence of liquid water. In the Dry Valleys of Antarctica, at high elevations, the day-average

surface temperature never approaches the ice melting point, and macroscopic amounts of liquid water never form. There exist two types of polygons in the Dry Valleys: low-centered sand wedges [Péwé, 1959; Berg and Black, 1966] and high centered sublimation polygons [Marchant et al., 2002]. The formation of both types of polygons is initiated by thermal cracking. Sand-wedge polygons form when fine grained material fills thermal contraction cracks and prevents crack closure during thermal expansion. Sublimation polygons form by increased sublimation at the thermal contraction cracks, exposing ice that underlies near-surface sediments. Mellon et al. [2008] suggests that Martian high latitude polygons are of the sand-wedge variety while Levy et al. [2009b] hypothesize that they are sublimation polygons. Both of these polygon types indeed share morphological similarities to Martian low-centered polygons and high-centered polygons in this region [Levy et al., 2009a].

3.1.2. Impact Craters

Craters larger than 2–3 km in the study area form a population with a well-defined early Amazonian crater retention age [e.g., Tanaka et al., 2003]. In contrast to these large craters, very few relatively unmodified craters smaller than ~1 km are found in the high latitudes of Mars in comparison with what would be expected for the early Amazonian age. There are, however, many smooth circular features (Figure 1) in the 0.1–1 km size range. These circular features were previously described by

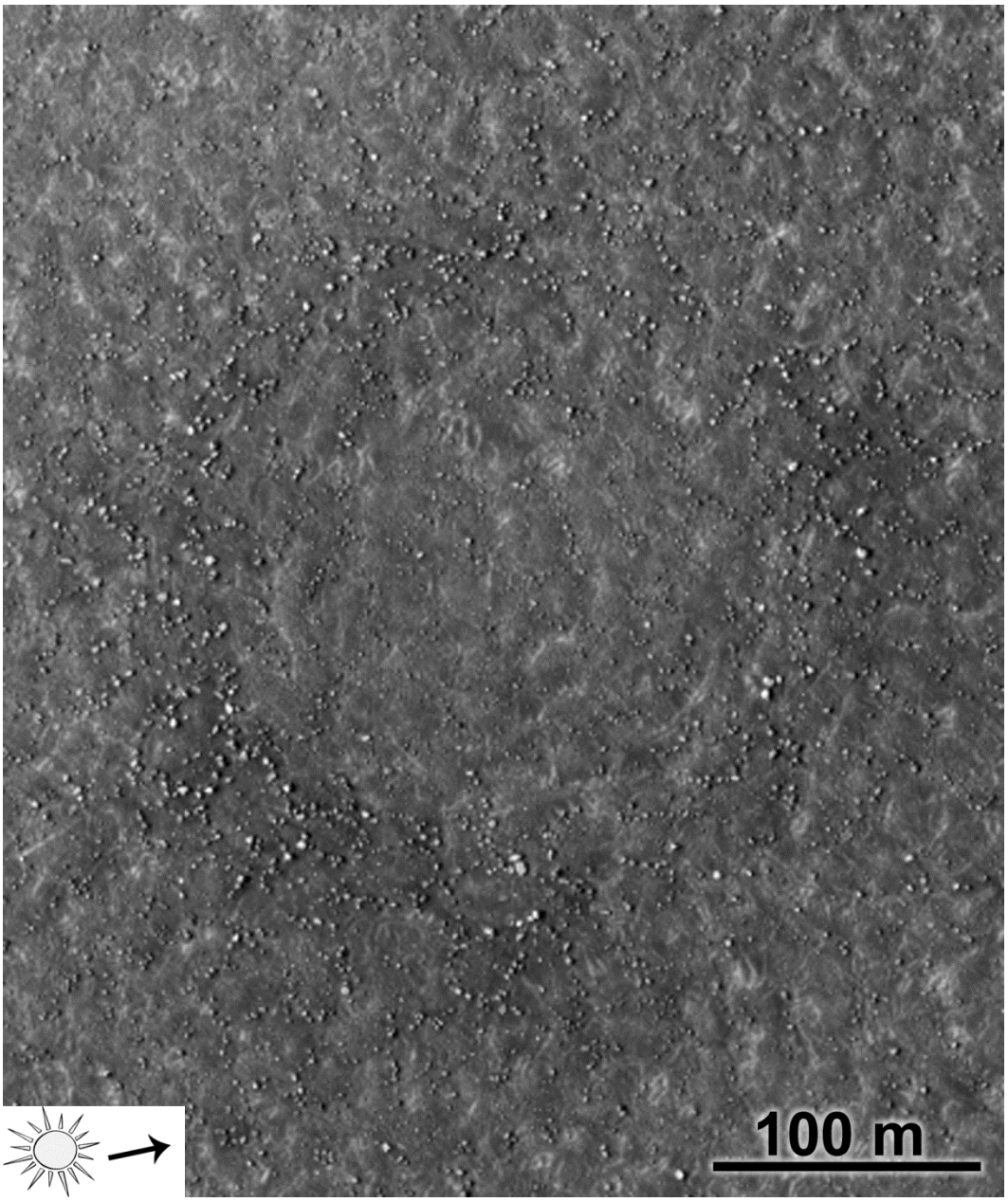

Figure 1. Ring of boulders outline former high-latitude crater (66.6°N, 320.1°E; illumination from the left; HiRISE image PSP_008219_2470). A crater is barely visible at the surface with only a remnant of a circular feature apparent. The boulder number density and size decrease outward from the crater.

Malin and Edgett [2001] and interpreted as heavily degraded impact craters. They were studied by Kostama et al. [2006], who supported their impact origin, but noted that some of these circular features may actually be some other degraded geologic features rather than primary impact craters. They found a break in the slope of the size-frequency distribution (SFD) of these features and interpreted it as the onset of nonimpact circular features smaller than ~250 m. They also found that the number of circular features varied greatly regionally, suggesting different retention ages at different locales.

These circular features span a wide range of topographic expressions ranging from smooth bowl-like depressions, to vague arcuate shapes, to relatively flat circular landforms that are apparent because of circular arrangements of enhancement of boulder number density (see Figure 1 for an example). They often are covered with the same type of patterned ground as the local terrain; orientation of the pattern-forming lineaments often follows the circular shape of these features; sometimes this orientation is their only apparent manifestation. Sometimes these circular features are slightly elevated above the local topography. A small percentage maintain the bowl-shaped depression indicative of the predecessor crater. In this case the boulders surrounding the circular feature indicate the extent of a proximal ejecta blanket surrounding the original crater.

The boulder distributions around these circular features resemble boulder distributions around Martian equatorial craters (Figure 2) and around fresh craters on the Moon [e.g., Bart and Melosh, 2010]. Boulders decrease in size and number with

distance from the rims of these circular features and often show local radially shaped enhancements in density, indicating crater-ejecta-like patterns. There is an observed continuous morphological sequence from such features with prominent central depressions to features without noticeable topography but with the same boulder pattern: this strongly suggests impact origin for the latter, more degraded landforms. The interiors usually display the polygonal fractures representative of local surroundings, while those most heavily degraded are almost indistinguishable from the surrounding terrain.

The size-frequency statistics of crater formation and retention support our premise that most of these circular features in the diameter range 0.1–1 km are degraded impact craters. First, the interior member of the Vastitas Borealis Formation that dominates our study area is old. Based on the density of large (D > 5 km) craters reported by Tanaka et al. [2003], its model age according to Neukum chronology [Ivanov, 2001] is 3.5 Ga, early Amazonian age, very close to the Hesperian boundary. The generally accepted cratering rate requires that old terrains have large populations of smaller craters. Second, according to Kostama et al. [2006], the SFD of these crater-like features approaches the Vastitas Borealis Formation age isochron for D = 1–2 km. In other words, the density of 1–2 km sized features is the same as the density of craters of these sizes expected to have formed over the duration this terrain has been exposed. At smaller diameters (D < 1 km) there is clear deflection from the isochron suggesting crater removal [Kostama et al., 2006], but the morphology is similar, suggesting that the features that are observed are the degraded crater

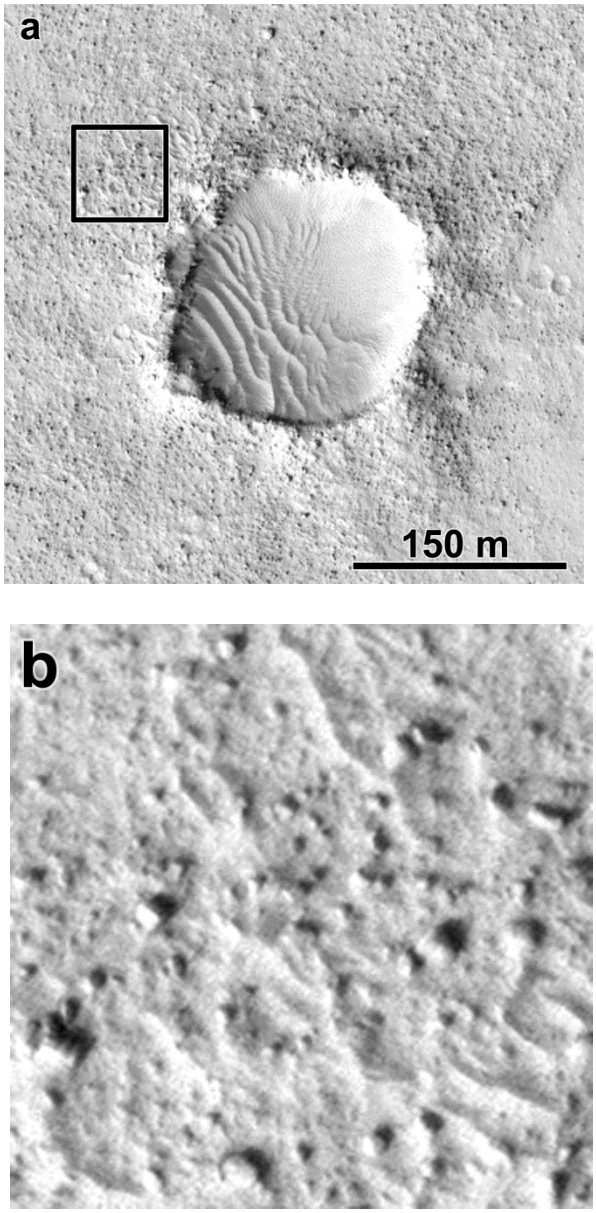

Figure 2. Equatorial crater with boulders: (a) A relatively fresh, equatorial crater in Elysium Planitia with associated boulders (9.7°N, 174.7°W; illumination is from the lower left; HiRISE image PSP_003623_1900). The boulder number density and size decrease outward from the crater. (b) Close up of boulders around crater in portion of Figure 2a outlined in the box.

remnants. Finally, the associated boulder patterns described above also suggest impact origins at least for those numerous features that have boulder fields associated with them.

For formal age estimates we assume that all circular shaped landforms in high latitudes in the size range 0.1–1 km diameter represent degraded craters, and call them “craters” for simplicity. Because we cannot exclude that some of them are features of different origin, our formal age estimates derived from crater densities should be considered as limits: actual retention ages are not older than these estimates.

3.1.3. Boulders

Boulders have been observed at the landing sites of all landers and rovers that have been sent to Mars, and they can be a potential hazard for future missions seeking to safely land and operate on the surface [Crumpler, 1996; Golombek et al., 2003; Marlow et al., 2006]. Boulders also represent potential sampling sources for observations such as those done by Spirit and Opportunity [McSween et al., 2008]. Despite the importance of boulders in Mars exploration, only a few studies [Sizemore and Mellon, 2006; Golombek et al., 2008; Sizemore et al., 2009] focus on the significance of boulders on the near surface.

Systematic study of individual boulders from orbit was made possible when the High Resolution Imaging Science Experiment (HiRISE) began imaging the surface of Mars at submeter resolutions in 2006, allowing a more detailed analysis than was previously possible [McEwen et al., 2007]. Figures 3 and 4 show meter-

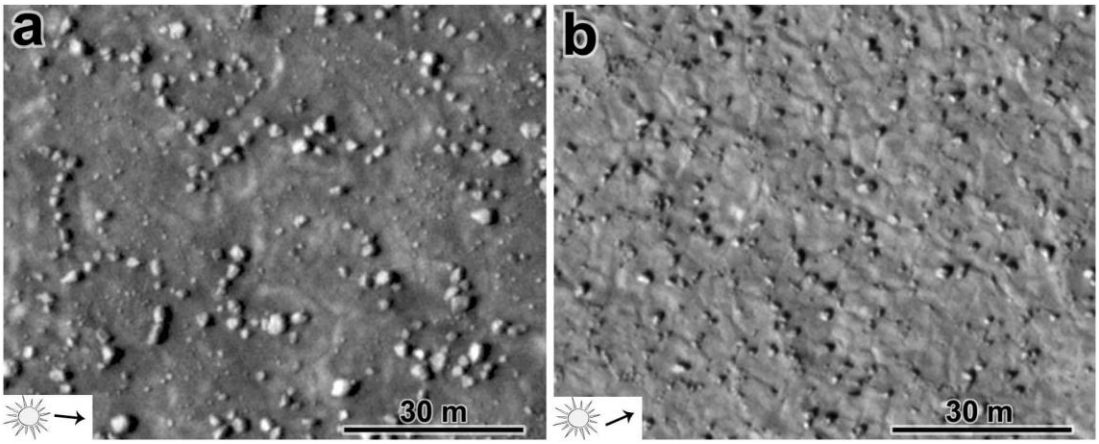

Figure 3. Boulders cluster on patterned ground in edges. (a) Boulders (bright faces with shadows) cluster in polygonal edges (66.6°N, 320.1°E; illumination from the left; HiRISE image PSP_008219_2470). (b) Boulders cluster in the cracks outlining polygons (68.4°N, 175.4°E; illumination from the left; HiRISE image PSP_001341_2485). Each image is 90 m across; north is to the top.

scale boulders as brightly lit blocks casting shadows on the surface around them. Boulders of different sizes are often found at the same locales. Boulders can appear both angular and round. Large numbers of boulders populate patterned ground terrains at high northern latitudes on Mars.

Golombek et al. [2008] analyzed boulder distributions on patterned ground terrain and noted a connection between impact crater proximity and boulder number density. As we described above (Figure 1), some boulders form distinctive fields around craters and are linked to them: they could form as ejecta deposits or as fractured rock within the ground later exposed during crater degradation. There are also many boulders not obviously related to any crater. They could be produced by totally obliterated craters or could be formed by other geological processes. For example, weathering and erosion of coherent rock through a variety of means will produce boulders.

We estimated the total volume of crater-associated boulders for the crater in Figure 1 and a few other similar craters with D = 100–200 m. To do this we applied an automated boulder identification algorithm similar to that used by Golombek et al. [2008]. We obtained boulder sizes and assumed that boulders are ellipsoids with axes ratios of 1: √2: 2, the shortest dimension being vertical, based on block fragmentation statistics [Fujiwara et al., 1989]. These estimates showed that the total volume of boulders makes approximately 1%–3% of the presumed volume of the original crater. The latter was calculated as $0.07D^3$, the volume of paraboloid-shaped bowl with diameter D and 35° steep slopes at the edge. Because of possible bias in boulder size

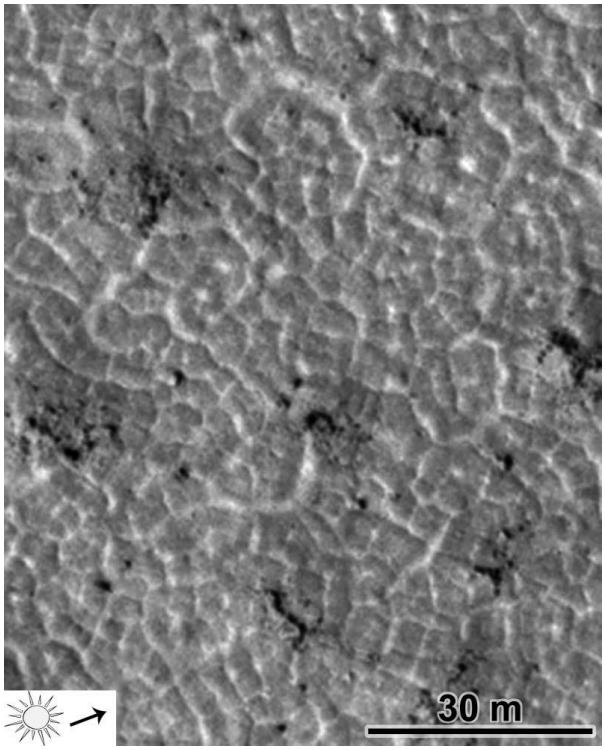

Figure 4. Boulders cluster on patterned ground in rubble piles. Boulders cluster in rubble piles defining polygonal interiors (69.8°N, 85.8°E; illumination is from the left; HiRISE image TRA_000856_2500). Image is 90 m top to bottom; north is to the top.

retrieval with the automated algorithm and uncertainty of the assumptions about shapes of boulders and craters, these estimates are accurate within a factor of 2 or 3. For two fresh lunar craters in the same size range, the size frequency distribution of ejected boulders, published by Bart and Melosh [2010], yield 1.4% and 4.8% under the same assumptions about the boulder shape and crater volume. Thus, we see that the total volume of boulders associated with craters has the same order of magnitude as the volume of ejected boulders on fresh impact craters.

Boulders on patterned ground terrain tend to cluster [Mellon et al. 2008; Levy et al., 2008, 2010]. Assuming an initially random distribution, one corresponding for instance to unpatterned lunar craters [Bart and Melosh, 2010], a mechanism or set of processes is required to remove boulders from their initial positions and toward their observed positions [Mellon et al., 2008]. Mellon et al. [2008] and Levy et al. [2010] propose possible mechanisms including (1) gravitational or aeolian sorting and slumping [Mellon et al., 2008], (2) surface creep [Mellon et al., 2008], (3) a complex dry cryoturbation process cycling boulders through troughs to polygon interiors [Mellon et al., 2008], or (4) gravitational sliding, rolling, and slumping due to oversteepening of polygon troughs by enhanced sublimation of buried ice along polygon margins [Levy et al., 2010]. Here we put the first dynamical constraints on the process of boulder movement and its time scale.

4.1. Investigation

We examine impact crater structures and boulder distributions between 60°N and 70°N. We chose this region for its relatively uniform patterned ground coverage

and geology as compared with more complex regions in lower latitudes and the southern hemisphere. In order to obtain a sample set of uniform high quality and to see the surface in detail, we selected only 25 cm/pixel HiRISE images with little to no seasonal frost (areocentric longitude of the Sun Ls between 30° and 175°). Since our interest is the typical behavior of a widely distributed surface unit, some images were omitted because of their proximity to anomalous features which may affect the development of surrounding polygons typical of the latitude band or the formation and evolution of impact craters. Such anomalies include interiors and ejecta fields of large impact craters (D > 5 km); pitted, fractured, and eroded regions often associated with nearby volcanic or tectonic features; and topographic slopes related to mesas, knobs, and scarps. In total, we selected 55 images in the region that fit this profile (Table 1, Figure 5); their total area is ~3200 km2. It should be noted that their spatial distribution is neither uniform nor random and clusters do occur in places, most notably near the Phoenix landing site. Thus, the results of statistical inferences should be treated with proper caution. We believe, however, that these images are a representative sample of the typical terrain in our study zone.

Within the resulting set of images we cataloged all circular features (see Table 1) in a diameter range of 0.1–1 km. Larger features are infrequent and cannot contribute significantly to statistical inferences; also they often are cut by image edges, which make diameter measurements less reliable. Smaller features are also

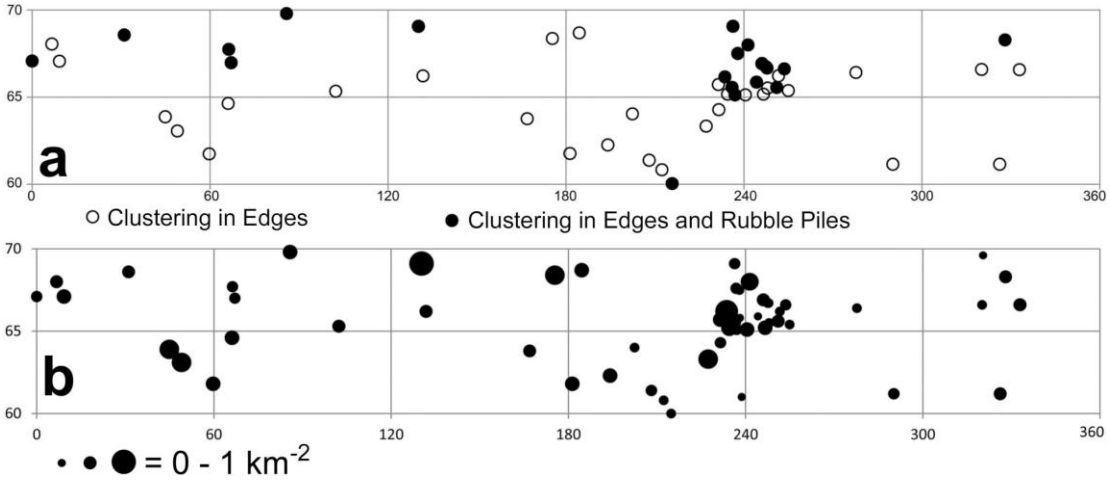

Figure 5. Image location information. (a) Circles show image locations within the 60°N–70°N latitude zone. Open circles show images where clustering occurs in polygon edges only. Solid circles show images where clustering occurs in both polygon edges and in rubble piles. Images without craters are not included. (b) Circles show the same image locations within the 60°N–70°N latitude zone. The sizes of the circles correspond to the number density of craters (0.1 km < D < 1 km) in the image that ranges linearly from 0 to 1 craters km−2.

infrequent, and they show a wider range of morphologies. We excluded them from consideration to ensure that we have uniform feature identification criteria. Our survey produced a catalog of 1018 craters. For each crater we kept note of the following parameters:

1. crater diameter,

2. the presence of boulders around the crater,

3. the clustering of boulders in the immediate vicinity of the crater.

Ambiguity in crater rim location may cause, in certain cases, significant error in measuring the crater diameter. The presence of boulders is very well seen in HiRISE images because of their bright sunlit faces and dark shadows. Clustering of boulders is determined and quantified through a visual assessment of areas around each crater extending for five crater radii.

We detect two types of boulder clustering: polygon edges (Figure 3) and rubble piles (Figure 4). Clustering in polygon edges is determined by examining boulders with diameters of <3 m for consistent placement in polygon edges. Polygon edges appear as slightly shaded linear features in HiRISE imagery. If more than ~25% of the boulders align with these linear features we consider the population clustered in polygon edges. The rubble pile detections are very reliable in that the compact clusters of boulders are surrounded by relatively boulder-free terrain. If we observe neither of these clustering types we consider boulders unclustered. It is interesting that except in one case we do not find rubble piles south of 65°N. We describe boulder clustering in detail below, in Section 6.

All craters in our catalog are heavily degraded. We attempted to quantify the degradation state of craters on the basis of apparent topography (elevated ring and central bowl) in HiRISE images with the goal of developing a relative aging classification. Because of the uniformly high degradation state of all craters in our catalog, we found objective, quantitative classification infeasible. Factors affecting detectability of apparent topography include the presence of contrasting details, patches of different albedo, illumination conditions, abundance of boulders, transparency of the atmosphere, and intensity of the scattered light illumination. It is important, however, that in our set of craters, we do not have any example of a relatively fresh crater with crisp rims and a deep bowl-shaped cavity.

5.1. Crater Distribution

Figure 6 shows two log-log plots of the crater SFD for 1018 impact crater features of our study. Figure 6a shows a cumulative SFD plot, and Figure 6b shows a log incremental SFD plot. For comparison, the plots show Neukum production function (NPF) isochrons [Ivanov, 2001] separating the Martian chronostratigraphic periods (as defined by Tanaka [1986]). Note that the plotted isochrones in Figure 6a are corrected to account for the exclusion of craters larger than 1 km from our sample; in other words the quantity plotted is the density of craters in size interval from D to 1 km, $N(D) - N(1\ km)$, rather than the usual N(D), the density of craters larger than D.

It is clearly seen that the SFDs are shallower (less steep) than the NPFs, at least for craters smaller than D ~500 m. This means that there are processes that

obliterate craters preferentially at smaller sizes. The crater population is not an accumulation population because craters are removed, and it does not have a single well-defined age. If we consider the density of craters within a certain size range, we can use the production rate for craters in this range and obtain a formal crater retention age of this subpopulation; this age can be interpreted as a characteristic time scale of obliteration of craters of given size. For example, crater densities for craters with diameters between D = 100–200 m yield retention ages of ~100 Ma (crater production function from Ivanov [2001] is used). Craters of diameter D = 200–300 m yield retention ages of ~900 Ma. For the largest craters, D = 500 m–1 km, the formal 90% confidence interval for retention age is 2.6–3.3 Ga, in the early Amazonian, as also seen from the isochrons in Figure 6. This retention age for the largest craters is somewhat younger than the age of the Vastitas Borealis Formation, the "geological" age of the northern lowlands, obtained from larger (D > 5 km) craters [Tanaka et al., 2003]. In their survey, Kostama et al. [2006] showed that for even larger craters (1–2 km) the SFD approaches the Vastitas Borealis isochron.

Crater densities within each image are scattered much more widely than can be expected from random fluctuations (Table 1). This suggests that crater obliteration rates differ geographically, e.g., due to local resurfacing. Inclusion of circular features of nonimpact origin and clusters of secondary craters can also contribute to this variation. This wide scattering means that the formal retention ages computed above

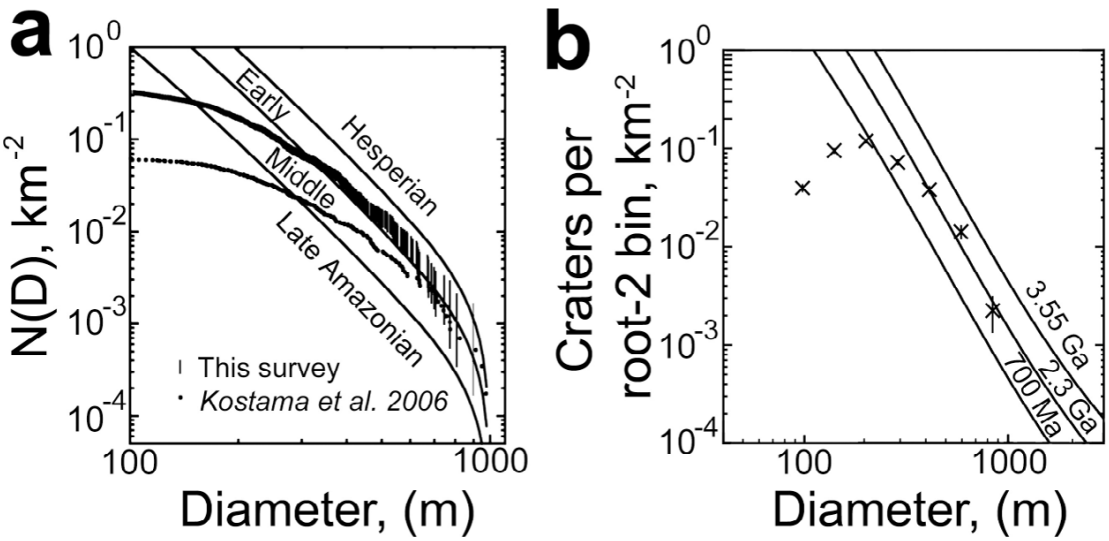

Figure 6. Size-frequency distributions of crater-like features. (a) A cumulative size-frequency distribution. Vertical lines indicate our data; each line shows a formal 90% confidence interval for densities of craters not smaller than given. Dots indicate a subset of data from Kostama et al. [2006] for 60–70 latitude and D < 1 km. Solid lines show impact crater production isochrones dividing the periods of geological history of Mars. The isochrones are computed using the Neukum-Hartmann production function recalculated to Mars [Ivanov, 2001]; the definition of periods is according to Tanaka [1986]. The drop down of the isochrones in the lower right corner is due to the removal of craters larger than 1 km from the production function. (b) A log-incremental size-frequency distribution. We plot our data as crosses with computed error bars showing a 1 sigma error. Solid lines show impact crater production isochrones for 700 Ma, 2.3 Ga, and 3.55 Ga in Mars past. The isochrones are computed using the Neukum-Hartmann production function recalculated to Mars [Ivanov, 2001].

give an order-of-magnitude crater obliteration time scale, but not a universal single rate.

For comparison, in Figure 6a we also plotted the SFD of a subset of features identified by Kostama et al. [2006]; only circular features between 100 m and 1 km and between 60°N and 70°N were included, a total of 355 features. For the largest features (700 m–1 km) the distributions from both surveys coincide within expected random fluctuations. The rollover of the SFD from the Kostama et al. [2006] survey is noticeably stronger. Data from Kostama et al. [2006] show an order-of-magnitude fewer craters at small diameters than our findings. The difference is too high to be explained by random fluctuations. The most probable reason for this discrepancy is that our higher-resolution imagery allows for the identification of more features. Our data do not confirm the break in the SFD slope at D ~250 m, as noted by Kostama et al. [2006].

For the given area (~3200 km2), for craters with diameter D > 100 m, the NPF gives the mean cratering rate of 1 crater per ~0.2 Ma. At this cratering rate, the youngest crater is younger than ~0.8 Ma (90% confidence). Since all craters in the study area are covered by the polygonal pattern and heavily degraded, this age (0.8 Ma) gives an upper limit for the time scale of pattern formation and crater degradation. This is a robust constraint, because it depends on the fact that there are no fresh craters in the study area and does not depend on subjective identification of subtle circular features and measurements of their size.

All ages considered above are formally obtained by making two assumptions, (1) that cratering is random, and (2) that cratering follows a commonly used production function. To assess the reliability of obtained age constraints we need to assess these two assumptions. The contribution of secondary craters to our observed population is the most important factor to examine when considering whether our first assumption of spatial randomness holds. Several researchers [e.g., Bierhaus et al., 2005; McEwen and Bierhaus, 2006; Zahnle et al., 2008] argue that the crater population is heavily contaminated with secondaries, which compromises age estimates. On the other hand, quantitative analysis of this problem by Werner et al. [2009] shows that our younger ages (age of the youngest crater in the population, Ma time scale) are safe, while for the early Amazonian ages the expected proportion of the secondaries among 0.5–1 km craters can be noticeable. The secondaries are effectively included in the production function [see discussion by Hartmann [2007]) and do not produce a systematical statistical bias in age estimates, but they do violate the assumption of randomness and the formal confidence interval should be widened. Nevertheless, the early Amazonian age of the 0.5–1 km crater subpopulation is probably a reliable inference, especially given consistency between the two surveys and sampling of all longitudes rather than a single region.

The validity of the second assumption is dependent on whether the cratering rate is well understood. The coincidence between the present-day observed rate of formation of 10 m size craters and the NPF [Daubar et al., 2010] gives the impression that we know the rate rather well. However, we have to admit that the absolute

cratering rate is measured at only a 10 year time scale and inferred for a 100 Ma time scale; thus, the assumed cratering rate at 1 Ma time scale is actually an interpolation over a very wide span and should be considered with caution.

6.1. Boulder Clustering Time Scale

Boulders are present around each impact crater feature in our catalog, suggesting the ubiquitous presence of boulders in our study region. Although the boulder sizes were not measured, Figures 3a, 3b, and 4 show that sizes vary within a given scene and regionally. Boulder number density also varies widely. Often high concentrations of boulders occur in proximity to impact craters. Their association suggests a genetic relationship between the boulders and the impact crater. Often the location of degraded craters is noticeable only because of circular fields of boulders. This indicates that the time scale of crater obliteration is shorter than the time scale of boulder destruction.

Boulders on patterned ground terrain cluster nearly everywhere, appearing ordered relative to random or landform-related distributions. As mentioned earlier, two kinds of boulder clustering are seen: (1) polygon edges (Figures 3a and 3b) and (2) rubble piles (Figure 4). Boulder clustering on polygon edges appears as chains of boulders outlining polygonal shapes (Figure 3a) or as individual boulders specifically on cracks (Figure 3b). These boulders touch but do not stack up on one another and often are strung together for tens of meters. Although clustering toward polygon edges is observed in each image, not all boulders appear clustered. A Low boulder number density is associated with the lack of clustering in many locales.

Rubble piles are groups of boulders clustered atop polygons. These rubble piles are separated by tens of meters of relatively boulder-free polygons. Malin and Edgett [2001] called this the "basketball terrain," named for the stippled appearance of albedo markings in Mars Orbiter Camera (MOC) imagery (4.8 m/pixel), which Mellon et al. [2008] showed using HiRISE imagery as shadows caused by groupings of boulders on the surface. Locations for each type are shown in Figure 5; see also Table 1. Note that edge boulder clustering occurs in all images surveyed, while rubble piles are found only in some of the images. Rubble piles and edge clustering coexist: boulders forming piles tend to prefer polygon-forming cracks (Figure 4). Figure 5 shows that rubble piles prefer higher latitudes in the surveyed latitude zone.

Only seven craters in our study present ambiguous cases: there are some (not many) boulders there, but no clustering is apparent. A few of these look relatively weakly degraded. Although it is possible that the boulder number density is just too low to make clustering apparent, it is also possible that boulders have not had time to cluster. For cratering according to the NPF, the seventh youngest crater in the surveyed area is younger than 2.4 Ma. This gives a conservative upper limit for the time scale of boulder clustering; however we cannot rule out that clustering happens more rapidly. Assuming random initial distribution, the average distance an average boulder in a cluster moves to create the observed patterning is comparable to the polygon size. Boulders that move approximately a polygon radius would then have seasonally averaged velocities Q ~1–10 mm/yr if clustering occurs at the 2.4 Ma upper limit time scales and more rapidly if the crater age is younger. These being

seasonal averages, it is quite likely that this movement is not gradual throughout the season, but has an active phase in which boulder movement primarily accrues.

7.1 Discussion

The preponderance of dense boulder fields associated with almost-obliterated craters provides us with insight into the surface mechanisms acting on Mars in the past million years. Only certain processes can significantly modify craters and leave much smaller objects (boulders) unaltered. We consider three end-member types of crater degradation mechanisms: deflation, deposition, and reworking.

1. Deflation. A process removes the surface layer, so the present surface was below the level of the surface when the crater formed. Intensive wind erosion of the Northern Lowlands was predicted by Armstrong and Leovy [2005] and evidence for very recent deflation in northern lowlands has been found by Meresse et al. [2006], Black and Stewart [2008] and Kadish et al. [2009]. This mechanism could explain generally positive topography associated with degraded craters: boulders and large clasts produced by impact armor the surface and reduce deflation. It is difficult, however, to reconcile quick degradation of craters (which requires at least 0.1 mm/yr deflation rate) with preservation of meter-scale boulders for crater retention ages of hundreds of Ma. No morphological features diagnostic of intensive wind erosion are observed. In addition, aeolian deflation is not strictly concentrated in the high-latitude areas, and this mechanism does not explain strongly zonal occurrences of the specific crater degradation morphologies. Thus, deflation has significant problems.

2. Deposition. A new surface layer is added, so the present surface is above the original level of the surface when the crater formed. Deposition of icy mantles at high latitudes was proposed by Kreslavsky and Head [2002] and Head et al. [2003] from geomorphological observations and by Mischna et al. [2003] and Levrard et al. [2004] based on climate modeling. Generally positive topography of degraded craters in this type of mechanism can be explained by preferential deposition of the icy mantles in local lows (including crater interiors and rough ejecta), which is supported by other morphological observations [Kreslavsky and Head, 2002, 2006]. The predicted age of mantles (0.5–3 Ma from the known history of spin axis obliquity) is generally consistent with the degradation time scale constraints that we have obtained here.

The main problem of the deposition model is how to explain that the boulders produced by impacts are not buried but persist at the surface. A "brazil nut" mechanism of size sorting potentially solves this problem [Williams, 1976; Rosato et al., 1987; Jullien and Meakin, 1990, 1992]. This mechanism predicts that smaller particles displace larger ones systematically toward the surface since they more easily fill in gaps created during fluctuations such as vibration in granular media. Still, it should not be taken for granted that such an active granular-mechanical mechanism is actually effective in the Martian regolith environment; it could be hindered significantly by ice cementation or higher boulder density in comparison to icy matrix.

3. In-place reworking, in which no global addition or removal of material occurs and the mean surface level is the same as it was at the moment of impact. In this kind of mechanisms the material locally moves downhill to reduce crater rims and fill crater cavities. Patterned ground formation processes are candidates for material mobilization agents. In-place reworking is unable to explain positive topography of the degraded craters: mechanisms of this kind conserve the total cavity volume of the original crater. This serious problem is difficult to avoid. Without the freeze thaw cycle the permafrost processes seem too slow to remove a significant part of 100 m crater topography in a 1 Ma time scale. Finally, except for boulder clustering, few morphological observations indicate horizontal movement of the surface material.

In summary, among considered end-members, none appear able to reconcile preservation of boulders and degradation of craters in a simple and straightforward way. It is interesting that boulders in some hyperarid environments on Earth also show evidence of extreme preservation over their surroundings [Matmon et al., 2009; Placzek et al., 2010]. For example, Placzek et al. [2010] measured cosmogenic nuclides in samples from the Atacama Desert and showed that in the most arid regions of the Atacama Desert boulders have exposure ages of 1.6–2.5 Ma, while bedrock and soil samples from the same locale have exposure ages between 0.6 and 1.2 Ma. This means that the boulders remain exposed longer than the surfaces they overlie. The mechanism for this effect on Earth also remains poorly understood, but

Placzek et al. [2010] suggest that in arid regimes boulders experience minimal erosion and may not degrade with the surrounding landscape.

Boulders on patterned ground in the study area show direct evidence of clustering. Boulders associated with degraded impact craters were probably created by impacts and not clustered initially; their clustering requires significant horizontal movement. The mechanism of such movement is also unclear. Our estimates show that this movement occurred recently, we discussed in Section 3.1, an active freeze-thaw cycle cannot have operated on Mars for the last 3 Ma. Longer ago in Martian history, numerous periods of very high obliquity (above 40°) [Laskar et al., 2004] would have made the freeze-thaw cycle at high latitudes possible [e.g., Costard et al., 2002], and a number of observations suggest that it indeed occurred, as discussed by Kreslavsky et al. [2008].

We cannot exclude that our estimates based on crateringrates are inaccurate by a factor of 3 or so and that reworking occurred in the more distant past. For instance, the most recent episode of intensive boulder movement could have occurred ~7.7 Ma ago, if our age estimate is 3 times too young; this is a time when the spin-orbit configuration was favorable to freeze-thaw. During a few thousand years long period the summer day-average temperature at high northern latitudes certainly exceeded 273 K. However, even during periods of freeze-thaw cycling, the particular mechanism of boulder movement is not obvious: Boulder size exceeds the thickness of the thawing layer; thawing beneath boulders probably does not occur; and meter-

sized boulders could not be entrained in permafrost sorting and convective motion. Some sort of indirect mechanism is needed.

Such old ages of boulder clustering events does not look very probable, however, at least for clustering at polygon edges. First, our analysis of possible biases in Section 5 showed that the actual ages are probably younger, not older, than our formal estimates. Second, we see that boulders tend to cluster near very small cracks that form the latest generation of polygons. Given that craters tens of meters in diameter are obliterated extremely quickly, at a 10 s ka time scale [Kreslavsky et al., 2010] and that the youngest craters in our studied population are uniformly covered with these polygonal cracks, it is reasonable to anticipate that these small cracks are very young and that boulder movement toward them occurred recently. Therefore it is important to consider possible mechanisms of boulder movement, at the rates considered here, that do not involve the freeze-thaw cycle and could operate in the past ~1 Ma.

In section 3.3 we discussed several mechanisms for boulder clustering. We find that aeolian sorting and slumping [Mellon et al., 2008] likely does not cluster boulders because of the lack of ventifacts around boulders. We cannot exclude gravitational sorting or surface creep [Mellon et al., 2008] as possible clustering mechanisms, processes that might apply similarly to boulder sorting in the Dry Valleys. Levy et al. [2010] suggested that at some stage of evolution the sublimation polygons attain significantly elevated centers, which cause boulders and smaller fragments to creep downhill toward polygon margins, which in turn favor sublimation

in the polygon centers and then lead to the much flatter topography seen today. This mechanism implicitly assumes the formation of recent icy mantles, in line with the works of Head et al. [2003], Levrard et al. [2004], and others; otherwise it is difficult to explain how material capable of quick sublimation survived until recently. The problem with this explanation is that the formation of recent icy mantles requires an additional explanation of how big dense boulders are not buried, but rather sit on top of freshly deposited mantles.

There are several specifically Martian factors that might in principle be related to boulder movement: (1) Tiny amount of brines can form in summer [Hecht et al., 2009], and frequent phase transitions may cause phenomena that are different from terrestrial frost heave, but have yet to be characterized, which do not require saturation of soil with water. (2) Boulders affect the depth of the ice table in the shallow subsurface [Sizemore et al., 2009]. (3) Deposition and sublimation of a rather massive seasonal CO2 frost layer occur every year at the high latitudes of our study region. However, at this point we cannot propose a scenario that fully explains all aspects of the boulder movement process.

8.1. Conclusions

We find that significant degradation of 0.1–1 km craters between 60°N and 70°N occurs very quickly (or occurred recently), at a time scale shorter than 1 Ma. Boulder clustering occurs at a time scale of a few Ma or significantly shorter. Boulders 1–10 m in diameter therefore migrate with a seasonally averaged velocity of at least ∼1–10 mm/yr or faster. Many craters formerly in patterned ground terrain are

now indiscernible except as rings of boulders, implying that crater obliteration occurs faster than boulder destruction. The complete degradation of ~100 m craters occurs on the order of 100 Ma; this can vary regionally.

This initial study of boulder movement in the high northern latitudes of Mars shows how quantitative studies of the evolution of boulder distributions on patterned ground terrain can lead to constraints on the rates of boulder clustering. By extension our study has implications for how boulders and geomorphic landforms on the Martian surface interact. While the mechanism for boulder movement remains enigmatic, we have constructed a first-order constraint on the dynamics.

Acknowledgments.

Research by T.O., M.K. and E.A. was supported by NASA Mars Fundamental Research Program award NNX08AT13G. M.K. was also supported by NASA Mars Data Analysis award NNX08AL07G. Work by J. K. was supported by NASA Mars Fundamental Research Program award NNX07AU77G. We would also like to thank Richard Soare and two other anonymous reviewers for their meaningful comments that greatly enhanced the quality of the manuscript.

Table 1 Details on HiRISE images used in the survey.

HiRISE Image Information					
Image I.D.	Latitude (°N)	Longitude (°E)	# of Circular Features	Image Area (km^2)	Clustering Configuration
ESP_016306_2410	60.8	212.3	25	195.1	Edges
ESP_016483_2420	61.8	59.7	32	78.5	Edges
ESP_016526_2415	61.2	326.2	22	59.8	Edges
ESP_017112_2440	63.8	166.9	68	180.5	Edges
ESP_017131_2485	68.0	6.7	45	140.8	Edges
ESP_017166_2465	66.2	131.8	34	100.8	Edges
ESP_017632_2475	67.1	9.2	100	200.4	Edges
ESP_017835_2435	63.3	227.3	62	77.6	Edges
ESP_018125_2445	64.3	231.5	14	61.5	Edges
ESP_018126_2445	64.0	202.4	10	59.7	Edges
ESP_018136_2415	61.2	290.2	13	59.0	Edges
ESP_018158_2435	63.1	49.0	46	59.6	Edges
ESP_018245_2425	62.3	194.1	19	39.9	Edges
ESP_018573_2415	61	238.7	0	23.3	
ESP_018646_2440	63.9	44.9	18	24.0	Edges
PSP_001341_2485	68.4	175.4	5	6.4	Edges
PSP_001345_2480	67.7	66.3	3	13.7	Rubble Piles and Edges
PSP_001375_2485	68.3	328.0	2	6.4	Rubble Piles and Edges
PSP_001477_2470	67.0	67.1	8	28.1	Rubble Piles and Edges
PSP_001497_2480	68.0	241.4	18	28.5	Rubble Piles and Edges
PSP_001520_2470	66.6	332.9	3	10.0	Edges
PSP_001523_2465	66.2	251.6	4	39.6	Edges
PSP_001565_2490	68.7	184.5	5	10.2	Edges
PSP_001588_2465	66.4	277.7	1	6.4	Edges
PSP_001655_2460	65.6	251.0	14	35.4	Rubble Piles and Edges
PSP_001663_2490	68.6	31.1	4	12.9	Rubble Piles and Edges

PSP_001669_2460	65.7	231.4	18	38.2	Edges
PSP_001682_2465	66.2	233.6	36	35.0	Rubble Piles and Edges
PSP_001695_2455	65.1	240.5	15	35.6	Edges
PSP_001708_2455	65.2	246.6	23	48.6	Edges
PSP_001721_2460	65.5	248.0	6	40.5	Edges
PSP_001734_2470	66.6	253.6	10	35.7	Rubble Piles and Edges
PSP_001748_2460	65.6	236.0	16	37.0	Rubble Piles and Edges
PSP_001774_2460	65.9	244.2	2	35.2	Rubble Piles and Edges
PSP_001801_2455	65.2	234.5	31	54.6	Edges
PSP_001813_2455	65.4	254.9	5	44.3	Edges
PSP_001814_2455	65.1	237.0	9	42.3	Rubble Piles and Edges
PSP_001827_2460	65.8	238.1	0	3.7	
PSP_001932_2470	66.7	247.8	3	25.3	Rubble Piles and Edges
PSP_002064_2470	66.9	246.1	16	59.8	Edges
PSP_002130_2470	66.7	247.5	18	148.3	Edges
PSP_002183_2495	69.1	236.3	4	20.0	Rubble Piles and Edges
PSP_002317_2420	61.8	181.3	25	53.6	Edges
PSP_006930_2480	67.6	236.8	23	119.6	Rubble Piles and Edges
PSP_007721_2480	67.5	237.9	28	199.8	Edges
PSP_008219_2470	66.6	320.1	15	120.7	Edges
PSP_008372_2455	65.3	102.3	60	200.8	Edges
PSP_009304_2405	60.0	214.8	2	19.6	Rubble Piles and Edges
PSP_009461_2470	66.9	246.0	22	59.2	Rubble Piles and Edges
PSP_009713_2415	61.4	208.1	11	58.3	Edges
PSP_010061_2450	64.6	66.1	2	4.0	Edges
PSP_010434_2500	69.6	320.4	0	4.3	
TRA_000828_2495	69.1	130.3	23	20.1	Rubble Piles and

					Edges
TRA_000846_2475	67.1	0.0	4	19.9	Rubble Piles and Edges
TRA_000856_2500	69.8	85.8	16	39.4	Rubble Piles and Edges

References

Armstrong, J.C., and C.B. Leovy (2005), Long term wind erosion on Mars, Icarus, 176, 57–74, doi:10.1016/j.icarus.2005.01.005.

Balme, M.R., and C. Gallagher (2008), An equatorial periglacial landscape on Mars, Earth Planet. Sci. Lett., 285(1–2), 1–15, doi:10.1016/j.epsl.2009.05.031.

Balme, M.R., C.J. Gallagher, D.P. Page, J.B. Murray, and J.-P. Muller (2009), Sorted stone circles in Elysium Planitia, Mars: Implications for recent Martian climate, Icarus, 200, 30–38, doi:10.1016/j.icarus.2008.11.010.

Bart, G.D., and H.J. Melosh (2010), Distributions of boulders ejected from lunar craters, Icarus, 209, 337–357, doi:10.1016/j.icarus.2010.05.023.

Berg, T.E., and R.F. Black (1966), Preliminary measurements of growth of nonsorted polygons, Victoria Land, Antarctica, in Antarctic Soils and Soil-Forming Processes, edited by J. C. F. Tedrow, pp. 61–108, AGU, Washington, D. C.

Bierhaus, E.B., C.R. Chapman, and W.J. Merline (2005), Secondary craters on Europa and implications for cratered surfaces, Nature, 437, 1125–1127, doi:10.1038/nature04069.

Black, B.A., and S.T. Stewart (2008), Excess ejecta craters record episodic ice-rich layers at middle latitudes on Mars, J. Geophys. Res., 113, E02015, doi:10.1029/2007JE002888.

Bockheim, J.G., I.B. Campbell, and M. McLeod (2007), Permafrost distribution and active-layer depths in the McMurdo Dry valleys, Antarctica, Permafrost Periglac. Process., 18, 217–227, doi:10.1002/ppp.588.

Boynton, W.V., W.C. Feldman, S.W. Squyres, T.H. Prettyman, J. Brückner, L.G. Evans, R.C. Reedy, R. Starr, J.R. Arnold, D.M. Drake, P.A.J. Englert, A.E. Metzger, I. Mitrofanov, J.I. Trombka, C. d'Uston, H. Wänke, O. Gasnault, D.K. Hamara, D.M. Janes, R.L. Marcialis, S. Maurice, I. Mikheeva, G.J. Taylor, R. Tokar, and C. Shinohara (2002), Distribution of hydrogen in the near surface of Mars: Evidence for subsurface ice deposits, Science, 297, 81–85, doi:10.1126/science.1073722.

Costard, F.M., and J.S. Kargel (1995), Outwash plains and thermokarst on Mars, Icarus, 114, 93–112, doi:10.1006/icar.1995.1046.

Costard, F., F. Forget, N. Mangold, and J.P. Peulvast (2002), Formation of recent Martian debris flows by melting of near-surface ground ice at high obliquity, Science, 295, 110–113, doi:10.1126/science.1066698.

Crumpler, L.S. (1996), The significance of rock abundances at the Viking lander sites: Implications for Mars Pathfinder and Surveyor landers, Lunar Planet. Sci., XXVII, 273–274.

Daubar, I.J., A.S. McEwen, S. Byrne, C.M. Dundas, M. Kennedy, and B.A. Ivanov (2010), The current Martian cratering rate, Lunar Planet. Sci., XLI, Abstract 1978.

Feldman, W.C., W.V. Boynton, R.L. Tokar, T.H. Prettyman, O. Gasnault, S.W. Squyres, R.C. Elphic, D.J. Lawrence, S.L. Lawson, S. Maurice, G.W. McKinney, K.R. Moore, and R.C. Reedy (2002), Global distribution of neutrons from Mars: Results from Mars Odyssey, Science, 297, 75–78, doi:10.1126/science.1073541.

Forget, F., F. Hourdin, R. Fournier, C. Hourdin, O. Talagrand, M. Collins, S.R. Lewis, P.L. Read, and J.-P. Huot (1999), Improved general circulation models of the Martian atmosphere from the surface to above 80 km, J. Geophys. Res., 104(E10), 24,155–24,175, doi:10.1029/1999JE001025.

Francou, B., N. Le Mehaute, and V. Jomelli (2001), Factors controlling spacing distances of sorted stripes in a low-latitude, alpine environment (Cordillera Real, 16°S, Bolivia), Permafrost Periglac. Process., 12, 367–377, doi:10.1002/ppp.398.

French, H.M. (1976), The Periglacial Environment, Longman, London.

French, H.M. (2003), The development of periglacial geomorphology: 1 up to 1965, Permafrost Periglac. Process, 14, 29–60, doi:10.1002/ppp.438.

Fujiwara, A., P. Cerroni, D. Davis, E. Ryan, E. Di Martino, K. Holsapple, and K. Housen (1989), Experiments and scaling laws on catastrophic collisions, in Asteroids II, edited by R. P. Binzel, T. Gehrels, and M. S. Matthews, pp. 240–268, Univ. of Arizona Press, Tucson, Az.

Gallagher, C., M.R. Balme, S.J. Conway, and P.M. Grindrod (2011), Sorted clastic stripes, lobes and associated gullies in high-latitude craters on Mars: Landforms indicative of very recent, polycyclic ground ice thaw and liquid flows, Icarus, 211, 458–471, doi:10.1016/j.icarus.2010.09.010.

Golombek, M.P., A. Haldemann, N. Forsberg-Taylor, E. Dimaggio, R. Schroeder, B. Jakosky, M. Mellon, and J. Matijevic (2003), Rock size-frequency distributions on Mars and implications for Mars Exploration Rover landing safety and operations, J. Geophys. Res., 108(E12), 8086, doi:10.1029/2002JE002035.

Golombek, M.P., A. Huertas, J. Marlow, B. McGrane, C. Klein, M. Martinez, R.E. Arvidson, T. Heet, L. Barry, K. Seelos, D. Adams, W. Li, J.R. Matijevic, T. Parker, H.G. Sizemore, M. Mellon, A.S. McEwen, L.K. Tamppari, and Y. Cheng (2008), Size-frequency distributions of rocks on the northern plains of Mars with special reference to Phoenix landing surfaces, J. Geophys. Res., 113, E00A09, doi:10.1029/2007JE003065.

Hallet, B. (1990), Spatial self-organization in geomorphology: From periodic bedforms and patterned ground to scale-invariant topography, Earth Sci. Rev., 29(1–4), 57–75, doi:10.1016/0012-8252(90)90028-T.

Hartmann, W.K. (2007), Martian cratering 9: Toward resolution of the controversy about small craters, Icarus, 189, 274–278, doi:10.1016/j.icarus.2007.02.011.

Head, J.W., J.F. Mustard, M.A. Kreslavsky, R.E. Milliken, and D.R. Marchant (2003), Recent ice ages on Mars, Nature, 426, 797–802, doi:10.1038/nature02114.

Hecht, M.H., S.P. Kounaves, R.C. Quinn, S.J. West, S.M.M. Young, D.W. Ming, D.C. Catling, B.C. Clark, W.V. Boynton, J. Hoffman, L.P. Deflores, K. Gospodinova, J. Kapit, and P.H. Smith (2009), Detection of perchlorate and the soluble chemistry of Martian soil at the Phoenix Lander site, Science, 325, 64–67, doi:10.1126/science.1172466.

Ivanov, B. (2001), Mars/Moon cratering rate ratio estimates, Space Sci. Rev., 96, 87–104, doi:10.1023/A:1011941121102.

Jullien, R., and P. Meakin (1990), A mechanism for particle size segregation in three dimensions, Nature, 344, 425–427, doi:10.1038/344425a0.

Jullien, R., and P. Meakin (1992), Three-dimensional model for particle-size segregation by shaking, Phys. Rev. Lett., 69, 640–643, doi:10.1103/PhysRevLett.69.640.

Kadish, S.J., N.G. Barlow, and J.W. Head (2009), Latitude dependence of Martian pedestal craters: Evidence for a sublimation-driven formation mechanism, J. Geophys. Res., 114, E10001, doi:10.1029/2008JE003318.

Kostama, V.-P., M.A. Kreslavsky, and J.W. Head (2006), Recent high latitude icy mantle in the northern plains of Mars: Characteristics and ages of emplacements, Geophys. Res. Lett., 33, L11201, doi:10.1029/2006GL025946.

Kreslavsky, M.A., and J.W. Head (2002), Mars: Nature and evolution of young latitude-dependent water-ice-rich mantle, Geophys. Res. Lett., 29(15), 1719, doi:10.1029/2002GL015392.

Kreslavsky, M.A., and J.W. Head (2006), Modification of impact craters in the northern plains of Mars: Implications for Amazonian climate history, Meteorit. Planet. Sci., 41, 1633–1646, doi:10.1111/j.1945-5100.2006.tb00441.x.

Kreslavsky, M.A., J.W. Head, and D.R. Marchant (2008), Periods of active permafrost layer formation during the geological history of Mars: Implications for circum-polar and mid-latitude surface processes, Planet. Space Sci., 56, 289–302, doi:10.1016/j.pss.2006.02.010.

Kreslavsky, M.A., J.W. Head, A. Maine, H. Gray, and E.I. Asphaug (2010), North-South Asymmetry in Degradation Rates of Small Impact Craters at High Latitudes on Mars: Implications for Recent Climate Change, Lunar Planet. Sci., XLI, Abstract 1533.

Lachenbruch, A.H. (1962), Mechanics of thermal contraction cracks and ice-wedge polygons in permafrost, Geol. Soc. Am. Spec. Pap., 70, 1–69.

Laskar, J., A.C.M. Correia, M. Gastineau, F. Joutel, B. Levrard, and P. Robutel (2004), Long term evolution and chaotic diffusion of the insolation quantities of Mars, Icarus, 170, 343–364, doi:10.1016/j.icarus.2004.04.005.

Leffingwell, E.K. (1915), Ground-ice wedges: The dominant form of ground ice on the north coast of Alaska, J. Geol., 23, 635–654, doi:10.1086/622281.

Lefort, A., P.S. Russell, N. Thomas, A.S. McEwen, C.M. Dundas, and R.L. Kirk (2009), Observations of periglacial landforms in Utopia Planitia with the High Resolution Imaging Science Experiment (HiRISE), J. Geophys. Res., 114, E04005, doi:10.1029/2008JE003264.

Levrard, B., F. Forget, F. Montmessin, and J. Laskar (2004), Recent ice rich deposits formed at high latitudes on Mars by sublimation of unstable equatorial ice during low obliquity, Nature, 431, 1072–1075, doi:10.1038/nature03055.

Levy, J.S., J.W. Head, and D.R. Marchant (2008), Origin and arrangement of boulders on the Martian Northern Plains: Assessment of emplacement and modification environments, Lunar Planet. Sci., XXXVIII, Abstract 1172.

Levy, J.S., J.W. Head, and D.R. Marchant (2009a), Thermal contraction crack polygons on Mars: Classification, distribution, and climate implications from HiRISE observations, J. Geophys. Res., 114, E01007, doi:10.1029/2008JE003273.

Levy, J.S., J.W. Head, and D.R. Marchant (2009b), Cold and dry processes in the Martian Arctic: Geomorphic observations at the Phoenix landing site and comparisons with terrestrial cold desert landforms, Geophys. Res. Lett., 36, L21203, doi:10.1029/2009GL040634.

Levy, J.S., D.R. Marchant, and J.W. Head (2010), Thermal contraction crack polygons on Mars: A synthesis from HiRISE, Phoenix, and terrestrial analog studies, Icarus, 206, 229–252, doi:10.1016/j.icarus.2009.09.005.

Lewis, S.R., M. Collins, P.L. Read, F. Forget, F. Hourdin, R. Fournier, C. Hourdin, O. Talagrand, and J.-P. Huot (1999), A Climate Database for Mars, J. Geophys. Res., 104(E10), 24,177–24,194, doi:10.1029/1999JE001024.

Lucchitta, B.K. (1981), Mars and Earth: Comparison of cold-climate features, Icarus, 45, 264–303, doi:10.1016/0019-1035(81)90035-X.

Malin, M.C., and K.S. Edgett (2001), Mars Global Surveyor Mars Observer Camera: Interplanetary cruise through primary mission, J. Geophys. Res., 106(E10), 23,429–23,570, doi:10.1029/2000JE001455.

Mangold, N. (2005), High latitude patterned ground on Mars: Classification, distribution and climate control, Icarus, 174, 336–359, doi:10.1016/j.icarus.2004.07.030.

Marchant, D.R., and J.W. Head (2007), Antarctic dry valleys: Microclimate zonation, variable geomorphic processes, and implications for assessing climate change on Mars, Icarus, 192, 187–222, doi:10.1016/j.icarus.2007.06.018.

Marchant, D.R., A.R. Lewis, W.M. Phillips, E.J. Moore, R.A. Souchez, G.H. Denton, D.E. Sugden, N. Potter, and G.P. Landis (2002), Formation of patterned ground and sublimation till over Miocene glacier ice in Beacon Valley, southern Victoria Land, Antarctica, Geol. Soc. Am. Bull., 114, 718–730, doi:10.1130/0016-7606(2002)114<0718:FOPGAS>2.0.CO;2.

Marlow, J.J., C. Klein, M. Martinez, B. McGrane, and M. Golombek (2006), Boulder hazard assessment of potential Phoenix landing sites, Lunar Planet. Sci., XXXVIII, Abstract 1094.

Matmon, A., O. Simhai, R. Amit, I. Haviv, N. Porat, E. McDonald, L. Benedetti, and R. Finkel (2009), Desert pavement-coated surfaces in extreme deserts present the longest-lived landforms on Earth, Geol. Soc. Am. Bull., 121, 688–697, doi:10.1130/B26422.1.

McEwen, A.S., and E.B. Bierhaus (2006), The importance of secondary craters to age constraints on planetary surfaces, Annu. Rev. Earth Planet. Sci., 34, 535–567, doi:10.1146/annurev.earth.34.031405.125018.

McEwen, A.S., E.M. Eliason, J.W. Bergstrom, N.T. Bridges, C.J. Hansen, W.A. Delamere, J.A. Grant, V.C. Gulick, K.E. Herkenhoff, L. Keszthelyi, R.L. Kirk, M.T. Mellon, S.W. Squyres, N. Thomas, and C.M. Weitz (2007), Mars Reconnaissance Orbiter's High Resolution Imaging Science Experiment (HiRISE), J. Geophys. Res., 112, E05S02, doi:10.1029/2005JE002605.

McGill, G.E., and L.S. Hills (1992), Origin of giant Martian polygons, J. Geophys. Res., 97(E2), 2633–2647, doi:10.1029/91JE02863.

McSween, H.Y., S.W. Ruff, R.V. Morris, R. Gellert, G. Klingelhöfer, P.R. Christensen, T.J. McCoy, A. Ghosh, J.M. Moersch, B.A. Cohen, A.D. Rogers, C. Schröder, S.W. Squyres, J. Crisp, and A. Yen (2008), Mineralogy of volcanic rocks in Gusev Crater, Mars: Reconciling Mossbauer, Alpha Particle X-Ray Spectrometer, and Miniature Thermal Emission Spectrometer spectra, J. Geophys. Res., 113, E06S04, doi:10.1029/2007JE002970.

Mellon, M.T. (1997), Small-scale polygonal features on Mars: Seasonal thermal contraction cracks in permafrost, J. Geophys. Res., 102(E11), 25,617–25,628, doi:10.1029/97JE02582.

Mellon, M.T., and B. Jakosky (1993), Geographic variations in the thermal and diffusive stability of ground ice on Mars, J. Geophys. Res., 98(E2), 3345–3364, doi:10.1029/92JE02355.

Mellon, M.T., R.E. Arvidson, J. Marlow, R. Phillips, and E. Asphaug (2008), Periglacial landforms at the Phoenix landing site and the northern plains of Mars, J. Geophys. Res., 113, E00A23, doi:10.1029/2007JE003039.

Mellon, M.T., R.E. Arvidson, H.G. Sizemore, M.L. Searls, D.L. Blaney, S. Cull, M.H. Hecht, T.L. Heet, H.U. Keller, M.T. Lemmon, W.J. Markiewicz, D.W. Ming, R.V. Morris, W.T. Pike, and A.P. Zent (2009a), Ground ice at the

Phoenix Landing Site: Stability state and origin, J. Geophys. Res., 114, E00E07, doi:10.1029/2009JE003417.

Mellon, M.T., M.C. Malin, R.E. Arvidson, M.L. Searls, H.G. Sizemore, T.L. Heet, M.T. Lemmon, H.U. Keller, and J. Marshall (2009b), The periglacial landscape at the Phoenix landing site, J. Geophys. Res., 114, E00E06, doi:10.1029/2009JE003418.

Meresse, S., F. Costard, N. Mangold, D. Baratoux, and J. M. Boyce (2006), Martian perched craters and large ejecta volume: Evidence for episodes of deflation in the northern lowlands, Meteorit. Planet. Sci., 41(10), 1647–1658, doi:10.1111/j.1945-5100.2006.tb00442.x.

Mischna, M.A., M.I. Richardson, R.J. Wilson, and D.J. McCleese (2003), On the orbital forcing of Martian water and CO2 cycles: A general circulation model study with simplified volatile schemes, J. Geophys. Res., 108(E6), 5062, doi:10.1029/2003JE002051.

Mitrofanov, I., D. Anfimov, A. Kozyrev, M. Litvak, A. Sanin, V. Tret'yakov, A. Krylov, V. Shvetson, W. Boynton, C. Shinohara, D. Hamara, and R.S. Saunders (2002), Maps of subsurface hydrogen from the High Energy Neutron Detector, Mars Odyssey, Science, 297, 78–81, doi:10.1126/science.1073616.

Morgenstern, A., E. Hauber, D. Reiss, S. van Gasselt, G. Grosse, and L. Schirmeister (2007), Deposition and degradation of a volatile-rich layer in Utopia Planitia and implication for climate history on Mars, J. Geophys. Res., 112, E06010, doi:10.1029/2006JE002869.

Murton, J.B., and M.D. Bateman (2007), Syngenetic sand veins and antisyngenetic sand wedges, Tuktoyaktuk coastlands, western Arctic Canada, Permafrost Periglac. Process., 18, 33–47, doi:10.1002/ppp.577.

Péwé, T.L. (1959), Sand-wedge polygons (tessellations) in the McMurdo Sound region, Antarctica: A progress report, Am. J. Sci., 257, 545–552, doi:10.2475/ajs.257.8.545.

Péwé, T.L. (1963), Ice-wedges in Alaska–classification, distribution and climatic significance, paper presented at 2nd International Conference on Permafrost, Russ. Acad. of Sci., Yakutsk, Siberia.

Placzek, C.J., A. Matmon, D.E. Granger, J. Quade, and S. Niedermann (2010), Evidence for active landscape evolution in the hyperarid Atacama from

multiple terrestrial cosmogenic nuclides, Earth Planet. Sci. Lett., 295, 12–20, doi:10.1016/j.epsl.2010.03.006.

Rempel, A.W. (2007), The formation of ice lenses and frost heave, J. Geophys. Res., 112, F02S21, doi:10.1029/2006JF000525.

Rosato, A., K.J. Strandburg, F. Prinz, and R.H. Swendsen (1987), Why the brazil nuts are on top: Size segregation of particulate matter by shaking, Phys. Rev. Lett., 58, 1038–1040, doi:10.1103/PhysRevLett.58.1038.

Schorghofer, N., and O. Aharonson (2005), Stability and exchange of subsurface ice on Mars, J. Geophys. Res., 110, E05003, doi:10.1029/2004JE002350.

Seibert, N.M., and J.S. Kargel (2001), Small-scale Martian polygonal terrain: Implications for liquid surface water, Geophys. Res. Lett., 28(5), 899–902, doi:10.1029/2000GL012093.

Sizemore, H.G., and M.T. Mellon (2006), Effects of soil heterogeneity on Martian ground-ice stability and orbital estimates of ice depth, Icarus, 185, 358–369, doi:10.1016/j.icarus.2006.07.018.

Sizemore, H.G., M.T. Mellon, and M.P. Golombek (2009), Ice table depth variability near small rocks at the Phoenix landing site, Mars: A pre-landing assessment, Icarus, 199, 303–309, doi:10.1016/j.icarus.2008.10.008.

Smith, P.H., L. Tamppari, R.E. Arvidson, D. Bass, D. Blaney, W. Boynton, A. Carswell, D. Catling, B. Clark, T. Duck, E. DeJong, D. Fisher, W. Goetz, P. Gunnlaugsson, M. Hecht, V. Hipkin, J. Hoffman, S. Hviid, H. Keller, S. Kounaves, C.F. Lange, M. Lemmon, M. Madsen, M. Malin, W. Markiewicz, J. Marshall, C. McKay, M. Mellon, D. Michelangeli, D. Ming, R. Morris, N. Renno, W.T. Pike, U. Staufer, C. Stoker, P. Taylor, J. Whiteway, S. Young, and A. Zent (2008), Introduction to special section on the Phoenix Mission: Landing site characterization experiments, mission overviews, and expected science, J. Geophys. Res., 113, E00A18, doi:10.1029/2008JE003083.

Soare, R.J., and G.R. Osinski (2009), Stratigraphical evidence of late Amazonian periglaciation and glaciation in the Astapus Colles region of Mars, Icarus, 202, 17–21, doi:10.1016/j.icarus.2009.02.009.

Soare, R.J., G.R. Osinski, and C.L. Roehm (2008), Thermokarst lakes and ponds on Mars in the very recent (late Amazonian) past, Earth Planet. Sci. Lett., 272, 382–393, doi:10.1016/j.epsl.2008.05.010.

Squyres, S.W., and M.H. Carr (1986), Geomorphic evidence for the distribution of ground ice on Mars, Science, 231, 249–252, doi:10.1126/science.231.4735.249.

Stoker, C.R., A. Zent, D.C. Catling, S. Douglas, J.R. Marshall, D. Archer Jr., B. Clark, S.P. Kounaves, M.T. Lemmon, R. Quinn, N. Renno, P.H. Smith, and S.M.M. Young (2010), Habitability of the Phoenix landing site, J. Geophys. Res., 115, E00E20, doi:10.1029/2009JE003421.

Tanaka, K.L. (1986), The stratigraphy of Mars, J. Geophys. Res., 91(B13), E139–E158, doi:10.1029/JB091iB13p0E139.

Tanaka, K.L., J.A. Skinner Jr., T.M. Hare, T. Joyal, and A. Wenker (2003), Resurfacing history of the northern plains of Mars based on geologic mapping of Mars Global Surveyor data, J. Geophys. Res., 108(E12), 8043, doi:10.1029/2002JE001908.

Tanaka, K.L., J.A. Skinner Jr., and T.M. Hare (2005), Geologic map of the northern plains of Mars, U.S. Geol. Surv. Sci. Invest. Map, 2888.

Washburn, A.L. (1973), Periglacial Processes and Environments, St. Martins Press, New York.

Werner, S.C., B.A. Ivanov, and G. Neukum (2009), Theoretical analysis of secondary cratering on Mars and an image-based study on the Cerberus Plains, Icarus, 200, 406–417, doi:10.1016/j.icarus.2008.10.011.

Williams, J.C. (1976), The segregation of particulate materials. A review, Powder Technol., 15, 245–251, doi:10.1016/0032-5910(76)80053-8.

Yershov, E.D. (1998), General Geocryology, Cambridge Univ. Press, Cambridge, U. K., doi:10.1017/CBO9780511564505.

Zahnle, K., J.L. Alvarellos, A. Dobrovloskis, and P. Hamill (2008), Secondary and sesquinary craters on Europa, Icarus, 194, 660–674, doi:10.1016/j.icarus.2007.10.024.

Zent, A.P., M.H. Hecht, D.R. Cobos, S.E. Wood, T.L. Hudson, S.M. Milkovich, L.P. DeFlores, and M.T. Mellon (2010), Initial results from the thermal and electrical conductivity probe (TECP) on Phoenix, J. Geophys. Res., 115, E00E14, doi:10.1029/2009JE003420.

CHAPTER THREE

Possible Mechanism of Boulder Clustering on Mars

In review: Orloff, T.C., M.A. Kreslavsky, and E.I. Asphaug (in review) Icarus.

Abstract

Whatever causes small-scale polygonal patterned ground (diameter < ~20 meters) to form pervasively in the northern plains of Mars, appears to also cause boulders to cluster at polygon margins. Assuming that these polygons are caused by the seasonal thermal contraction and expansion of ice in the near-surface to meters of depth, we propose a mechanism that ratchets boulders towards the edges in seasonal cycles on present day Mars. During the contraction (cooling) phase, a CO_2 frost layer embeds the boulders. Buffered by condensation and sublimation, the solid CO_2 is isothermal and does not contract; we propose that it locks the boulders in place while the H_2O ice in the near surface continues cooling and contracts beneath them. In spring/summer seasons when the frost sublimates and heating of the surface begins, the boulders freely move with the expanding near surface ice. We show that over many seasons this process would lead to progressive boulder movement towards polygon edges, with an estimated rate of boulder migration ~0.1 mm/yr under present Mars conditions.

1. Introduction

Patterned ground forms in many regions on Mars. Small scale (diameter <~20m) polygons dominate patterned ground terrains at high latitudes (>55°) (Mangold, 2005, Levy et al., 2009); the same regions found to possess large volumes of water equivalent hydrogen in the near surface (within the uppermost meter) (Boynton et al., 2002; Feldman et al., 2002; Mitrofanov et al., 2003, Bandfield and Feldman, 2008). Previous research indicates that the high latitude polygons form due to thermal contraction of the ground ice, which cements the near surface (Mellon et al., 1997). With current high resolution imagery we see individual boulders (a meter to a few meters size) on patterned ground terrain (Golombek et al., 2008). Often these boulders appear clustered compared to a random population (Figure 1). Analysis (Orloff et al., 2011) has shown that this clustering should involve actual horizontal movement of the boulders at geologically short time scales (around ~ 1 Ma, and possibly much shorter).

Here we propose, develop and discuss a new physical mechanism for boulder movement toward polygon margins. First, we review the current hypotheses for boulder movement on Martian patterned ground terrains and show that they do not adequately explain the boulder clustering on Mars. Then we develop our hypothesis and describe its fundamental aspects. We follow with order of magnitude calculations and discuss our thermal and elastic model in detail, and conclude with a discussion of our results and its implications.

Clustering (patterning delineated with stones) occurs on patterned ground landforms on Earth (Washburn, 1956). Stones on patterned ground may cluster due to different mechanisms including particle sorting (Anderson, 1988), freeze-thaw (Taber, 1929, Fowler and Krantz, 1994), deformation of frozen soil (Li et al., 2000), and soil creep (Matsuoka, 2001), but no one process explains the entire range of clustering forms. Many of these mechanisms require liquid water but some cluster without liquid water more similar to Mars, for example, in the stable upland zone in Dry Valleys, Antarctica (Marchant and Head, 2007).

The meter-scale boulders we observe clustering in patterned ground on Mars, from satellite imagery, are an order of magnitude larger than the sizes found clustering in patterned ground on Earth. Sorting and other periglacial-induced clustering mechanisms on Earth generate patterns with stones the size of pebbles (~1 cm) or cobbles (~5 cm. – 25 cm.). Boulders up to several meters in size are found clustering in patterned ground related on Mars. Although gravity is different by a factor of ~3 between the planets, it is clear that none of the mechanisms for clustering of patterned ground on Earth can readily account for the clustering of boulders on Mars.

The morphological similarities between polygons in the stable upland zone in the Dry Valleys of Antarctica and high-latitude polygons on Mars and also the meteorological constraints of aridity and year round sub-zero temperature conditions on Mars led previous researchers to hypothesize they are the same type of polygons – thermal contraction polygons (sublimation type) (Marchant and Head, 2007; Levy et

al., 2009). But the presence of large scale boulders might tell a different story. Martian patterned ground exhibits two primary types of boulder clustering: (1) at polygon edges (Figure 1a,b), and (2) in rubble piles. In this paper we consider only boulder clustering at polygon edges although we should note that in the hypothesis of Levy et al., 2010 the boulders must cluster in polygon edges first, before transitioning to rubble piles.

Previous researchers hypothesize that boulders may cluster on Mars due to any one or a combination of the following processes: 1) Gravitational Slumping or Creep (Mellon et al., 2008, Levy et al., 2010), 2) Dry Cryoturbation (Mellon et al., 2008), or 3) Ice Lensing / Frost Heave (Balme et al., 2009, Zent et al., 2011, Gallagher et al., 2011). However, none of these explanations adequately fit the details of the situation presented on Mars.

Gravitational slumping occurs when the slope exceeds the angle of repose or when static friction between the boulder and sloped surface is overcome. This usually occurs on slopes greater than 30° (e.g., Clover, 1998, Kleinhans, 2011) but typical polygon relief is usually less than 10°. Thus, the gravitational slumping does not occur in the present-day patterned ground terrain on Mars, or would require some kind of active trigger such as seismic vibration.

Gravitational creep occurs on gentler slopes when some agent in the environment initiates downslope movement (e.g. Roering et al. 2001). On Earth, this often occurs due to action of the biosphere or wind or water, but there are fewer options for Martian patterned ground terrains. Aeolian deflation may initiate

Figure 1: Boulders cluster. a) Boulders cluster toward polygon margins in patterned ground in HiRISE image PSP_008219_2470 (66.6ºN, 320.1ºE). b) HiRISE image PSP_001341_2485 (68.4ºN, 175.4ºE) shows boulders clustering in cracks outlining polygons. Each image's width is 90 m and the scenes are illuminated from the left. Images from Orloff et al., (2011) and credit to HiRISE team NASA/JPL/University of Arizona.

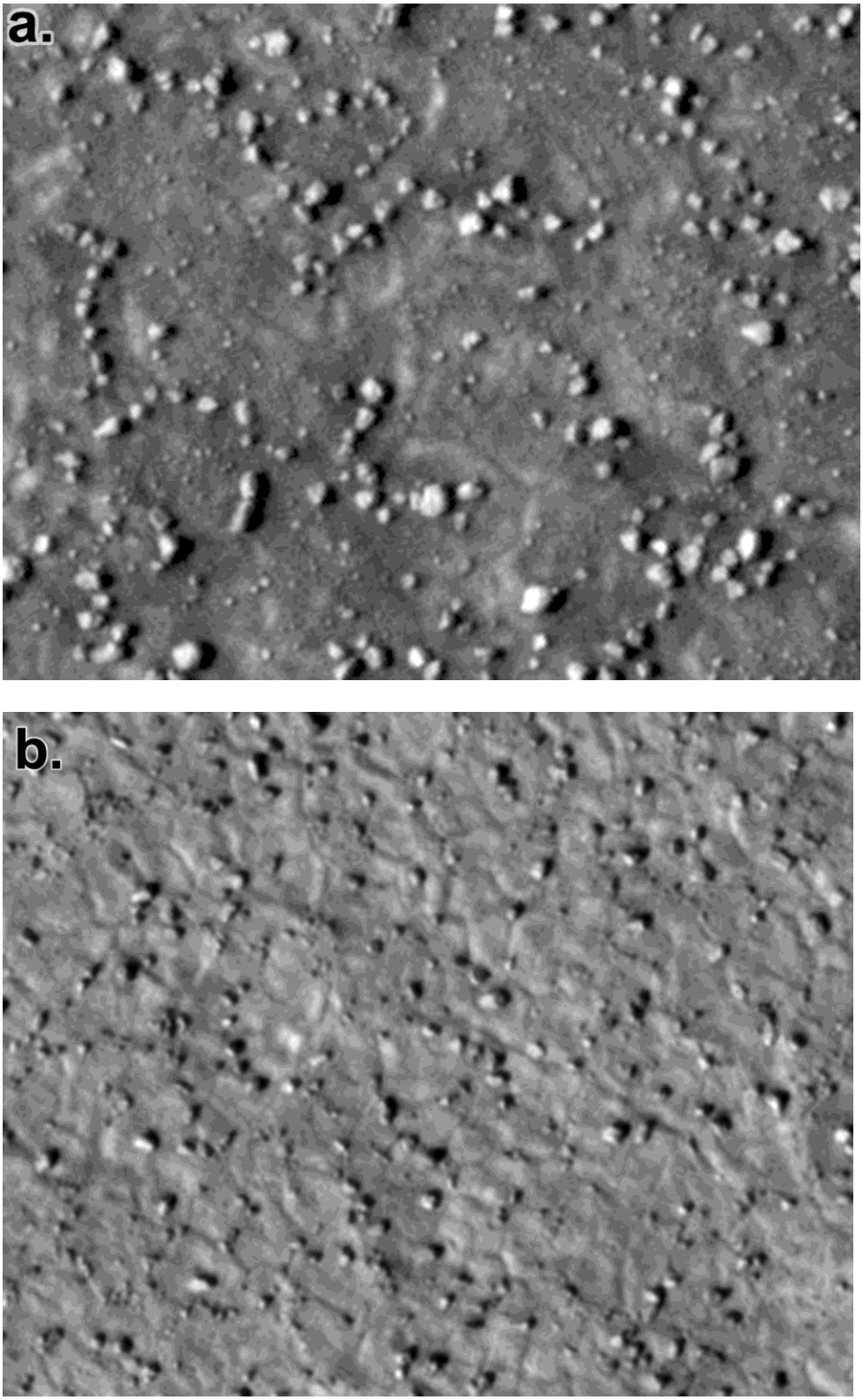

Figure 1

gravitational creep on Mars; however, we do not find it likely that this can be the case over such ubiquitous terrains on Mars. For one thing, we do not see ventifacts or other aeolian features in satellite imagery of high-latitude patterned ground terrains.

Levy et al. (2010) propose that sublimation of ground ice could generate the necessary slopes and initiate gravitational creep. They predict that surface slopes increase due to faster rates of sublimation of ice at thermal contraction cracks than in the polygon interiors. To increase slopes to the point that boulders would move requires removing meters of ice. This ice must furthermore sublimate away in a geologically short period of time because we do not find steep slopes today. The lack of steep slopes today would mean that boulder movement does not occur on Mars currently but did so in the past. To reconcile the boulder movement mechanism by Levy et al. (2010) with our constraints on time scales of boulder emplacement and movements (Orloff et al., 2011), we need to assume rather recent deposition of meters thick icy mantle and quick movement of the boulders from the base to the top of this mantle. The physical mechanism of the latter remains unclear, at best, which makes us uncomfortable with the scenario of Levy et al. (2010).

Mellon et al. (2008) propose a dry cryoturbation process which cycles soil particles from the polygon edges, down thermal contraction cracks, back to the center of the polygon and then up to the surface. Details regarding the exact nature of the processes in this mechanism remain vague; no good terrestrial or laboratory analogs are known. However, we expect two outcomes as the result of any process that cycles

material from the contraction cracks back to the center of the polygon, and this makes it a testable hypothesis. First, we expect boulders to get buried at polygon margins or for material to pile up around boulders at polygon margins. We see neither; however, a "brazil nut" mechanism (Williams, 1976, Rosato et al., 1987, Jullien and Meakin, 1990, 1992, Orloff et al., 2011) could potentially keep boulders sitting atop the finer grained sediments. Instead of buried or crowded boulders we see boulders at most touching edge to edge in a row (Figure 1). Second, we would expect the excavation of boulders at polygon centers. We have not encountered specific cases of buried boulders with signs of excavation from polygon centers but it is likely we cannot observe any such traces with current imagery. We also do not see boulders stacked on top of each other, which could suggest burial if the stacked boulders are at polygon margins or excavation if the stacked boulders at the polygon center.

We cannot completely rule out ice lensing or frost heave as a cause for boulder movement. When water freezes in a soil it can form crystals larger than the pore spaces in the soil causing the surface to rise or "heave". The Phoenix lander did indeed find massive ice deposits in the polygons surrounding the polar lander. Frost heave on Earth occurs within the active layer of saturated soils that experience seasonal melting and freezing. Thaw, which is a required part of heave, does not occur on Mars today, but calculations by Zent et al. (2011) show that ice lensing of pure water may occur between 2-3 Ma ago during periods of high obliquity when more sunlight reaches higher latitudes.

Orloff et al. (2011) predict boulder clustering in the high latitudes of the northern hemisphere occurred within the past 1 Ma based on crater age estimates of 0.1-1 km circular features assumed to be craters. Very few bowl shaped craters in this size range remain on patterned ground terrain yet many flattened circular features with boulder distributions similar to equatorial craters exist so these were also counted as highly degraded craters. They found the boulders around all craters in this size range appeared clustered in some fashion.

The time frame for thaw calculated by Zent et al. (2011) is within the error bars for age of boulder clustering assessed by Orloff et al. (2011). Orloff et al. (2011) also found that the size frequency distribution of craters did not follow predicted isochrones at smaller sizes, which means that craters degrade and disappear over time. The degradation of ~100 m scale diameter craters on rapid timescales and the appearance of clustered boulders around every crater in their study suggest that boulder clustering may be a continuous process because these craters form throughout Mars history yet all of them experience boulder clustering. In this case a pure liquid water mechanism does not work.

In any case, even if frost heave happens on Mars today or in the past, this process is known to sort pebbles and cobbles in periglacial landscapes on Earth but not boulders similar in size to those observed in the northern plains of Mars. We know of no terrestrial examples of frost heave resulting in the clustering of meter-scale boulders such as are found clustering around typical polygons on Mars.

Instead of appealing to terrestrial analogues, we suggest a process specific to the unique environment of Mars, one in which ground ice is a pervasive component of the near surface in the mid- to high latitudes, and in which the atmosphere condenses out seasonally as CO_2 as a massive surface layer. We now consider the physics of this seasonal setting.

2. Hypothesis

We suggest the following mechanism for boulder clustering on thermal contraction polygons. During the winter the water ice and/or ice-rich soil in the near surface cools and contracts (opening cracks) and during the summer it heats and expands (closing cracks). We propose that the carbon dioxide frost layer formed in Martian winters lock boulders in place during the contraction phase of the near surface ice contraction / expansion cycle, then, when the seasonal frost disappears in the summer, boulders shift outward with expanding near surface ice; after many seasonal cycles, this leads to boulder clustering in polygon margins.

Figure 2 depicts a cartoon of the proposed mechanism. Figure 2a shows boulders of different sizes sitting at different radial positions at the surface on thermal contraction polygons. We picture boulders at the very surface. Many of the boulders on patterned ground terrains are directly associated with impact craters which would leave them at or near the very surface. Even boulders not directly associated with an impact event are likely impact related. Orloff et al. 2011 found that most craters on patterned ground terrain were highly degraded and they suggested that craters on the surface become erased over time. Those boulders that are buried either during the

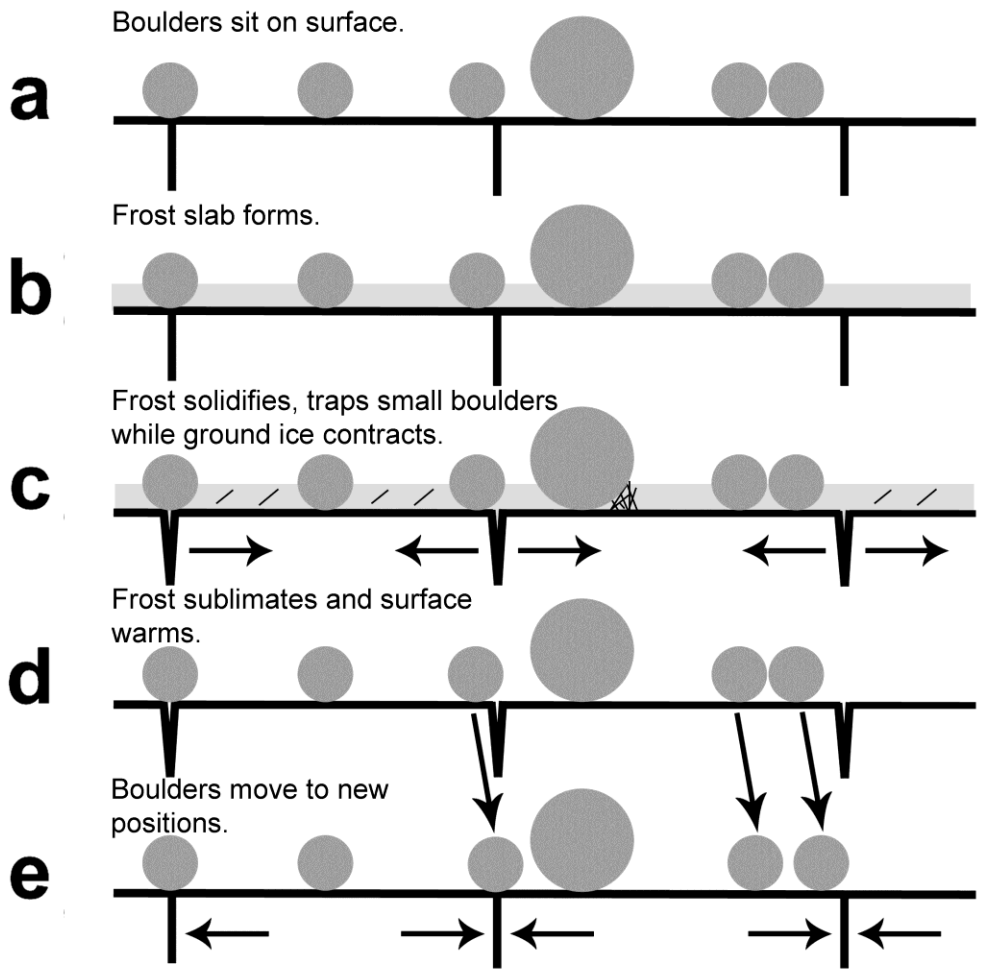

Figure 2: Cartoon of mechanism for boulder clustering. (a) Boulders sitting on the ground at different radial positions on polygons. We describe these boulders as: one very large boulder near the edge, one boulder already in a polygon crack, one boulder in the center of the polygon, one boulder near a crack, and two boulders close to each other near another crack. (b) Seasonal CO_2 frost forms a layer. (c) The frost layer solidifies into a slab locking in all small boulders (but not the large boulder) while the near surface ice continues to contract beneath the isothermal frost slab. (d) The frost slab sublimates away and the ground starts to heat up. (e) The boulders are free to move with the expansion of the near surface ice. The boulder already in a crack remains in the crack. The boulder in the center of the polygon stays in the center. The one boulder near a crack falls into the crack. The two boulders close to each other both move towards the crack but separation between them increases.

impact or during the degradation of the crater could migrate to the very surface in media experiencing repeated perturbations via a Brazil nut effect (Williams, 1976, Rosato et al., 1987, Jullien and Meakin, 1990, 1992, Orloff et al., 2011) which would bring them to the surface. In Figure 2b a seasonal CO_2 frost layer forms and covers the terrain.

When the seasonal CO_2 frost layer covers the surface, the surface temperature is fixed at the CO_2 frost point, which is lower than the year-average temperature. The frost layer remains isothermal due to the latent heat involved in the phase change of CO_2 from gas to solid and back to gas. Not until the ground itself becomes exposed to the atmosphere does the surface temperature start to rise in the spring. This causes heat flux from beneath the frost to the surface and progressive cooling of the seasonal thermal skin layer. The near surface ice continues to contract until the seasonal frost disappears in late spring.

The upward heat flux causes sublimation of solid CO_2 at its boundary with soil. Due to this, the CO_2 slab is detached from the soil through the whole winter season, even if initially the CO_2 frost condenses on soil particles. The CO_2 gas produced at the soil - frost boundary migrates through the cold CO_2 slab and condenses in it, at least, partially, which causes pore filling, sintering, and strengthening of the CO_2 frost. Exact degree of sintering is not known, but different lines of observational evidence indicate that this indeed occurs. Transparency of the seasonal frost [e.g., Kiefer, 2007] and its spectral properties [e.g., Langevin, 2007] suggest that the grain sizes of CO_2 crystals in the frost layer grow through the winter.

This produces a seasonal CO_2 layer more similar to a solid slab rather than fluffy snow.

The observed venting and formation of plumes, evidently by pressurized gas concentrated beneath the frost layer (Kieffer et al., 2006, Thomas et al., 2011), indicates that the slab is impermeable for gas and hence sintered to a high degree. The observed spring-time cracks of a wide spacing (tens of meters) in the frost (Portyankina et al., 2010) suggest that the slab can support significant stresses. These cracks do not form due to thermal-induced stresses within the frost itself because, as noted above, the slab remains isothermal. Rather we suspect these cracks form from mechanical stresses induced from the underlying water ice contraction in the subsurface or from the pressure of vapor generated at the frost-surface interface.

Order of magnitude calculations (see Section 3.2) show that depending on the coefficient of thermal expansion the ice may contract a few millimeters over the course of the winter. Figure 2c shows both the continued contraction of the near surface ice and cemented soil under the CO_2 frost slab and boulders underneath a size threshold locked in the CO_2 frost. Estimates below (see Section 3.1) show that the slab can be strong enough to withstand the frictional forces exerted by the boulder in contact with the ground.

In the late spring the CO_2 frost sublimates away. The boulders become unlocked from the CO_2 frost and rest gently on the surface; the subsurface icy material thermally expands as it warms up, narrows polygonal cracks and transports boulders outward from the polygon centers, as shown in Figure 2d and Figure 2e,

respectively. This leads to gradual boulder migration towards polygon margins. Once the boulders reach the polygon margin they become trapped there.

3. Calculations and Models

Here we describe our orders of magnitude estimate for critical quantities for the proposed mechanism. We consider a boulder of a characteristic diameter $d \sim 1$ m sitting at a distance x from the center of a polygon of a diameter $L \sim 10$ m.

3.1. Required Strength of the Carbon Dioxide Slab to Lock Boulders in Place

To lock a boulder, the slab strength should exceed shear stress σ caused by the maximal drag force F applied to the boulder by the moving substrate. The stress is scaled as $\sigma \sim F / A$, where A is the cross-section area of the boulder - slab interface; $A \sim d\,h$, where h is the slab thickness. The drag force is limited by the maximal dry friction force, which is proportional to weight of the boulder: $F = f\,m\,g$, where f is static dry friction coefficient ($f \sim 0.5$), $m \sim \rho\,d^3$ is boulder mass, g is gravity ($g = 3.7$ m s^{-2}), and ρ is boulder density ($\rho \approx 3000$ kg m^{-3}). Thus, we obtain:

$$\sigma \sim f\ \rho\, g\, \frac{d^2}{h}. \qquad (1)$$

Figure 3 shows this stress as a function of boulder diameter d for different carbon dioxide ice thicknesses h. The strength of the CO_2 slab is bracketed between the strength of dry soil layer of thickness h and the strength of the solid CO_2. The

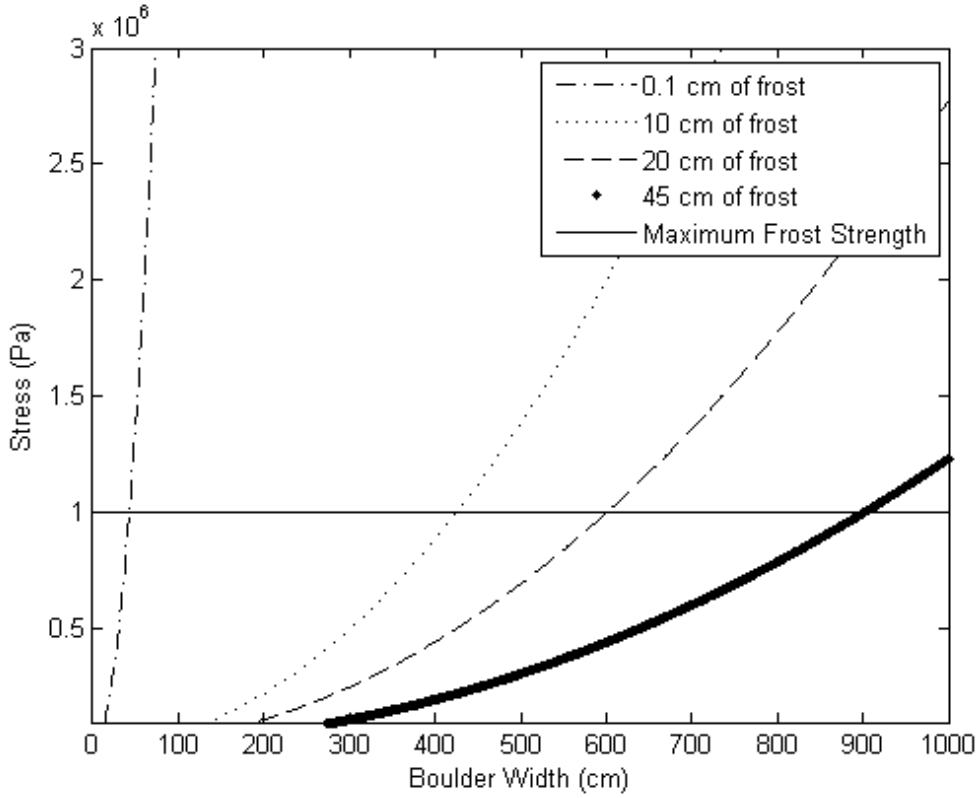

Figure 3: Stress induced in frost layers of different thicknesses due to frictional force from boulder of given radius. We show lines for frost layers 0.1 cm thick, 10 cm thick, 20 cm thick, and 45 cm thick. Even with large uncertainties in frost strength 10's of centimeters of frost can lock in boulders several meters in diameter.

former is scaled as the layer lithostatic pressure and is obviously below our estimate of σ. However, as we discussed above, we expect at least some degree of sintering of the seasonal frost. Bulk dry ice is significantly weaker than water ice (Clark and Mullin, 1975), however its strength (0.1 - 1 MPa) well exceeds the stress (1) required to lock a boulder, unless the boulder is too big. Thus, with some sintering, the CO_2 slab can lock boulders of the appropriate size.

If the CO_2 ice is strong enough to lock the boulders, it will be strong enough to withstand the frictional forces exerted by the contracting near surface ice; it will not move with the seasonally contracting near surface ice and will act as a coherent layer much greater in size than any individual polygon. The stress induced by the frictional force of a block of CO_2 ice in contact with the ground, similarly to (1) is scaled as $f\, m_i\, g\, /\, A_i$, where m_i is a mass of an ice block overlying a coherently displacing part of a polygon, which size we assume to be ~0.2 L, $m_i \sim 0.04\, \rho_i\, L^2\, h$, ρ_i is the CO_2 ice density ($\rho_i \approx 1500$ kg m^{-3} or lower, if porosity is high), and A_i is a cross-section of the ice block over a coherently displacing part, $A_i \sim 0.2\, L\, h$. Thus, the stress is scaled as:

$$\sigma \sim 0.2\, f\, \rho_i\, g\, L, \qquad (2)$$

which is less than (1) for our characteristic sizes of boulders and polygons. Therefore, in all cases, where frost traps boulders, the frost itself also remains locked in place. High-resolution spring-time images of the seasonal frost indeed do not reveal any cracking spatially associated with polygon margins (however, such cracks, if they exist, might be unresolved).

3.2. Seasonal movement scale

We now estimate the movement of boulders in a given seasonal cycle by our proposed mechanism. Seasonal thermal crack opening is scaled as

$$\Delta L \sim \alpha \, \Delta T \, L, \qquad (3)$$

where α is the coefficient of thermal expansion and ΔT is the seasonal change in daily average temperature. The near surface ice contracts towards the center of a polygon, so a boulder placed some distance x from the center of the polygon would then experience a seasonal displacement Δx:

$$\Delta x \sim \alpha \, \Delta T \, x. \qquad (4)$$

For $\alpha = 2\times10^{-5}$ K^{-1} (value for a linear mixture of ice and basalt at 200°K assuming a soil with 40% porosity completely filled with ice, parameters used in Mellon, 1997; Mellon et al., 2008) and ΔT = 100 K (the order of magnitude of seasonal surface temperature change), Δx ranges from 0 at the polygon's center to ~5 mm near the edge of a 5 m diameter polygon. This estimate depends strongly on the coefficient of thermal expansion, which varies significantly depending on the mixture of the materials and temperature.

If we assume that boulders move outward during warm season and do not move inward during cold season, (3) gives a dimension estimate of the net shift during one Martian year. Boulders near the centers of polygons migrate slower than boulders near the exteriors. Far from the centers boulder movement rate would be a

few mm per martian year, and it takes several hundreds of years for a boulder to reach the polygon edge.

The dimension relationship (3), however, significantly overestimates the annual boulder shift on two reasons. First, the temperature field is not uniform within the seasonal thermal skin, and the thermal skin depth is comparable to the polygon size, which makes seasonal displacement amplitude smaller than given by (3). Second, some part of the cold-season contraction occurs before the seasonal frost is emplaced and sintered. Thus, the actual migration rates are slower and migration time scales are longer. The difference can be significant, and to ensure the viability of the mechanism we need more accurate estimates of surface displacement due to thermal contraction during the season when boulders are locked by the seasonal frost.

Below we consider a simple model to estimate this displacement. It consists of two parts, a thermal model that gives vertical distribution of temperature inside the seasonal thermal skin, and an elastic model that uses the temperature field to calculate displacements due to thermal contraction and expansion.

3.3. Thermal model

Our simple order of magnitude thermal model of the subsurface (in the fashion of James, 1952) simulates changes of the temperature $T(z, t)$ with depth z and time t. For the accuracy we need, we can ignore the processes in the thin diurnal thermal skin and solve the linear diffusive heat conduction equation in the thicker seasonal thermal skin modeled as semi-infinite solid bounded by the plane z = 0, with

the boundary condition of prescribed model surface temperature $T(z=0, t) = T_0(t)$ equal to the actual day-average surface temperature. We take daily average surface temperatures $T_0(t)$ for the Phoenix landing site from the Mars Climate Database (available at http://www-mars.lmd.jussieu.fr/mars/mars.html [Forget et al., 1999, Lewis et al., 1999]) as appropriate boundary conditions for the model. The surface temperatures in the climate database include results from more accurate thermal model calculations, and these have been validated against observations and are sufficiently accurate for our purposes. We use a cubic spline to interpolate the day-average surface temperatures between the seasons listed in the database and set the temperature equal to the CO_2 frost point during the period when the seasonal frost is present.

The periodic solution for the linear heat conduction equation with constant thermal diffusivity χ can be obtained by Fourier method as a sum of Fourier series:

$$T(z,t) = T_{ya} + \mathrm{Re}\sum_{n=1}^{\infty} \tilde{T}_{0n} \exp\left(-(1+i)z\sqrt{\frac{\pi n}{\chi\tau}}\right)\exp\left(2\pi i\frac{t}{\tau}\right), \quad (5)$$

where T_{ya} is the year-average temperature, τ is the length of the Martian year, and

$$\tilde{T}_{0n} = \frac{1}{\tau}\int_0^{\tau} T_0(t)\exp\left(-2\pi i n\frac{t}{\tau}\right)dt, \quad n = 1,2,\ldots. \quad (6)$$

We use the standard implementation of the discrete Fourier transform to evaluate the sum in (5) and the integral in (6). For χ we used thermal diffusivity of water ice (10^{-4} m^2 s^{-1}), knowing that it makes a dominant part of the material volume in the upper meters. Figure 4 shows examples of calculated temperature profiles for various days

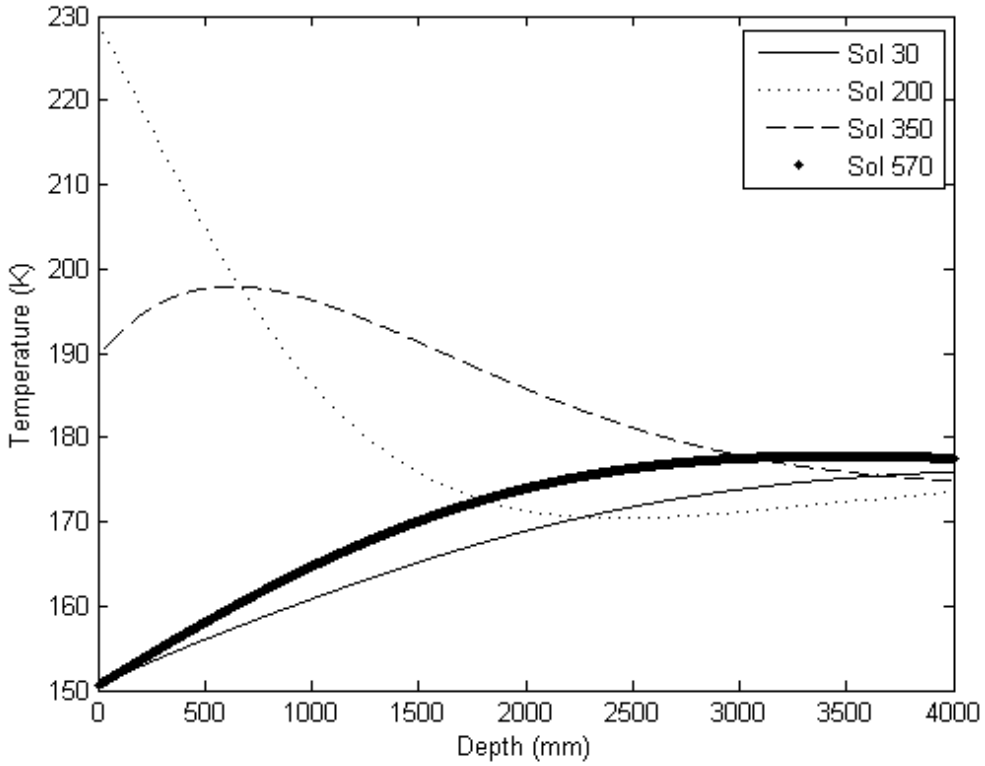

Figure 4: Temperature profiles with depth at the Phoenix Landing site (68.15°N, 233.98°E) for different Sols in the Mars year. We show 5 different days here: one summer, one spring, and three winter. The 2 winter days occur at L_s = 305 and 370 which correspond to Sol 570 and Sol 30 next martian year, respectively.

in the Martian year. We show 3 winter profiles, a spring, and a summer profile. After deriving these temperatures we then use these data as feed for our elastic model described in the next section.

3.4. Elastic model

We chose to develop our model using software called Automatic Dynamic Incremental Nonlinear Analysis (ADINA) (Bathe, 1996). ADINA offers a wide range of efficient and reliable finite element procedures with multi-physics capabilities. We simulate the stress, strain, and displacement using a freely available academic version of the ADINA structure and thermal analysis software.

We model a single polygon as a rotationally symmetric cylinder with a depth of 4 meters (comparable to the seasonal thermal skin thickness) and a radius of 2.5 m. In ADINA we create a grid with 20 cm cell size representing a cross section of the model domain from the cylinder axis to the outer edge. The top and outer boundaries act as free surfaces while the bottom boundary remains fixed at zero displacement. Because we find that the frost slab and surface are detached, we treat the upper boundary as a free surface and do not include the weight of the frost on the surface in our model. The unstressed condition corresponds to uniform temperature field of T_{ya}. Then we impose a temperature profile calculated with the thermal model (Section 3.3). We apply a constant Young's modulus (7.8×10^{10} Pa), coefficient of thermal expansion $\alpha = 4.5\times10^{-5}$ °K^{-1}, and Poisson ratio of 0.33 representative of pure water ice. ADINA computes the displacement, stress, and strain using finite element

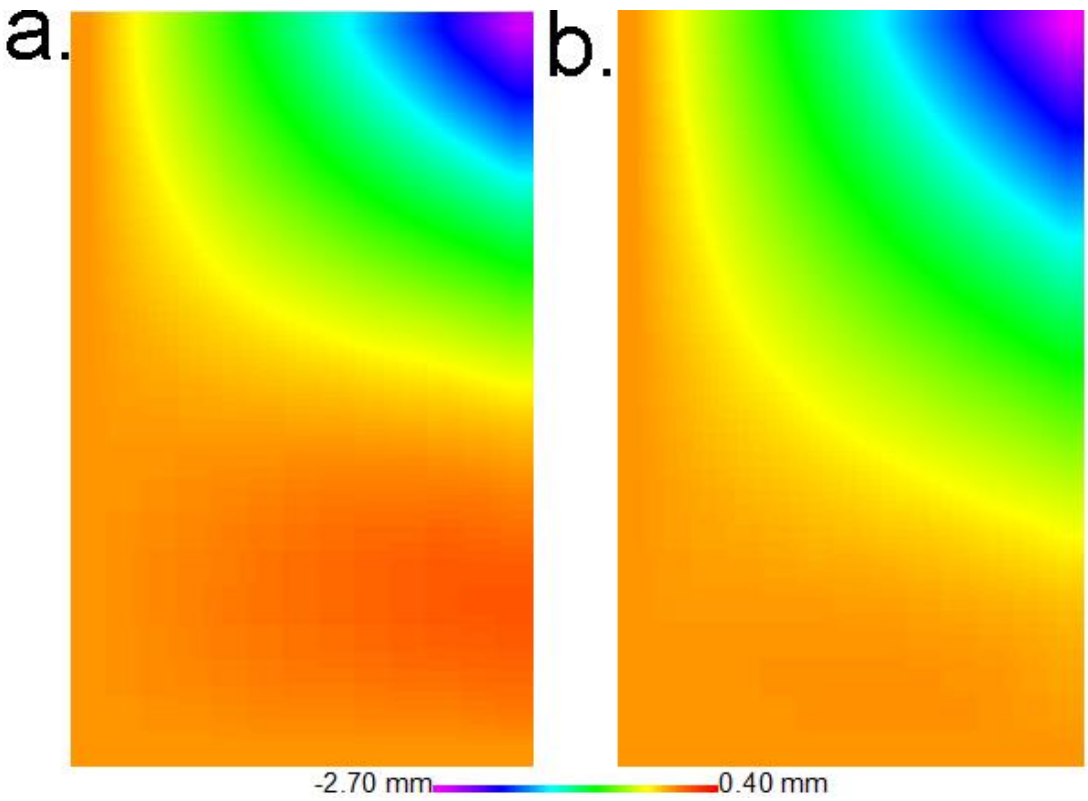

Figure 5: Color-coded radial displacement distribution in our elastic model of an ice polygon. Symmetry axis is at the left edge of the domain shown, the surface is at the top, positive displacement is outward. Results for Sols (A) 570 and (B) 30 are shown. These two days represent the dates within which the frost layer is thicker than 20 cm.

procedures from Bathe (1996). Figure 5 for example shows the amount of radial displacement in the polygon at two times in late winter. Note that the maximum contraction (~2.5 cm) occurs at the surface of the near the edge and that the contraction decreases both towards the center and at depth.

Our interest lies in the comparisons between points in time when frost traps and releases boulders. We discussed previously several reasons and lines of observational evidence for why the CO_2 frost appears to become strong through the course of the winter. In constructing our estimates, we assume that a boulder gets trapped into the frost slab in winter, when its thickness reaches 20 cm, and gets released in spring, when the slab thins down to 20 cm. Kelly et al. (2007) presented a model that gives the evolution of the frost layer thickness through the course of the Martian winter and spring (Figure 6). We used their results to determine the trapping and release dates. We input the temperatures fields from Sol 570 (L_s = 305°; first appearance of 20 cm of frost (Figure 5a)) and Sol 30 (L_s = 15°; last appearance of 20 cm of frost (Figure 5b)) into the boundary thermal conditions our elastic model. ("Sol" is the number of martian day within a martian year starting at the vernal equinox.)

Figure 7 shows the difference in radial displacement between these two times. The change in displacement at the uppermost outer edge between these two states is the maximum amount of boulder movement we predict. In this example we predict 0.1 mm of radial displacement. Decreasing the thickness of frost necessary to trap the boulder increases the amount of time the boulder remains locked in the frost and also

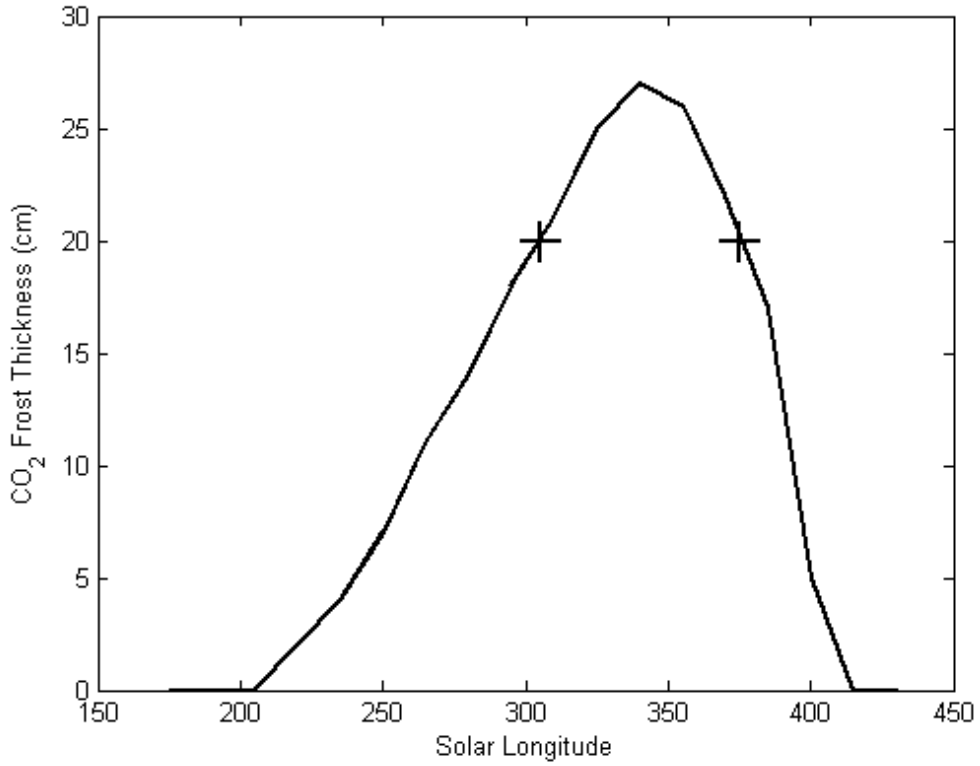

Figure 6: Model of CO_2 frost thickness for the Martian winter adapted from Kelly et al. (2007). For the constant strength scenario we imagine a boulder that gets locked in place in 20 cm of frost at L_s = 305º and released at L_s = 375º. These times are indicated on the plot and the temperature profiles that correspond with these times are shown in Figure 4.

allows for more cooling of the subsurface with the boulder locked; these would both increase the magnitude of the contraction that occurs while the boulder remains locked in the CO_2 ice. In this case the boulder would move further than the 0.1 mm of radial displacement. Conversely, increasing the thickness of frost necessary would decrease the amount of time the boulder remains locked in frost and would allow for less cooling and contraction.

It is reasonable to consider a similar case, that instead of using different thicknesses of frost at a single location, we consider different thicknesses of frost as a function of latitude. Less frost forms equatorward, and for a shorter duration, so that a boulder requiring 20 cm of frost would spend less time locked in place and would perhaps move less than our scenario. Conversely, more frost forms poleward for a longer duration so that same boulder would spend more time locked in place and might migrate farther than our canonical case.

The primary goal for now is to place order of magnitude estimates in order to reject or validate the hypothesis. As we expected, the cumulative displacement is significantly (almost by two orders of magnitude) less than that predicted by the scaling relationship established above (Eq. 3). However, it still leaves us with estimated annual displacement on the order of 0.1 mm. Consequently, the time scale for significant boulder clustering is on the order of hundred thousands of years (the polygon diameter divided by the displacement velocity), and this is short compared with the observational constraints for the timescale of boulder clustering established in our previous work (Orloff et al., 2011).

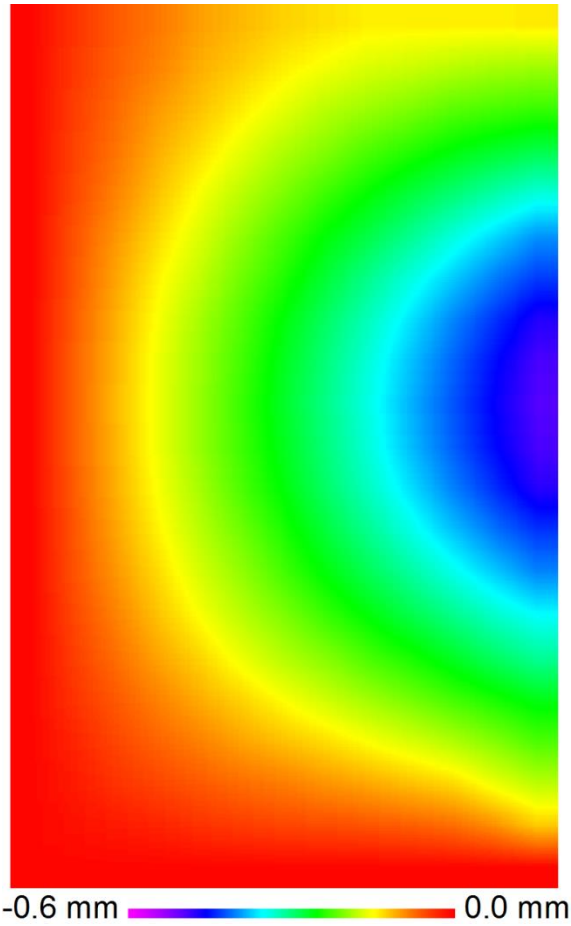

Figure 7: Difference in radial displacement in the polygon between the times in Figure 5a and 5b. At the top outermost (upper right) edge of the polygon additional 0.1 mm of contraction occurs between Sols 570 and 30 (next year).

4. Discussion

The displacement velocity 0.1 mm/yr represents roughly the order of magnitude of annual boulder movement we expect. We cannot present an exact number due to many uncertainties like local variations of soil texture, uncertainty in seasonal frost properties, dependence on boulder size and shape, etc. Additionally, our thermal modeling simulations show the magnitude of displacement decreases towards the centers of the polygons. Annual movement that is even 2 orders of magnitude less than our example (0.001 mm/yr) would cluster boulders on timescales of millions of years. In summary, these numbers are very well consistent with our previous findings in Orloff et al. (2011) which constrain the maximum age of boulder clustering to around ~2.4 Ma.

Our mechanism assumes that boulders sit at the surface and are not partly buried. Analysis in Sizemore and Mellon, (2006) showed that the boulders, unless they are deeply buried, are not frozen into the ground ice, and thus can be dragged with respect to the surface, if the CO_2 slab is strong enough. Partial burial of boulders would increase friction with the ground. This result means a decrease in the likelihood of moving any given boulder holding other factors constant. Buried boulders are likely to move with the contraction/expansion of the near surface ice in the polygons since the subsurface continues cooling while the seasonal frost is present. These factors mean that our mechanism for boulder movement probably does not work on partially buried boulders. We suspect the torque on partially buried boulders from the seasonal frost as the near surface ice contracts could, over time,

ratchet boulders to the surface. Clustered boulders on patterned ground on Mars do not appear partially buried (see boulders in Figure 1) but it will take detailed studies of statistics of boulder vertical and horizontal dimensions to check. Furthermore, modifications of our thermal model that include the partial burial of high thermal inertia boulders would give better insight. These projects are beyond the scope of this paper.

Our proposed mechanism predicts a size threshold for boulder clustering depending on the thickness of the seasonal frost and the strength of the frost: the largest boulders cannot be locked by the frost slab and do not move. The thickness of the CO_2 frost slab depends on climate (a function of latitude). At progressively lower latitudes, where the seasonal frost is thinner, we would expect only progressively smaller boulders to cluster. Conversely, with thicker frost at higher latitudes we expect clustering of progressively larger boulders. Since the largest boulders do not form dense fields and appear sporadically, these predicted dependences (or their absence) are not readily obvious in the images. Figure 1B hints that our prediction may be true, because the small boulders appear consistently in polygon edges compared to large boulders, but to rigorously test this aspect of our hypothesis we aim to develop analysis techniques to determine boulder distribution characteristics.

During periods of higher obliquity (e.g. >0.3 Ma ago) the seasonal temperature amplitude is higher, and the seasonal frost is thicker. Thus, this period is overall considered favorable for boulder movement. Thicker and longer lasting (thus stronger) frost is more capable of trapping boulders. The additional time that frost is

present during higher obliquity also allows increased ground cooling which contracts the near surface ice further. It is possible that migration actually occurred only at high obliquity. However, our calculations show that even under the current martian climate boulders can cluster on timescales of thousands of years.

We do not see traces left by moving boulders. Other moved boulders indeed leave visible tracks, for example those that fall down gullies or crater walls. The lack of boulder tracks means that either boulders do not leave tracks or the tracks were since removed. For boulders of this size to not leave tracks requires well-cemented rigid surfaces, which is certainly not the case. Kreslavsky et al. (2010) have shown that the time scale of significant modification (smoothing) of 5 - 10 m - size craters at high latitudes is on the order of thousands to tens thousands of years. The same processes that effectively smooth the craters would obliterate boulder tracks. Aeolian action could erode a hypothetical boulder track or perhaps interaction between the surface and the seasonal frost could eliminate them.

The required rate of track obliteration is comparable to the predicted rate of boulder movement, about 0.1 mm/yr. As we discussed above, each winter the near surface ice contracts and the surface could be rubbed by the overlying solid CO_2 slab. This may be responsible for or contribute to quick obliteration of boulder traces.

According to our considerations above (section 3.2), boulders in the very centers of polygons should remain in place because no displacement occurs in the center. However, we generally do not find boulders in the exact centers of polygons in images. For this we have two explanations that do not exclude each other. First,

polygons do not have perfectly symmetrical shapes, and slight asymmetry may lead to the absence of a point of zero displacement in the center. Once off center, boulder migration begins and accelerates towards the edges. Moreover, any material that drops into the polygon-forming cracks when they are open does so unevenly in time, and the stress field could significantly change year to year, which would make the zero-displacement point to move about the polygon center. This would lead to gradual movement of boulders away from polygon centers.

Second, formation of polygons can occur concurrently with boulder movement. Mellon et al. (2008) show that the highest thermal contraction stresses occur in the polygon center, and it is the most likely location for new crack formation. A boulder in the center of a polygon forming a new crack would end up appearing in a new polygon edge.

5. Conclusions

The clustering of boulders in the youthful polygonal terrains of Mars implies boulder movement on a relatively rapid timescale (Orloff et al. 2011). Obtaining a mechanism for this movement is important, as it links closely to recent and ongoing epochs of martian climate, and the cycling of martian volatiles. It can provide insight into analysis of boulder distributions preserved in older terrains and their implications for climate evolution.

In this paper we have proposed a mechanism to account for boulder movement inside thermal contraction polygons that is driven by the seasonal covering of this terrain by an approximately 1-m thick layer of carbon dioxide frost. CO_2 frost,

buffered by the atmosphere, forms an isothermal planar slab that locks boulders in place during the winter contraction of the underlying near surface ice, preventing them from moving. This applies a net displacement relative to the inward contraction of the near surface ice in winter. When the frost sublimates the boulders are free to move with the expansion of near surface ice during warming. This leads to progressive movement of boulders towards polygon edges.

We estimate the rate of this movement to be approximately 0.1 mm per year, based on the ages of the polygonal terrains and the results of thermal models of the ice-rich regolith. Our model has at least three testable aspects deserving further focused attention:

1) The small boulders should migrate and large boulders should remain in place; the threshold boulder size should increase poleward. Detailed studies of statistics of boulder populations may test this prediction.

2) Boulders should become unlocked at the end of winter in order by size, from larger to smaller, causing faults in the frost layer that might allow for the CO_2 gas trapped under the translucent frost slab to escape and form plumes. Repeat imagery of a scene known to contain boulders and plumes through the late winter could determine whether plumes tend to occur at boulder locations starting from larger and progressing to smaller boulders.

3) Boulders (and other meter scale objects like the Phoenix lander itself) should migrate toward polygon edges. With current technology on or orbiting Mars we

cannot observe these small rates of boulder movement at this time but with increased image resolution or future missions such direct measurements may become possible.

6. Acknowledgements.

Research by T.O., M.K. and E.A. was supported by NASA Mars Fundamental Research Program award NNX08AT13G. M.K. was also supported by NASA Mars Data Analysis award NNX08AL07G. We also would like to acknowledge the HiRISE team for the spectacular images of the surface of used in this study.

References

Anderson, S.P. (1988), The upfreezing process: Experiments with a single clast. Geol. Soc. Am. Bull. 100, no. 4, 609-621.

Balme, M.R., C.J. Gallagher, D.P. Page, J.B. Murray, and J.-P. Muller (2009), Sorted stone circles in Elysium Planitia, Mars: Implications for recent Martian climate, Icarus, 200, 30–38, doi:10.1016/j.icarus.2008.11.010.

Bandfield, J.L., and W. Feldman (2008), Martian high latitude permafrost depth and surface cover thermal inertia distributions. J. Geophys. Res. 113, E8, E08001.

Bathe, K.J. (1996), Finite Element Procedures. Prentice Hall, Upper Saddle River, New Jersey, pp. 1-1037.

Boynton, W.V., W.C. Feldman, S.W. Squyres, T.H. Prettyman, J. Brückner, L.G. Evans, R.C. Reedy, R. Starr, J.R. Arnold, D.M. Drake, P.A.J. Englert, A.E. Metzger, I. Mitrofanov, J.I. Trombka, C. d'Uston, H. Wänke, O. Gasnault, D.K. Hamara, D.M. Janes, R.L. Marcialis, S. Maurice, I. Mikheeva, G.J. Taylor, R. Tokar, and C. Shinohara (2002), Distribution of hydrogen in the near surface of Mars: Evidence for subsurface ice deposits, Science, 297, 81–85, doi:10.1126/science.1073722.

Clark, B.R., and R.P. Mullin (1975), Martian Glaciation and Flow of Solid CO_2. Icarus 27, 215-228.

Clover, T. J. (1998), Pocket Ref. Littleton, Colorado: Sequoia Publishing.

Feldman, W.C., W.V. Boynton, R.L. Tokar, T.H. Prettyman, O. Gasnault, S.W. Squyres, R.C. Elphic, D.J. Lawrence, S.L. Lawson, S. Maurice, G.W. McKinney, K.R. Moore, and R.C. Reedy (2002), Global distribution of neutrons from Mars: Results from Mars Odyssey, Science, 297, 75–78, doi:10.1126/science.1073541..

Forget, F., F. Hourdin, R. Fournier, C. Hourdin, O. Talagrand, M. Collins, S. R. Lewis, P. L. Read, and J.-P. Huot (1999), Improved general circulation models of the Martian atmosphere from the surface to above 80 km, J. Geophys. Res., 104(E10), 24,155–24,175, doi:10.1029/1999JE001025.

Fowler, A.C., and W.B. Krantz, W.B. (1994), A Generalized Secondary Frost Heave Model. SIAM J. Appl. Math 54, 6, 1650-1675.

Gallagher, C., M.R. Balme, S.J. Conway, P.M. Grindrod (2011), Sorted clastic stripes, lobes and associated gullies in high-latitude craters on Mars:

Landforms indicative of ground-ice thaw and liquid flows. Icarus 211, 1, 458-471.

Golombek, M.P., A. Huertas, J. Marlow, B. McGrane, C. Klein, M. Martinez, R.E. Arvidson, T. Heet, L. Barry, K. Seelos, D. Adams, W. Li, J.R. Matijevic, T. Parker, H.G. Sizemore, M. Mellon, A.S. McEwen, L.K. Tamppari, and Y. Cheng (2008), Size-frequency distributions of rocks on the northern plains of Mars with special reference to Phoenix landing surfaces, J. Geophys. Res., 113, E00A09, doi:10.1029/2007JE003065.

James, R.W. (1952), Heat diffusion from a plane, periodic source. Pure and Applied Geophys. 22, 3-4, 174-188.

Jullien, R., and P. Meakin (1990), A mechanism for particle size segregation in three dimensions. Nature 355, 425-427.

Jullien, R., and P. Meakin, (1992), Three dimensional model for particle-size segregation by shaking. Phys. Rev. Lett. 69, 640-643.

Kelly, N.J., W.V. Boynton, K. Kerry, D. Hamara, D. Janes, R.C. Reedy, K.J. Kim, and R.M. Haberle (2007), Seasonal polar carbon dioxide frost on Mars: CO2 mass and columnar thickness distribution. J. Geophys. Res. 111, E03S07.

Kiefer, H.H. (2007), Cold jets in the Martian polar caps. J, Geophys. Res. Planet 112, E08005.

Kieffer, H.H., P.R. Christensen, and T.N. Titus (2006), CO_2 jets formed by sublimation beneath translucent slab ice in Mars' seasonal polar ice cap. Nature 442, 793-796.

Kleinhans, M.G., H. Markies, S.J. de Vet, S.J. in 't Veld, and F.N. Postema (2011), Static and dynamic angles of repose in loose granular materials under reduced gravity. J. Geophys. Res. 116, E11004, doi:10.1029/2011JE003865.

Kreslavsy, M.A., J.W. Head, A. Maine, H. Gray, and E.I. Asphaug (2010), North-South Asymmetry in Degradation Rates of Small Impact Craters at High Latitudes on Mars: Implications for Recent Climate Change, Lunar Planet. Sci. XLI, 1533.

Langevin, Y., J.-P. Bibring, F. Montmessin, F. Forget, M. Vincendon, S. Douté, F. Poulet, and B. Gondet (2007), Observations of the south seasonal cap of Mars during recession in 2004-2006 by the Omega visible/near infrared imaging spectrometer on board Mars Express. J. Geophys. Res. Planets 112, E8, E08S12.

Levy, J.S., J.W. Head, and D.R. Marchant (2009), Thermal contraction crack polygons on Mars: Classification, distribution, and climate implications from HiRISE observations. J. Geophys. Res. 114, E01007.

Levy, J.S., D.R. Marchant, and J.W. Head (2010), Thermal contraction crack polygons on Mars: A synthesis from HiRISE, Phoenix, and terrestrial analog studies. Icarus 206, 229-252.

Lewis, S.R., M. Collins, P.L. Read, F. Forget, F. Hourdin, R. Fournier, C. Hourdin, O. Talagrand, and J.-P. Huot (1999), A Climate Database for Mars, J. Geophys. Res., 104(E10), 24,177–24,194, doi:10.1029/1999JE001024.

Li, N., B. Chen, C. Feixong, and X. Xiaozu (2000), The coupled heat-moisture-mechanic model of the frozen soil. Cold Regions Sci. Technol. 31, 3, 199-205.

Malin, M.C., and K. Edgett (2001), Mars Global Surveyor Mars Orbiter Camera: Interplantary cruise through primary mission. J. Geophys. Res. Planet 106, E10, 23429-23570.

Mangold, N. (2005), High latitude patterned grounds on Mars: Classification, distribution and climatic control. Icarus 174, 2, 336-359.

Marchant, D.R., and J.W. Head (2007), Antarctic Dry Valleys: Microclimate zonation, variable geomorphic processes, and implications for assessing climate change on Mars. Icarus 192, 187-222.

Matsuoka, N. (2001), Solifluction rates, processes and landforms: a global review. Earth Sci. Rev. 55, 1-2, 107-134.

Mellon, M.T. (1997), Small-scale polygonal features on Mars: Seasonal thermal contraction cracks in permafrost. J. Geophys. Res. Planet 102, E11, pp. 25617-25628.

Mellon, M.T., R.E. Arvidson, J.J. Marlow, R.J. Phillips, and E.I. Asphaug (2008), Periglacial landforms at the Phoenix landing site and the northern plains of Mars. J. Geophys. Res. Planet 113, E00A23.

Mitrofanov, I.G., M.T. Zuber, M.L. Litvak, W.V. Boynton, D.E. Smith, D. Drake, D. Hamara, A.S. Kozyrev, A.B. Sanin, C. Shinohara, R.S. Saunders, and V. Tretyakov (2003), CO_2 snow depth and subsurface water-ice abundance in the northern hemisphere of Mars. Science 300, 5628, 2081-2084.

Orloff, T., M. Kreslavsky, E. Asphaug, and J. Korteniemi (2011), Boulder movement at high northern latitudes of Mars. J. Geophys. Res. Planet 116, E11006.

Portyankina, G., W.J. Markiewicz, N. Thomas, C.J. Hansen, and M. Milazzo (2010), HiRISE observations of gas sublimation-driven activity in Mars' southern polar regions: III. Models of processes involving translucent ice. Icarus 205, 1, 311-320.

Roering, J.J., J.W. Kirchner, and W.E. Dietrich (2001), Hillslope evolution by nonlinear, slope-dependent transport: Steady state morphology and equilibrium adjustment timescales. J. Geophys. Res. 106, B8, 16499-16513.

Rosato, A., K.J. Strandburg, F. Prinz, and R.H. Swendsen (1987), Why the brazil nuts are on top: Size segregation of particulate matter by shaking. Phys. Rev. Lett. 58, 1038-1040.

Sizemore, H.G., and M.T. Mellon (2006), Effects of soil heterogeneity on martian ground-ice stability and orbital estimates of ice table depth. Icarus 185, 2, 358-369.

Taber, S. (1929), Frost Heaving. J. Geol. 37, 5, 428-261.

Thomas, N., G. Portyankina, C.J. Hansen, and A. Pommerol (2011), HiRISE observations of gas sublimation-driven activity in Mars' southern polar regions: IV. Fluid dynamics models of CO_2 jets. Icarus 212, 1, 66-85.

Washburn, A.L. (1956), Classification of Patterned Ground and Review of Suggested Origins. Bull. Geol. Soc. Am. 67, 823-866.

Williams, J.C. (1976), The segregation of particulate materials. A review. Powder Technol. 15, 245-251.

Zent, A.P., H.G. Sizemore, and A.W. Rempel (2011), Ice lens formation and frost heave at the Phoenix landing site. Lunar Planet. Sci. XLII, 2543.

Bibliography

Anderson, S.P. (1988), The upfreezing process: Experiments with a single clast. Geol. Soc. Am. Bull. 100, no. 4, 609-621.

Armstrong, J.C., and C.B. Leovy (2005), Long term wind erosion on Mars, Icarus, 176, 57–74, doi:10.1016/j.icarus.2005.01.005.

Balme, M.R., and C. Gallagher (2008), An equatorial periglacial landscape on Mars, Earth and Planet. Sci. Lett., 285(1-2), 1-15, doi:10.1016/j.epsl.2009.05.031.

Balme, M.R., C.J. Gallagher, D.P. Page, J.B. Murray, and J.-P. Muller (2008), Sorted stone circles in Elysium Planitia, Mars: Implications for recent martian climate, Icarus, 200(1), 30-38, doi:10.1016/j.icarus.2008.11.010.

Bandfield, J.L., and W. Feldman (2008), Martian high latitude permafrost depth and surface cover thermal inertia distributions. J. Geophys. Res. 113, E8, E08001.

Bart, G.D., and H.J. Melosh (2010), Distributions of boulders ejected from lunar craters, Icarus, 209, 337–357, doi:10.1016/j.icarus.2010.05.023.

Bathe, K.J. (1996), Finite Element Procedures. Prentice Hall, Upper Saddle River, New Jersey, pp. 1-1037.

Berg, T.E., and R.F. Black (1966), Preliminary measurements of growth of nonsorted polygons, Victoria Land, Antarctica, in Antarctic Soils and Soil-Forming Processes, edited by J. C. F. Tedrow, pp. 61–108, AGU, Washington, D. C.

Beucher, S., and F. Meyer (1993), The morphological approach to segmentation: The watershed transformation. In Mathematical Morphology in Image Processing. (E.R. Dougherty, Ed.) 433-482, Marcel Dekker, New York.

Bierhaus, E.B., C.R. Chapman, and W.J. Merline (2005), Secondary craters on Europa and implications for cratered surfaces, Nature, 437, 1125–1127, doi:10.1038/nature04069.

Black, B.A., and S.T. Stewart (2008), Excess ejecta craters record episodic ice-rich layers at middle latitudes on Mars, J. Geophys. Res., 113, E02015, doi:10.1029/2007JE002888.

Bleau, A., and L.J. Leon (2000), Watershed-based segmentation and region merging. Computer Vision and Image Understanding, 77, 317-370.

Bockheim, J.G., I.B. Campbell, and M. McLeod (2007), Permafrost distribution and active-layer depths in the McMurdo Dry valleys, Antarctica, Permafrost Periglac. Process., 18, 217–227, doi:10.1002/ppp.588.

Boynton, W.V., W.C. Feldman, S.W. Squyres, T.H. Prettyman, J. Brückner, L.G. Evans, R.C. Reedy, R. Starr, J.R. Arnold, D.M. Drake, P.A.J. Englert, A.E. Metzger, I. Mitrofanov, J.I. Trombka, C. d'Uston, H. Wänke, O. Gasnault, D.K. Hamara, D.M. Janes, R.L. Marcialis, S. Maurice, I. Mikheeva, G.J. Taylor, R. Tokar, and C. Shinohara (2002), Distribution of hydrogen in the near surface of Mars: Evidence for subsurface ice deposits, Science, 297, 81–85, doi:10.1126/science.1073722.

Clark, B.R., and R.P. Mullin (1975), Martian Glaciation and Flow of Solid CO_2. Icarus 27, 215-228.

Clover, T. J. (1998), Pocket Ref. Littleton, Colorado: Sequoia Publishing.

Costard, F.M., and J.S. Kargel (1995), Outwash Plains and Thermokarst on Mars, Icarus, 114(1), 93- 112.

Costard, F., F. Forget, N. Mangold, and J.P. Peulvast (2002), Formation of recent Martian debris flows by melting of near-surface ground ice at high obliquity, Science, 295, 110–113, doi:10.1126/science.1066698.

Crumpler, L.S. (1996), The significance of rock abundances at the Viking lander sites: Implications for Mars Pathfinder and Surveyor landers, Lunar Planet. Sci., XXVII, 273–274.

Daubar, I.J., A.S. McEwen, S. Byrne, C.M. Dundas, M. Kennedy, and B.A. Ivanov (2010), The current Martian cratering rate, Lunar Planet. Sci., XLI, Abstract 1978.

Feldman, W.C., W.V. Boynton, R.L. Tokar, T.H. Prettyman, O. Gasnault, S.W. Squyres, R.C. Elphic, D.J. Lawrence, S.L. Lawson, S. Maurice, G.W. McKinney, K.R. Moore and R.C. Reedy (2002), Global distribution of neutrons from Mars: Results from Mars Odyssey, Science, 297(5578), 75-78, DOI:10.1126/science.1073541.

Forget, F., F. Hourdin, R. Fournier, C. Hourdin, O. Talagrand, M. Collins, S.R. Lewis, P.L. Read, and J.-P. Huot (1999), Improved general circulation models of the Martian atmosphere from the surface to above 80 km, J. Geophys. Res., 104(E10), 24,155–24,175, doi:10.1029/1999JE001025.

Fowler, A.C., and W.B. Krantz, W.B. (1994), A Generalized Secondary Frost Heave Model. SIAM J. Appl. Math 54, 6, 1650-1675.

Francou, B., N. Le Mehaute, and V. Jomelli (2001), Factors controlling spacing distances of sorted stripes in a low-latitude, alpine environment (Cordillera Real, 16°S, Bolivia), Permafrost Periglac. Process., 12, 367–377, doi:10.1002/ppp.398.

French, H.M. (1976), The Periglacial Environment, Longman, London.

French, H.M. (2003), The development of periglacial geomorphology: 1 up to 1965, Permafrost Periglac. Process, 14, 29–60, doi:10.1002/ppp.438.

Fujiwara, A., P. Cerroni, D. Davis, E. Ryan, E. Di Martino, K. Holsapple, and K. Housen (1989), Experiments and scaling laws on catastrophic collisions, in Asteroids II, edited by R. P. Binzel, T. Gehrels, and M. S. Matthews, pp. 240–268, Univ. of Arizona Press, Tucson, Az.

Gallagher, C., M.R. Balme, S.J. Conway, and P.M. Grindrod (2011), Sorted clastic stripes, lobes and associated gullies in high-latitude craters on Mars: Landforms indicative of very recent, polycyclic ground ice thaw and liquid flows, Icarus, 211, 458–471, doi:10.1016/j.icarus.2010.09.010.

Gallant, J.C. (1997), Scale and structure in landscapes, PhD thesis, Australian National University.

Golombek, M.P., A. Haldemann, N. Forsberg-Taylor, E. Dimaggio, R. Schroeder, B. Jakosky, M. Mellon, and J. Matijevic (2003), Rock size-frequency distributions on Mars and implications for Mars Exploration Rover landing safety and operations, J. Geophys. Res., 108(E12), 8086, doi:10.1029/2002JE002035.

Golombek, M.P., A. Huertas, J. Marlow, B. McGrane, C. Klein, M. Martinez, R.E. Arvidson, T. Heet, L. Barry, K. Seelos, D. Adams, W. Li, J.R. Matijevic, T. Parker, H.G. Sizemore, M. Mellon, A.S. McEwen, L.K. Tamppari, and Y. Cheng (2008), Size-frequency distributions of rocks on the northern plains of Mars with special reference to Phoenix landing surfaces, J. Geophys. Res., 113, E00A09, doi:10.1029/2007JE003065.

Hallet, B. (1990), Spatial self-organization in geomorphology: From periodic bedforms and patterned ground to scale-invariant topography, Earth Sci. Rev., 29(1–4), 57–75, doi:10.1016/0012-8252(90)90028-T.

Hanley, J.T. (1977), Fourier analysis of the Catawba Mountain knolls, Roanoke county, Virginia, Mathematical Geology, 9(2), 159-163.

Hartmann, W.K. (2007), Martian cratering 9: Toward resolution of the controversy about small craters, Icarus, 189, 274–278, doi:10.1016/j.icarus.2007.02.011.

Head, J.W., J.F. Mustard, M.A. Kreslavsky, R.E. Milliken, and D.R. Marchant (2003), Recent ice ages on Mars, Nature, 426, 797–802, doi:10.1038/nature02114.

Hecht, M.H., S.P. Kounaves, R.C. Quinn, S.J. West, S.M.M. Young, D.W. Ming, D.C. Catling, B.C. Clark, W.V. Boynton, J. Hoffman, L.P. Deflores, K. Gospodinova, J. Kapit, and P.H. Smith (2009), Detection of perchlorate and the soluble chemistry of Martian soil at the Phoenix Lander site, Science, 325, 64–67, doi:10.1126/science.1172466.

Ivanov, B. (2001), Mars/Moon cratering rate ratio estimates, Space Sci. Rev., 96, 87–104, doi:10.1023/A:1011941121102.

James, R.W. (1952), Heat diffusion from a plane, periodic source. Pure and Applied Geophys. 22, 3-4, 174-188.

Jullien, R., and P. Meakin (1990), A mechanism for particle size segregation in three dimensions, Nature, 344, 425–427, doi:10.1038/344425a0.

Jullien, R., and P. Meakin (1992), Three-dimensional model for particle-size segregation by shaking, Phys. Rev. Lett., 69, 640–643, doi:10.1103/PhysRevLett.69.640.

Kadish, S.J., N.G. Barlow, and J.W. Head (2009), Latitude dependence of Martian pedestal craters: Evidence for a sublimation-driven formation mechanism, J. Geophys. Res., 114, E10001, doi:10.1029/2008JE003318.

Kelly, N.J., W.V. Boynton, K. Kerry, D. Hamara, D. Janes, R.C. Reedy, K.J. Kim, and R.M. Haberle (2007), Seasonal polar carbon dioxide frost on Mars: CO2 mass and columnar thickness distribution. J. Geophys. Res. 111, E03S07.

Kiefer, H.H. (2007), Cold jets in the Martian polar caps. J, Geophys. Res. Planet 112, E08005.

Kieffer, H.H., P.R. Christensen, and T.N. Titus (2006), CO_2 jets formed by sublimation beneath translucent slab ice in Mars' seasonal polar ice cap. Nature 442, 793-796.

Kleinhans, M.G., H. Markies, S.J. de Vet, S.J. in ‘t Veld, and F.N. Postema (2011), Static and dynamic angles of repose in loose granular materials under reduced gravity. J. Geophys. Res. 116, E11004, doi:10.1029/2011JE003865.

Korteniemi, J., and M.A. Kreslavsky (2012), Patterned ground in Martian high northern latitudes: Morphology and age constraints. Icarus, in press.

Kostama, V.-P., M.A. Kreslavsky, and J.W. Head (2006), Recent high latitude icy mantle in the northern plains of Mars: Characteristics and ages of emplacements, Geophys. Res. Lett., 33, L11201, doi:10.1029/2006GL025946.

Kreslavsky, M.A., and J.W. Head (2002), Mars: Nature and evolution of young latitude-dependent water-ice-rich mantle, Geophys. Res. Lett., 29(15), 1719, doi:10.1029/2002GL015392.

Kreslavsky, M.A., and J.W. Head (2006), Modification of impact craters in the northern plains of Mars: Implications for Amazonian climate history, Meteorit. Planet. Sci., 41, 1633–1646, doi:10.1111/j.1945-5100.2006.tb00441.x.

Kreslavsky, M.A., J.W. Head, and D.R. Marchant (2008), Periods of active permafrost layer formation during the geological history of Mars: Implications for circum-polar and mid-latitude surface processes, Planet. Space Sci., 56, 289–302, doi:10.1016/j.pss.2006.02.010.

Kreslavsky, M.A., J.W. Head, A. Maine, H. Gray, and E.I. Asphaug (2010), North-South Asymmetry in Degradation Rates of Small Impact Craters at High Latitudes on Mars: Implications for Recent Climate Change, Lunar Planet. Sci., XLI, Abstract 1533.

Lachenbruch, A.H. (1962), Mechanics of thermal contraction cracks and ice-wedge polygons in permafrost, Geol. Soc. Am. Spec. Pap., 70, 1–69.

Langevin, Y., J.-P. Bibring, F. Montmessin, F. Forget, M. Vincendon, S. Douté, F. Poulet, and B. Gondet (2007), Observations of the south seasonal cap of Mars during recession in 2004-2006 by the Omega visible/near infrared imaging spectrometer on board Mars Express. J. Geophys. Res. Planets 112, E8, E08S12.

Laskar, J., A.C.M. Correia, M. Gastineau, F. Joutel, B. Levrard, and P. Robutel (2004), Long term evolution and chaotic diffusion of the insolation quantities of Mars, Icarus, 170, 343–364, doi:10.1016/j.icarus.2004.04.005.

Leffingwell, E.K. (1915), Ground-ice wedges: The dominant form of ground ice on the north coast of Alaska, J. Geol., 23, 635–654, doi:10.1086/622281.

Lefort, A., P.S. Russell, N. Thomas, A.S. McEwen, C.M. Dundas, and R.L. Kirk (2009), Observations of periglacial landforms in Utopia Planitia with the High Resolution Imaging Science Experiment (HiRISE), J. Geophys. Res., 114(E4), E04005, doi:10.1029/2008JE003264.

Levrard, B., F. Forget, F. Montmessin, and J. Laskar (2004), Recent ice rich deposits formed at high latitudes on Mars by sublimation of unstable equatorial ice during low obliquity, Nature, 431, 1072–1075, doi:10.1038/nature03055.

Levy, J.S., J.W. Head, and D.R. Marchant (2008), Origin and arrangement of boulders on the Martian Northern Plains: Assessment of emplacement and modification environments, Lunar Planet. Sci., XXXVIII, Abstract 1172.

Levy, J.S., J.W. Head, and D.R. Marchant (2009), Thermal contraction crack polygons on Mars: Classification, distribution, and climate implications from HiRISE observations, J. Geophys. Res., 114, E01007, doi:10.1029/2008JE003273.

Levy, J.S., J.W. Head, and D.R. Marchant (2009b), Cold and dry processes in the Martian Arctic: Geomorphic observations at the Phoenix landing site and comparisons with terrestrial cold desert landforms, Geophys. Res. Lett., 36, L21203, doi:10.1029/2009GL040634.

Levy, J.S., D.R. Marchant, and J.W. Head (2010), Thermal contraction crack polygons on Mars: A synthesis from HiRISE, Phoenix, and terrestrial analog studies, Icarus, 206, 229–252, doi:10.1016/j.icarus.2009.09.005.

Lewis, S.R., M. Collins, P.L. Read, F. Forget, F. Hourdin, R. Fournier, C. Hourdin, O. Talagrand, and J.-P. Huot (1999), A Climate Database for Mars, J. Geophys. Res., 104(E10), 24,177–24,194, doi:10.1029/1999JE001024.

Li, N., B. Chen, C. Feixong, and X. Xiaozu (2000), The coupled heat-moisture-mechanic model of the frozen soil. Cold Regions Sci. Technol. 31, 3, 199-205.

Lucchitta, B.K. (1981), Mars and Earth: Comparison of cold-climate features, Icarus, 45, 264–303, doi:10.1016/0019-1035(81)90035-X.

Malin, D.R. and K.S. Edgett (2001), Mars Global Surveyor Mars Observer Camera: Interplanetary cruise through primary mission, J. Geophys. Res., 106(E10), 23429-23570, doi:10.1029/2000JE001455.

Mangold, N. (2005), High latitude patterned ground on Mars: Classification, distribution and climate control, Icarus, 174, 336– 359, doi:10.1016/j.icarus.2004.07.030.

Marchant, D.R., and J.W. Head (2007), Antarctic dry valleys: Microclimate zonation, variable geomorphic processes, and implications for assessing climate change on Mars, Icarus, 192(1), 187-222, doi:10.1016/j.icarus.2007.06.018.

Marchant, D.R., A.R. Lewis, W.M. Phillips, E.J. Moore, R.A. Souchez, G.H. Denton, D.E. Sugden, N. Potter, and G.P. Landis (2002), Formation of patterned ground and sublimation till over Miocene glacier ice in Beacon Valley, southern Victoria Land, Antarctica, Geol. Soc. Am. Bull., 114, 718–730, doi:10.1130/0016-7606(2002)114<0718:FOPGAS>2.0.CO;2.

Marlow, J.J., C. Klein, M. Martinez, B. McGrane, and M. Golombek (2006), Boulder hazard assessment of potential Phoenix landing sites, Lunar Planet. Sci., XXXVIII, Abstract 1094.

Matmon, A., O. Simhai, R. Amit, I. Haviv, N. Porat, E. McDonald, L. Benedetti, and R. Finkel (2009), Desert pavement-coated surfaces in extreme deserts present the longest-lived landforms on Earth, Geol. Soc. Am. Bull., 121, 688–697, doi:10.1130/B26422.1.

Matsuoka, N. (2001), Solifluction rates, processes and landforms: a global review. Earth Sci. Rev. 55, 1-2, 107-134.

McEwen, A.S., and E.B. Bierhaus (2006), The importance of secondary craters to age constraints on planetary surfaces, Annu. Rev. Earth Planet. Sci., 34, 535–567, doi:10.1146/annurev.earth.34.031405.125018.

McEwen, A.S., E.M. Eliason, J.W. Bergstrom, N.T. Bridges, C.J. Hansen, W.A. Delamere, J.A. Grant, V.C. Gulick, K.E. Herkenhoff, L. Keszthelyi, R.L. Kirk, M.T. Mellon, S.W. Squyres, N. Thomas, and C.M. Weitz (2007), Mars Reconnaissance Orbiter's High Resolution Imaging Science Experiment (HiRISE), J. Geophys. Res., 112, E05S02, doi:10.1029/2005JE002605.

McGill, G.E., and L.S. Hills (1992), Origin of giant Martian polygons, J. Geophys. Res., 97(E2), 2633–2647, doi:10.1029/91JE02863.

McSween, H.Y., S.W. Ruff, R.V. Morris, R. Gellert, G. Klingelhöfer, P.R. Christensen, T.J. McCoy, A. Ghosh, J.M. Moersch, B.A. Cohen, A.D. Rogers, C. Schröder, S.W. Squyres, J. Crisp, and A. Yen (2008), Mineralogy of volcanic rocks in Gusev Crater, Mars: Reconciling Mossbauer, Alpha Particle

X-Ray Spectrometer, and Miniature Thermal Emission Spectrometer spectra, J. Geophys. Res., 113, E06S04, doi:10.1029/2007JE002970.

Mellon, M.T. (1997), Small-scale polygonal features on Mars: Seasonal thermal contraction cracks in permafrost, J. Geophys. Res., 102(E11), 25,617–25,628, doi:10.1029/97JE02582.

Mellon, M.T., and B. Jakosky (1993), Geographic variations in the thermal and diffusive stability of ground ice on Mars, J. Geophys. Res., 98(E2), 3345–3364, doi:10.1029/92JE02355.

Mellon, M.T., R.E. Arvidson, J. Marlow, R. Phillips, and E. Asphaug (2008), Periglacial landforms at the Phoenix landing site and the northern plains of Mars, J. Geophys. Res., 113, E00A23, doi:10.1029/2007JE003039.

Mellon, M.T., R.E. Arvidson, H.G. Sizemore, M.L. Searls, D.L. Blaney, S. Cull, M.H. Hecht, T.L. Heet, H.U. Keller, M.T. Lemmon, W.J. Markiewicz, D.W. Ming, R.V. Morris, W.T. Pike, and A.P. Zent (2009a), Ground ice at the Phoenix Landing Site: Stability state and origin, J. Geophys. Res., 114, E00E07, doi:10.1029/2009JE003417.

Mellon, M.T., M.C. Malin, R.E. Arvidson, M.L. Searls, H.G. Sizemore, T.L. Heet, M.T. Lemmon, H.U. Keller, and J. Marshall (2009b), The periglacial landscape at the Phoenix landing site, J. Geophys. Res., 114, E00E06, doi:10.1029/2009JE003418.

Meresse, S., F. Costard, N. Mangold, D. Baratoux, and J. M. Boyce (2006), Martian perched craters and large ejecta volume: Evidence for episodes of deflation in the northern lowlands, Meteorit. Planet. Sci., 41(10), 1647–1658, doi:10.1111/j.1945-5100.2006.tb00442.x.

Mischna, M.A., M.I. Richardson, R.J. Wilson, and D.J. McCleese (2003), On the orbital forcing of Martian water and CO2 cycles: A general circulation model study with simplified volatile schemes, J. Geophys. Res., 108(E6), 5062, doi:10.1029/2003JE002051.

Mitrofanov, I., D. Anfimov, A. Kozyrev, M. Litvak, A. Sanin, V. Tret'yakov, A. Krylov, V. Shvetsov, W. Boynton, C. Shinohara, D. Hamara, and R. Saunders (2002), Maps of Subsurface Hydrogen from the High Energy Neutron Detector, Mars Odyssey, Science, 297(5578), 78-81, doi:10.1126/science.1073616.

Mitrofanov, I.G., M.T. Zuber, M.L. Litvak, W.V. Boynton, D.E. Smith, D. Drake, D. Hamara, A.S. Kozyrev, A.B. Sanin, C. Shinohara, R.S. Saunders, and V.

Tretyakov (2003), CO_2 snow depth and subsurface water-ice abundance in the northern hemisphere of Mars. Science 300, 5628, 2081-2084.

Morgenstern, A., E. Hauber, D. Reiss, S. van Gasselt, G. Grosse, and L. Schirmeister (2007), Deposition and degradation of a volatile-rich layer in Utopia Planitia and implication for climate history on Mars, J. Geophys. Res., 112(E6), E06010, doi:10.1029/2006JE002869.

Mulla, D.J. (1988), Using geostatistics and spectral analysis to study spatial patterns in the topography of southeastern Washington state, USA Earth Surface Processes and Landforms, 13, 389-405.

Murton, J.B., and M.D. Bateman (2007), Syngenetic sand veins and antisyngenetic sand wedges, Tuktoyaktuk coastlands, western Arctic Canada, Permafrost Periglac. Process., 18, 33–47, doi:10.1002/ppp.577.

Orloff, T., M. Kreslavksy, E. Asphaug, and J. Korteniemi (2011), Boulder movement at high northern latitudes of Mars, J. Geophys. Res., 116, E11006, doi:10.1029/2011JE003811.

Perron, J.T., J.W. Kirchner and W.E. Dietrich (2008), Spectral signatures of characteristic spatial scales and nonfractal structure in landscapes, J. Geophys. Res., 113, F04003, doi:10.1029/2007JF000866.

Péwé, T.L. (1959), Sand-wedge polygons (tessellations) in the McMurdo Sound region, Antarctica: A progress report, Am. J. Sci., 257, 545–552, doi:10.2475/ajs.257.8.545.

Péwé, T.L. (1963), Ice-wedges in Alaska–classification, distribution and climatic significance, paper presented at 2nd International Conference on Permafrost, Russ. Acad. of Sci., Yakutsk, Siberia.

Pina, P., J. Saraiva, L. Bandeira, and T. Barata (2006), Identification of Martian polygonal patterns using the dynamics of watershed contours, Lect. Notes Comput. Sci,. 4142, 691–699.

Pina, P., J. Saraiva, L. Bandeira, and J. Antunes (2008), Polygonal terrains on Mars: A contribution to their geometric and topological characterization, Planet. And Space Sci., 56, 1919-1924.

Placzek, C.J., A. Matmon, D.E. Granger, J. Quade, and S. Niedermann (2010), Evidence for active landscape evolution in the hyperarid Atacama from multiple terrestrial cosmogenic nuclides, Earth Planet. Sci. Lett., 295, 12–20, doi:10.1016/j.epsl.2010.03.006.

Portyankina, G., W.J. Markiewicz, N. Thomas, C.J. Hansen, and M. Milazzo (2010), HiRISE observations of gas sublimation-driven activity in Mars' southern polar regions: III. Models of processes involving translucent ice. Icarus 205, 1, 311-320.

Rayner, J.N. (1972), The application of harmonic and spectral analysis to the study of terrain, in Spatial Analysis in Geomorphology, edited by R. J. Chorley, pp. 283-302, Methuen.

Rempel, A.W. (2007), The formation of ice lenses and frost heave, J. Geophys. Res., 112, F02S21, doi:10.1029/2006JF000525.

Ricard, Y., C. Froidevaux, and R. Simpson (1987), Spectral analysis of topography and gravity in the Basin and Range Province, Tectonophysics, 133, 175-187.

Roering, J.J., J.W. Kirchner, and W.E. Dietrich (2001), Hillslope evolution by nonlinear, slope-dependent transport: Steady state morphology and equilibrium adjustment timescales. J. Geophys. Res. 106, B8, 16499-16513.

Rosato, A., K.J. Strandburg, F. Prinz, and R.H. Swendsen (1987), Why the brazil nuts are on top: Size segregation of particulate matter by shaking, Phys. Rev. Lett., 58, 1038–1040, doi:10.1103/PhysRevLett.58.1038.

Schorghofer, N., and O. Aharonson (2005), Stability and exchange of subsurface ice on Mars, J. Geophys. Res., 110, E05003, doi:10.1029/2004JE002350.

Seibert, N.M., and J.S. Kargel (2001), Small-scale Martian polygonal terrain: Implications for liquid surface water, Geophys. Res. Lett., 28(5), 899-902.

Sizemore, H.G., and M.T. Mellon (2006), Effects of soil heterogeneity on Martian ground-ice stability and orbital estimates of ice depth, Icarus, 185, 358–369, doi:10.1016/j.icarus.2006.07.018.

Sizemore, H.G., M.T. Mellon, and M.P. Golombek (2009), Ice table depth variability near small rocks at the Phoenix landing site, Mars: A pre-landing assessment, Icarus, 199, 303–309, doi:10.1016/j.icarus.2008.10.008.

Smith, P.H., L. Tamppari, R.E. Arvidson, D. Bass, D. Blaney, W. Boynton, A. Carswell, D. Catling, B. Clark, T. Duck, E. DeJong, D. Fisher, W. Goetz, P. Gunnlaugsson, M. Hecht, V. Hipkin, J. Hoffman, S. Hviid, H. Keller, S. Kounaves, C.F. Lange, M. Lemmon, M. Madsen, M. Malin, W. Markiewicz, J. Marshall, C. McKay, M. Mellon, D. Michelangeli, D. Ming, R. Morris, N. Renno, W.T. Pike, U. Staufer, C. Stoker, P. Taylor, J. Whiteway, S. Young,

and A. Zent (2008), Introduction to special section on the Phoenix Mission: Landing site characterization experiments, mission overviews, and expected science, J. Geophys. Res., 113, E00A18, doi:10.1029/2008JE003083.

Soare, R.J., and G.R. Osinski (2009), Stratigraphical evidence of late Amazonian periglaciation and glaciation in the Astapus Colles region of Mars, Icarus, 202, 17–21, doi:10.1016/j.icarus.2009.02.009.

Soare, R.J., G.R. Osinski, and C.L. Roehm (2008), Thermokarst lakes and ponds on Mars in the very recent (late Amazonian) past, Earth Planet. Sci. Lett., 272, 382–393, doi:10.1016/j.epsl.2008.05.010.

Squyres, S.W., and M.H. Carr (1986), Geomorphic evidence for the distribution of ground ice on Mars, Science, 231, 249–252, doi:10.1126/science.231.4735.249.

Stoker, C.R., A. Zent, D.C. Catling, S. Douglas, J.R. Marshall, D. Archer Jr., B. Clark, S.P. Kounaves, M.T. Lemmon, R. Quinn, N. Renno, P.H. Smith, and S.M.M. Young (2010), Habitability of the Phoenix landing site, J. Geophys. Res., 115, E00E20, doi:10.1029/2009JE003421.

Stromberg, W.D., and T.G. Farr (1986), A Fourier-based textural feature extraction procedure, IEEE Transactions on Geoscience and Remote Sensing, 24, 722-731.

Taber, S. (1929), Frost Heaving. J. Geol. 37, 5, 428-261.

Tanaka, K.L. (1986), The stratigraphy of Mars, J. Geophys. Res., 91(B13), E139–E158, doi:10.1029/JB091iB13p0E139.

Tanaka, K.L., J.A. Skinner Jr., T.M. Hare, T. Joyal, and A. Wenker (2003), Resurfacing history of the northern plains of Mars based on geologic mapping of Mars Global Surveyor data, J. Geophys. Res., 108(E12), 8043, doi:10.1029/2002JE001908.

Tanaka, K.L., J.A. Skinner Jr., and T.M. Hare (2005), Geologic map of the northern plains of Mars, U.S. Geol. Surv. Sci. Invest. Map, 2888.

Thomas, N., G. Portyankina, C.J. Hansen, and A. Pommerol (2011), HiRISE observations of gas sublimation-driven activity in Mars' southern polar regions: IV. Fluid dynamics models of CO_2 jets. Icarus 212, 1, 66-85.

Washburn, A.L. (1956), Classification of Patterned Ground and Review of Suggested Origins. Bull. Geol. Soc. Am. 67, 823-866.

Washburn, A.L. (1973), Periglacial Processes and Environments, St. Martins Press, New York.

Werner, S.C., B.A. Ivanov, and G. Neukum (2009), Theoretical analysis of secondary cratering on Mars and an image-based study on the Cerberus Plains, Icarus, 200, 406–417, doi:10.1016/j.icarus.2008.10.011.

Williams, J.C. (1976), The segregation of particulate materials. A review, Powder Technol., 15, 245–251, doi:10.1016/0032-5910(76)80053-8.

Yershov, E.D. (1998), General Geocryology, Cambridge Univ. Press, Cambridge, U. K., doi:10.1017/CBO9780511564505.

Zahnle, K., J.L. Alvarellos, A. Dobrovloskis, and P. Hamill (2008), Secondary and sesquinary craters on Europa, Icarus, 194, 660–674, doi:10.1016/j.icarus.2007.10.024.

Zent, A.P., M.H. Hecht, D.R. Cobos, S.E. Wood, T.L. Hudson, S.M. Milkovich, L.P. DeFlores, and M.T. Mellon (2010), Initial results from the thermal and electrical conductivity probe (TECP) on Phoenix, J. Geophys. Res., 115, E00E14, doi:10.1029/2009JE003420.

Zent, A.P., H.G. Sizemore, and A.W. Rempel (2011), Ice lens formation and frost heave at the Phoenix landing site. Lunar Planet. Sci. XLII, 2543.